CRANFIELD UNIVERSITY

SCHOOL OF ENGINEERING

PHD THESIS

HUGO PERVIER

EMISSIONS MODELLING FOR ENGINE CYCLE AND AIRCRAFT TRAJECTORY OPTIMISATION

SUPERVISOR: DR. VISHAL SETHI

JUNE 2013

This thesis is submitted in the fulfilment of the requirement for the degree of Doctor of Philosophy

Abstract

The aviation industry is currently experiencing a growth rate of about 4% per annum and this trend is expected to continue into the future. One concern about this growth rate is the impact it will have on the environment particularly in terms of emissions of CO_2, NO_x and relatively recently also cirrus clouds induced by contrails.

The ACARE has set emissions reduction targets of 50% reduction of CO_2 and noise and 80% reduction of NO_x by 2020 relative to Y2000 technology. Clean Sky and other large EU collaborative projects have been launched in an effort to identify new, more efficient, aircraft and engine technologies, greener operational and asset management practices and lower life cycle emissions. This PhD research was funded by and contributed to the Systems for Green Operations Integrated Technology Demonstrator (SGO-ITD) of the Clean Sky project.

The key contribution to knowledge of this research is the development and application of a methodology for simultaneous optimisation of aircraft trajectories and engine cycles. Previous studies on aircraft trajectory optimisation studies, published in the public domain, are based on relatively low fidelity models. The case studies presented in this thesis are multi-objective and based on higher fidelity, verified aircraft, engine and emissions models and also include assessments of conceptual engines with conceptual LPP combustors.

The first task involved the development of reactor based NO_x emission prediction models for a conventional aero gas turbine combustor and a novel conceptual lean pre-mixed pre-vaporised combustor. A persistent contrails prediction model was also developed.

A multi-disciplinary framework comprising a genetic algorithm based optimiser integrated with an engine performance, an aircraft performance and an emission prediction model was then developed. The framework was initially used to perform multi-disciplinary aircraft trajectory optimisation studies and subsequently both aircraft trajectory and engine cycle optimisation studies simultaneously to assess trade-offs between mission fuel burn, flight time, NO_x production and persistent contrails formation.

The main result of the work shows that when optimising the trajectory only, the range of environmental gain is limited. NO_x can only be reduced by about 3% compared to a fuel optimised trajectory. Additional case studies have shown that NO_x emitted can potentially be drastically reduced by either changing the combustor technology to a lean pre-mixed pre-vaporised combustor or by radically changing the engine design toward lower overall pressure ratio while accepting a significant fuel penalty. The use of a 2-objective optimisation technique has led to the generation of optimum Pareto fronts from which it is possible to directly choose trade off solutions between environmental gain (NO_x and length of persistent contrails in this study) and fuel consumed. In all cases, and based on the vertical atmospheric profile chosen, contrails were completely avoided with a relatively small fuel penalty (0.5% fuel penalty in case 1 and 2 and 0.3% for case 3).

Acknowledgments

I would like to thank my supervisor Dr. Vishal Sethi for his support and precious technical help along the course of this PhD.

I also have a special thanks to my fellow colleague and friend Dr. Devaiah K. Nalianda who was always there for a cup of tea and enlightening topic of discussions.

The work presented in this document was achieved thanks to the funding from the European Union's Seventh Framework Program (FP7/2007-2013) for the Clean Sky Joint Technology Initiative under grant agreement n° CJSU-GAM-SGO-2008-001.

Contents

List of Figures

List of tables

Glossary

ACARE	Advisory Council for Aeronautics Research in Europe
ATM	Air Traffic Management
BADA	Base of Aircraft Data
BFF2	Boeing Fuel Flow Method 2
BPR	By-Pass Ratio
CAEP	Committee on Aviation Environmental Protection
CAS	Calibrated Air Speed
CEA	Chemical Equilibrium with Application
CF	Contrails Factor
CFD	Computational Fluid Dynamic
CO_2	carbon dioxide
Contrails	Condensation Trails
Δ	Diversity metric
DLR	Zentrum fur Luft and Raumfahrt
DVM	Dynamic Vector Mutate
EGT	Exhaust Gas Temperature
FP	Framework Program
FPR	Fan Pressure Ratio
GA	Genetic Algorithm
GATAC	Green Aircraft Trajectory under ATM Constraints
GE	General Electric
GUI	Graphical User Interface
HPC	High Pressure Compressor
ICAO	International Civil Aviation Organisation
IPCC	Intergovernmental Panel on Climate Change
ISA	International Standard Atmosphere
LPC	Low Pressure Compressor
LPP	Lean Pre-mixed Pre-vaporised
LTO	Landing and Take-Off
MLW	Maximum Landing Weight
MTOW	Maximum Take-Off Weight
MZFW	Maximum Zero Fuel Weight
N_2O	Dinitrogen oxide
nm	Nautical mile
NO_x	Oxides of nitrogen
NO_2	Nitrogen Dioxide
NO	Nitrogen oxide
NSGA	Non-dominated Sorting Genetic Algorithm
OEW	Operating Empty Weight
OPR	Overall Pressure Ratio
PaSR	Partially Stirred Reactor
pdf	Probability distribution function
ppmvd	Parts Per Million, Volumetric Dry
PR	Pressure Ratio or Payload range

PSR	Perfectly Stirred Reactor
PSRS	Series of Perfectly Stirred Reactors
RH	Relative humidity
SBX	Simulated Binary Cross-over
SLS	Sea level, Static
SPEA	Strength Pareto Evolutionary Algorithm
SUS	Stochastic Universal Sampling
TAS	True Air Speed
TERA	Techno-economic and Environmental Risk Assessment
TET	Turbine Entry Temperature
UHC	Unburned Hydro Carbon
UN	United Nations
WSR	Well Stirred Reactor
ZDT	Zitzler, Deb and Thiele test functions

Nomenclature

A	area	m^2
β	drag to lift coefficient ratio	-
C_L	lift coefficient	-
C_D	drag coefficient	-
C_{D0}	parasitic drag coefficient	-
C_{D2}	induced drag coefficient	-
c_p	specific heat capacity	$J.kg^{-1}.K^{-1}$
D	aerodynamic drag	N
d	Euclidean distance	-
δ_{amb}	relative ambient pressure	-
e_w	saturation pressure with respect to water	Pa
esw_0	water saturation pressure at critical temperature	Pa
ε	molar mass ratio of water and air	-
η	overall engine efficiency	-
EIH_2O	emissions index of water	g/kg of fuel
$EINO_X$	emissions index of oxides of nitrogen	g/kg of fuel
f	mixture fraction	-
F_{00}	rated net thrust at sea level static conditions	N or kN
FAR	fuel air ratio	-
FN	net Thrust	N or kN
G	mixing line slope	$Pa.K^{-1}$
g_0	earth gravitational acceleration	$m.s^{-2}$
γ_c	convergence metric	-
γ	ratio of specific heat of air	-
H	humidity factor	-
h	altitude	m
L	aerodynamic lift	N
LHV	lower Heating Value	MJ/kg
M	Mach number	-
$\bar{M}$	molar weight	$g.mol^{-1}$
m	mass	kg
$\dot{m}_A$	air mass flow rate	$kg.s^{-1}$
$\dot{m}_f$	fuel mass flow rate	$kg.s^{-1}$
$\dot{m}_{ff}$	corrected fuel mass flow rate	$kg.s^{-1}$
μ	runway coefficient of friction	-
N	number of solutions in the non-dominated front	-
P	pressure	Pa
P_v	saturation vapour pressure	Pa
ϕ	equivalence ratio	-
ρ	density	$kg.m^{-3}$
R	specific gas constant	$J.kg^{-1}.K^{-1}$
r	arc radius	m
R_{ac}	specific air range	km
RH	relative humidity	-

ROC	rate of climb	$ft.min^{-1}$
ROD	rate of descent	$ft.min^{-1}$
S	mixing parameter	-
s_g	distance covered on the ground	m
SFC	specific fuel consumption	$mg.N^{-1}.s^{-1}$
σ	standard deviation	-
t	time	s
t_r	residence time	ms
T	temperature	K
θ_{amb}	relative ambient temperature	-
τ	NO_x formation time	ms
V	speed	$m.s^{-1}$
V_2	take-off Safety speed	kt
V_c	combustor volume	m^3
W	aircraft weight	kg
w	specific humidity	-
x	number of carbon atoms per fuel molecule	-
Y	mass fraction	-

Units are as indicated unless specifically given in the text.

Subscripts

A	air
alt	altitude
amb	ambient
c	combustion
cr	critical
e	evaporation
eq	equilibrium
f	fuel
ff	corrected fuel
GL	ground level
LOF	lift off ground
m	mean
pz	primary zone
ref	reference
r	rotation
s	stall
st	stoichiometric
stag	stagnation
trans	transition
pz	primary zone

Chapter 1 Introduction

1.1 CONTEXT

The 20th century has seen the first design of a self-propelled flying machine. By the end of the century, the development of this industry has largely enabled the economy of many countries to reach a global scale. Nowadays, aircraft engines are much more fuel-efficient with 70% reduction fuel consumption since the early days of commercial flights; however the drastic increase of the passenger and freight volume has completely overcome those improvements. In the context of global warming all sectors of activities are asked to produce solutions in order to reduce their emissions. The aviation industry is therefore also facing challenges to achieve significant reduction of pollutant. Institutional bodies such as ICAO or ACARE for Europe are setting stringent targets to tackle the global warming issue and steer the aviation sector towards a "greener" industry.

It is well known that aviation industry is one of the smallest contributors in term of global CO_2 emission with only about 2 % [1] when comparing against industry sectors such as electricity generation, road transport, etc. Figure 1, shows the distribution of CO_2 emission per sector. However, concerns about aircraft emissions are seriously taken into account for several reasons. One reason is that aviation industry is a fast growing sector with an average of 4% growth per annum and is expected to continue for the next few decades [2]. Second is that aircraft are also emitting other gaseous pollutant than CO_2. The other main pollutant of concern is NO_x (NO and NO_2), in which case high concentration can be severely detrimental to people living around airports. Moreover aviation is the only emitter of NO_x at cruise altitude (8-10km) and is known to have effect on the ozone layer and global warming potential [3]. For these reasons efforts are being undertaken since the 70's to limit the impact of aviation emissions. Since few decades, policies have been enforced by international organisation such as ICAO [6] forcing engine manufacturer to comply with ever stronger emissions regulation. More recently the introduction of the Emission Trading Scheme (ETS) in Europe will force airliners to reduce their CO_2 emission [4]. In Europe, ACARE (Advisory Council for Aeronautics Research in Europe) has set goal for aviation to be achieved by 2020. The goal stated are a reduction of 50% of CO_2, 80% reduction in NO_x and halving the noise produced with datum taken in the year 2000 [5].

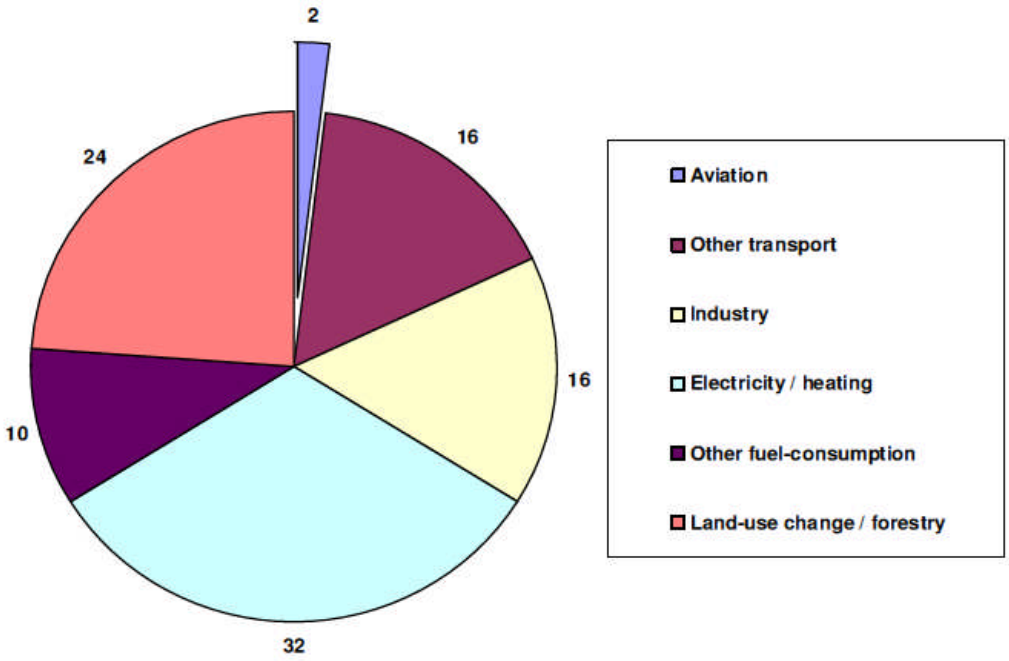

Figure 1 – CO_2 emissions per sector [1]

Due to the constant growth in air traffic and the increased public concerns about global climate change, environmental issues related to aircraft operations has become one of the most important aspect of commercial aviation.

As describes by Clarke [88], there are three main options in order to decrease the environmental impact of aviation. The first option is to reduce the number of flights, the second is to change the type of aircraft used or finally the air traffic regulation and procedure needs to be changed. For obvious reasons the first option is not likely to be feasible given the expected growing trend of air traffic, only option two and three will enable reduction in environmental impact of aviation.

According to Riddlebaugh [89], the main concerns of aircraft design has been, for a long time, focusing on meeting performance requirement with the least operating cost. Environmental considerations were looked at as a final design step to ensure compliance with specific environmental constraints. Nowadays, with ever stringent environmental requirements the early design phase needs to include the environmental performance. Thus, trade-off using systematic quantitative performance and environmental impact assessment needs to be done at an early stage of the design.

With respect to change in air traffic rules and procedures, it is regarded as a shorter term option than aircraft design or component improvement. Identifying greener aircraft trajectories has a potential for reducing the impact of aircraft operations on the environment.

This section leads to the following research questions that this research work aims at answering.

- Can conventional combustor emissions model provide reasonable NO_x estimation for use in preliminary design phase?

- Can the NO_x model be adapted to more advanced combustor concept?
- Can the model be integrated and effectively used in trajectory and engine cycle optimisation?
- How scalable the developed methodology is with respect to optimiser capability and increased problem complexity (higher number of variables, multiple models)
- Is there a noticeable benefit in doing simultaneous trajectory and engine cycle optimisation?

1.2 OBJECTIVES

The objectives of this PhD study were the following:

- Development of an environmental-based methodology for aircraft trajectory and engine cycle optimisation.
- Development of a specific aircraft/engine integration framework linked with a Genetic Algorithm (GA) optimiser to perform trajectory and engine cycle optimisation.
- Development/improvement of a stirred reactor model enabling representative NO_x emission trends prediction from conventional single annular combustor technology.
- Development of a stirred reactor model for NO_x trend estimations from a potentially low NO_x lean pre-mixed and pre-vaporised (LPP) combustor technology using concept of variable geometry.
- Developing a condensation trails (contrails) models to be used in optimisation framework to assess environmental benefits.
- Generating optimum trajectories and engine designs and assessing trade-offs in term of fuel consumed, time of flight, NO_x emitted and persistent contrails formation.

1.3 CONTRIBUTION TO KNOWLEDGE

From the outcome of the achievement of the objectives mentioned in the previous section and from the literature review presented in the thesis, the contribution to knowledge of the present study is the following:

- Development of a methodology for the analysis and comparison of aircraft trajectory and engine optimisations using a genetic algorithm capable of generating Pareto fronts for 2 objectives. The aircraft trajectory calculations are derived from representative aircraft, engine and emissions models.
- Use of a hypothetical LPP combustor emissions model within a trajectory optimisation to assess environmental benefits and prove the flexibility of the developed methodology.

1.4 SCOPE

The scope of the proposed research is mainly in the perspective of flight operations and early engine design stage. The flight operation point of view encompass limits of aircraft flight envelop. In this work, the use of a detailed aircraft model ensures that generated trajectories are physically flyable. Limitation such as rate of climb and maximum thrust are taken into account in the aircraft model. Usual ATM constraints in term of speeds range have been included. This ensures that generated trajectories are within limit of what ATM operator would allow. However, it is assumed throughout the work that the aircraft is flying a trajectory without additional air traffic. All trajectories are defined by their vertical profile only (no aircraft banking). On-board fuel caters for diversion, hold and contingency fuel as per flight regulations. All trajectories were simulated in no-wind conditions. In term of engine design, the work focuses on the twin spool turbofan technology. Design variable ranges ensure that engine designs generated do not require the use of different engine technologies to be feasible. Constraints on engine parameters also ensure similar mass flow rates which in turn impose similar engine fan size. Engine integration effect and weight are not taken into account in the simulations performed in this work.

1.5 METHODOLOGY

In order to achieve the overall thesis objectives a research methodology has been carried out. The first step was to perform a literature review on all the techniques available to predict NO_x emissions from gas turbine engines. Then an appropriate model was selected based on criteria such as computational speed, representative of physical phenomena, flexibility and adaptability to different combustor technologies. The next step was to perform a similar literature review regarding potential optimisers to be used in complex trajectory and engine cycle optimisation. The outcome was the benchmarking and selection of an appropriate optimiser designed for two-objective and constraint handling capabilities. Subsequently aircraft and engine models were selected based on the availability of public domain information as well as specific features required for the study. Finally, test cases to perform were selected in order to answers the research questions set for this study.

The novelty of the methodology lies in the use of different models compared to previous studies. In particular, the reactor based model was used instead of a simple correlation method for NO_x emissions prediction. The engine models used was not based on a database or simple correlation model but used a fully regressed thermodynamic modelling approach ensuring representative physical engine behaviour.

1.6 THESIS STRUCTURE

Chapter 2 is a review of the literature available regarding the various ways of modelling NO_x for aircraft engines. Main methods are Boeing fuel flow, DLR method, P3T3 method, reactor based modelling and CFD modelling. The survey then review, how NO_x regulation is currently enforced by international organisations. This chapter also goes into explaining in details how multi-objectives optimisation works and especially for genetic algorithm. It provides the metrics generally used to assess the performance of multi-objectives optimisers. Finally, the last part of chapter 2 deals with studies published in the past regarding trajectory optimisations and points out the area of the contribution to knowledge of the current work.

Chapter 3 is dedicated to the testing and benchmarking of the optimiser against other genetic algorithm optimisers to ensure that the optimiser used in the subsequent optimisation studies will perform adequately with a good level of performance. The outcome was that all optimisers performed similarly and to high level of convergence and diversity for all tested functions.

Chapter 4 details the emissions models to be used in chapter 5 optimisation studies. This chapter firstly focuses on the improvement made of an existing reactor based NO_x emissions model. The outcome is a comparison for different engine model on the level of NO_x emitted. The improved reactor based model indicates good agreement. The next part of the chapter describes the modelling of a hypothetical LPP combustor that could potentially fit future generation of aircraft. The combustor is modelled after a currently existing LPP combustor developed by Rizk and Mongia [6]. Finally to assess the length of persistent contrails generated by aircraft flying at cruise level, a contrails model has been developed and validated. The details are given in chapter 4.

Chapter 5 focuses on the test cases developed for the present work that uses all the models described in chapter 4 and uses the optimisation technique detailed in chapter 3. Three test cases have been defined. The first case is a trajectory optimisation for which objectives sets were as follows: fuel/time, fuel/NO_x and fuel/contrails. All objectives were to be minimised. The second case is essentially the same as the first case except the combustor model is replaced with the LLP combustor. The last case is a trajectory and engine optimisation. This case essentially allows the optimiser to modify trajectory related and engine design point related parameters. This case is designed to assess how engine optimisation can further improve fuel, time, NO_x or contrails compared to case 1.

Chapter 2: Literature review

Chapter 2 is a review of the literature available regarding the various ways of modelling NO_x for aircraft engines. Main methods are Boeing fuel flow, DLR method, P3T3 method, reactor based modelling and CFD modelling. The survey then review, how NO_x regulation is currently enforced by international organisations. This chapter also goes into explaining in details how multi-objectives optimisation works and especially for genetic algorithm. It provides the metrics generally used to assess the performance of multi-objectives optimisers. Finally, the last part of chapter 2 deals with studies published in the past regarding trajectory optimisations and points out the area of the contribution to knowledge of the current work.

2.1 NO_X EMISSIONS PREDICTION MODELLING METHODOLOGIES

2.1.1 EMPIRICAL AND SEMI-EMPIRICAL MODELS

2.1.1.1 Legacy empirical and semi-empirical NO_X emissions model

To predict pollutant emissions, many empirical models have been developed in the past. A large number of models have been specifically developed to predict NO_X for different applications (stationary gas turbine or aero-gas turbine) and different combustor designs and technologies. This section will briefly review some of the available empirical or semi-empirical NO_X emissions models.

Lefebvre [7] has published a correlation for estimating NO_x emissions index and is shown in equation [2.1].

$$EINO_X = 9 \times 10^{-8} P^{1.25} V_C \exp(0.01 T_{st}) / \dot{m}_A T_{pz} \quad \text{in g/kg of fuel} \qquad [2.1]$$

Where, $EINO_x$ is the emissions index of NO_x given in grams of NO_x emitted per kilogram of fuel burnt. P is the combustor pressure, V_c is the combustor volume, T_{st} and T_{pz} are the temperature at stoichiometry and in the primary zone respectively. $\dot{m}_A$ is the air mass flow rate.

This empirical formula was experimentally obtained using NO_x emissions data from aero-engine. This equation mainly assumes that the formation of NO_x in heterogeneous fuel-air mixture is dependent on the stoichiometric flame temperature rather than the average

flame temperature. The average temperature in the primary zone (T_{pz}) takes into account the residence time dependency on the NO_x formation. The particular set of constants and exponent in Eq. 2.1 make this correlation suitable only for conventional spray combustors. [8].

Odgers and Kretschmer [9] have proposed a correlation for NO_x that directly uses the NO_x formation time (τ) as a variable as can be seen in Eq. 2.2. The authors suggest using 0.8 ms for aero-combustors design with airblast atomizer and 1.0 ms when the combustor is fitted with pressure atomizer. T_c is the combustion temperature.

$$EINO_X = 29exp\left(-\frac{21670}{T_C}\right)P^{0.66} \times [1 - exp(-250\tau)] \qquad \text{in g/kg of fuel} \qquad [2.2]$$

Rizk and Mongia [10] proposed a correlation that includes the effect of fuel evaporation on NO_x emissions. In equation Eq. 2.3, a reduction in fuel droplet size leads to an increase in NO_x formation.

$$EINO_X = 15.10^{14}(t_r - 0.5t_e)^{0.5}\exp(-71100/T_{st})P^{-0.05}(\Delta P/P)^{0.5} \qquad \text{in g/kg of fuel} \quad [2.3]$$

Where, t_r is the residence time and t_e is the evaporation time.

Other authors have proposed correlation for NO_x emissions such as in [11], [12] and [13]. Overall most work on NO_x correlation was done with specific combustor application rather than being general NO_x correlation that can be applied in many fields.

2.1.1.2 Boeing Fuel Flow method 2

The Boeing fuel flow method has been developed to specifically assess civil aircraft engine emissions such as NO_X, CO and UHC [14]. The method relies on the knowledge of known engine emissions information provided by the ICAO emissions databank [15] at ground level. The purpose of the model is to estimate emissions at other atmospheric conditions (temperature, pressure, humidity) while also providing a fuel flow correction factor for the engine installation effect. This correction is required since the ICAO databank emissions data is provided directly by the engine manufacturer who has tested his engines un-mounted. In final, this allows to calculate emissions from aircraft engine at any altitudes. Jelinek [16] shows that this method can be used for a wide range of aircraft/engines configuration for NO_X, CO and UHC emission indices estimation.

BBF2 calculation steps

The BFF2 method estimates emission indices through a 5-step procedure (see Kim et al. [17]) which can be summarised as follow for the case of NO_X prediction. The first step is the application of the correction factor on the fuel flow for the four ICAO points. The correction factor values are shown in Table 1.

Table 1 - Fuel flow correction factors for the four ICAO points.

ICAO point	Take-off	Climb out	Approach	Idle
Correction factor	1.010	1.013	1.020	1.100

The second step is to build a log-log plot of $EINO_X$ versus fuel flow. The plot is used to obtain the best fit linear equation of $EINO_X$ versus fuel flow in a log-log scale. There are two approaches possible, either defining a single best fit equation for the whole set of points or defining an equation between each ICAO reference point (called point to point fitting) leading to the creation of 3 equations. The latter option is said to lead to more accurate results [14]. Each method is illustrated in Figure 2.

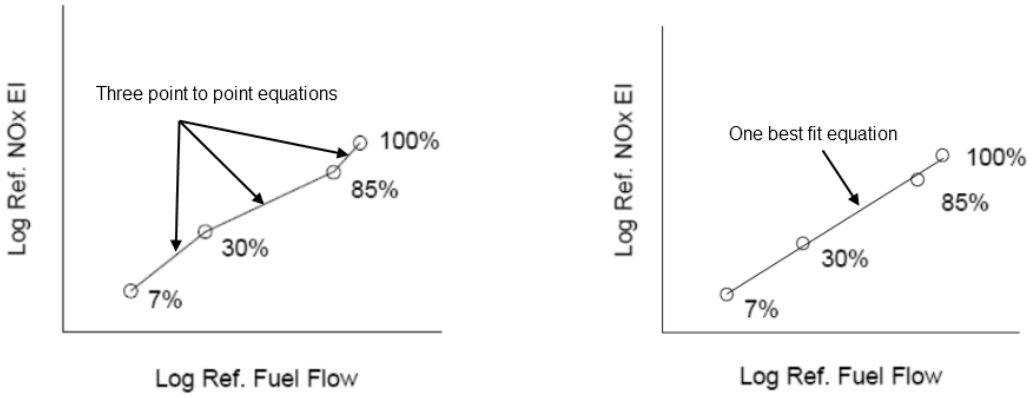

Figure 2 - Left: point to point fitting method. Right: single best fit equation

The next step is to correct the fuel flow for the reference conditions given by the following equation.

$$\dot{m}_{ff} = \frac{\dot{m}_f}{\delta_{amb}}[\theta_{amb}^{3.8}\exp(0.2M^2)] \quad [2.4]$$

With $\delta_{amb} = P_{amb}/101325$ and $\theta_{amb} = T_{amb}/288.15$.

Once the reference fuel flow is calculated it is possible to obtain the corresponding reference EI ($EINO_{Xref}$) (step 4) using the equation derived from step 2. At last, in step 5, the $EINO_x$ at altitude can be calculated using equation 2.5.

$$EINO_{X_{alt}} = EINO_{X_{ref}}\left(\frac{\delta_{amb}^{1.02}}{\theta_{amb}^{3.3}}\right)^{0.5} exp(H) \quad [2.5]$$

In equation (2.5), the term H is the humidity factor. It is defined as follows.

$$H = -19.0(w - 0.0063) \quad [2.6]$$

In the original BBF2 method, the specific humidity w is defined as in equation 2.7.

$$w = \frac{0.62198.\mathrm{RH}.P_v}{P_{amb} - \mathrm{RH}.P_v} \quad [2.7]$$

However, it is reported in [16], that the formula should be corrected to the following.

$$w = \frac{0.62198 \Phi P_v}{P_{amb} - 0.37802 \Phi P_v} \quad [2.8]$$

In equations 2.7 and 2.8, RH is the relative humidity and P_v is the saturation vapour pressure in psia and is given by

$$P_v = 0.014504.\,10^{\beta} \quad [2.9]$$

Where,

$$\beta = 7.90298\left(1 - \frac{373.16}{T_{amb}+273.16}\right) + 3.00571 + 5.02808.\log\left(\frac{373.16}{T_{amb}+373.16}\right) + 1.3816.\,10^{7}\left[1 - 10^{11.344\left(1-\frac{T_{amb}+273.16}{373.16}\right)}\right] + 8.1328.\,10^{-3}.\,10^{3.49149(1-373.16/(T_{amb}+273.16))} \quad [2.10]$$

2.1.1.3 DLR method

The Zentrums fur Luft and Raumfahrt (DLR) [18] has developed a slightly modified version of the BFF2 method. The basic principle remains the same in the sense that it is still using only fuel flow to predict the engine emission indices. In this method, the ICAO emissions databank is also used to obtain the $EINO_X$ reference value (in this case only using a second order polynomial fit).

The fuel flow correction factor is modified as shown in equation 2.11.

$$\dot{m}_{ff} = \frac{\dot{m}_f}{\delta_t \sqrt{\theta_t}} \quad [2.11]$$

And the NO_X emission index at altitude is calculated using the following equations.

$$EINO_{X,alt} = EINO_{X,ref} \exp(H) {\delta_t}^{a} {\theta_t}^{b} \quad [2.13]$$

With $\delta_t = \frac{Pstag}{101325}$ and $\theta_t = \frac{Tstag}{288.15}$.

Where P_{Stag} and T_{Stag} are the stagnation pressure and temperature respectively and shown in equations 2.14 and 2.15.

$$P_{Stag} = P_{amb}(1 + 0.2M^2)^{3.5} \quad [2.14]$$

$$T_{Stag} = T_{amb}(1 + 0.2M^2) \quad [2.15]$$

2.1.1.4 P3T3 method

The P3T3 method [19 and 20] can be classified in the semi-empirical method because instead of simply using the fuel flow as the only input (like for the BFF2 and DLR approach), this method relies on engine condition parameters such as pressure and temperature at combustor inlet. As a consequence, this method is considered more advanced compared to BFF2 or DLR methods, but it is also necessary to obtain more information about the combustor inlet conditions compared BFF2 or DLR methods. The common point with the P3T3 method and the BFF2 and DLR methods is again the use of the ICAO emissions databank as the reference emissions index.

The principle of the method is to plot the $EINO_X$ at ground level against the combustor inlet temperature ($T3_{GL}$) for the four ICAO emission points. Two other plots are also initially constructed for the ground level reference, that is, the combustor inlet pressure ($P3_{GL}$) against combustor inlet temperature and the overall fuel-air ratio (FAR_{GL}) against the combustor inlet temperature. Temperature and pressure at the combustor inlet and the fuel-air ratio at ground level are not information given by the ICAO emissions databank and thus need to be computed by engine simulation software. The level of accuracy of this simulation software will therefore have a significant impact on the accuracy of the P3T3 method. For each plot, similarly to the BFF2 and DLR method, a second order polynomial fit is obtained. One main difference compared to BFF2 and DLR method is that the plots are not in a log-log scale.

Once the three plots and the three equations are set, it is possible to compute the NO_X at altitude using equation 2.16.

$$EINO_{X_{ALT}} = EINO_{X_{GL}} \left(\frac{P_{ALT}}{P_{GL}}\right)^n \left(\frac{FAR_{ALT}}{FAR_{GL}}\right)^m \exp(H) \qquad [2.16]$$

In order to use equation 2.16, it is necessary to know the engine condition at altitude (using the engine model). The parameters are pressure ($P3_{ALT}$) and temperature ($T3_{ALT}$) at combustor inlet and overall fuel-air ratio (FAR_{ALT}) at altitude.

$EINO_{X_{GL}}$, P_{GL} and FAR_{GL} are interpolated using their respective polynomial equations given $T3_{ALT}$. P_{ALT} and FAR_{ALT} are directly taken from the engine model.

Finally, similarly to the BFF2 and DLR method, a humidity correction factor (H) is taken into account for the calculation of the emission index of NO_x at altitude.

In equation 2.16, two exponents, n and m can be adjusted for a given engine. In fact the exponent m is usually set to zero since it has been observed that the overall fuel-air ratio had not a significant impact on the predicted NO_X at altitude. Madden and Park [19] reports variation of only 3% in NO_X emission index for a 20% change in FAR.

For the exponent n, it is recommended by [19] to use 0.4 if no specific information is available for the engine to be assessed. [20] reports a number of possible value for n, generally ranging from 0.2 to 0.49.

2.1.2 REACTOR BASED MODEL

In general, flows in actual combustors show high level of turbulence, time dependency and mass transport and energy transfer in three dimensions. Obtaining the solution on such a complex problem where partial differential equations need to be solved for mass, energy and momentum conservation can be very computationally intensive. As such, different approaches are used to approximate the combustion process in order to reduce complexity and computing time. One type of approximation is to focus on the finite rate chemistry and to assume that the mixing takes place at an infinite rate or in a defined way. When mixing is assumed infinite the reactor is called a Perfectly Stirred Reactor (PSR). If one the other hand the mixing is defined by probability distribution functions, the reactor is called a Partially Stirred Reactor (PaSR) or a Well Stirred Reactor (WSR). In both cases, this approximation leads to the reactor theory as discussed in more detailed in section 4.1. As opposed to the finite rate chemistry, another type of approximation is to consider the chemical reaction to happen instantaneously and to focus on the mixing processes. This approach leads to Computational Fluid Dynamics (CFD) applied to combustion processes.

The basic concept of the reactor-based modelling method is to break down the combustor into a number of regions simulated through reactors and to calculate within each the production or elimination of pollutants of interest. Reactors can be modelled differently depending on the specificities of the region they represent. In all reactors, the principle is to capture sufficiently well the combustion process in order to assess pollutant formation rates. This includes the use of chemical equilibrium to obtain information about temperature, density, residence time, mass fraction and so on, within each reactor. In addition, since most pollutants are not formed in chemical equilibrium, it is necessary to include chemical kinetic considerations.

A model using this concept has been developed by Celis [21]. The following section focus on describing how the model has been designed.

As stated, the basic principle is to split the combustor using different reactors to model different part of the combustor. In the work of Celis [21] three different types of reactors have been developed based on the work of Aksit [22], Pratt [23], Fletcher et al. [24] and Swithenbank et al [25] and are discussed below.

2.1.2.1 Perfectly Stirred Reactor (PSR)

As described in [21] the PSR model inputs two streams. One is the air or combustion products stream entering the reactor with specific temperature, pressure and species mass fraction, the second stream is the fuel. As stated above both stream mixes instantly and chemical equilibrium is assumed to occur instantaneously. The calculation of the chemical equilibrium is done through the use of the NASA Chemical Equilibrium with Application (CEA) program [26, 27] which uses the minimisation of Gibbs free energy at constant pressure and temperature under the constraint of elements conservation. The main aim of the NASA program is to compute combustion parameters such as equilibrium temperature, density and species mass fraction for a given reactor.

Typical residence times in aero-engine gas turbine are usually significantly shorter than the time needed to achieve chemical equilibrium for most of the pollutant of interest. This is particularly true for NO_x emissions. In order to ensure sensible quantitative calculation of NO_x emissions, it is therefore necessary to include adequate kinetic model within each reactor. Celis [21] list a number of important assumptions used for the PSR model, but also for the other two types of reactors (PSRS and PaSR). Firstly, the kinetics of radical formation is neglected and equilibrium radical concentration prevails. Secondly, the heat release from the formation of pollutants is considered small compared to the combustion products heat release at chemical equilibrium conditions and is therefore neglected.

2.1.2.2 Series of Perfectly Stirred Reactors (PSRS)

Celis [21] developed a second type of reactor called series of perfectly stirred reactors. This type of reactor was first conceptualised by Hammond and Mellor [28-30]. The idea is to stack a number of perfectly stirred reactors in order to further discretise the air and fuel addition in certain region of the combustor. The number of reactor is set in relation with requirements of a region. In general, the number of reactors is increased until emissions output does not show dependence on this parameter.

2.1.2.3 Partially Stirred Reactor (PaSR)

The last type of reactor is designed to represent macro-mixing within the primary zone of the combustor. The model firstly published by Fletcher and Heywood [24] statistically describes the variation in gas composition, temperature and residence time occurring in the primary zone and outputs a global parameter such as temperature, density and species concentration amongst other. The principle of the partially stirred reactor (or sometimes called well-stirred reactor) is to assume that the mixture fraction distribution follows a

Gaussian probability density function (pdf). To model the PaSR, Celis [21] also uses a clipped Gaussian instead of the classical Gaussian. The reason behind, is that the probability density function of the classical Gaussian tends to zero when the variable (here mixture fraction) tends to ±∞. However, by definition, the mixture fraction can only vary between 0 and 1. The use of the clipped Gaussian is to renormalize and truncate between 0 and 1 the probability density of the Gaussian function so that the integral between 0 and 1 of the clipped pdf still equals 1. Celis [21] uses the same approach as Fletcher and Heywood [24] to define the shape of the clipped Gaussian. They introduced a parameter called the mixing parameter, S, given by equation 2.17.

$$S = \frac{\sigma}{f_m} \qquad [2.17]$$

Where, f_m is the mean value of the mixture fraction and σ corresponds to its standard deviation. One can see that if uniform mixing is assumed the mixing parameter simply becomes zero. In order to determine both the mean and standard deviation, it is necessary to obtain a correlation for the mixing parameter. Sturgess [31-32] has shown that the mixing parameter can be derived from experiments. By matching measured emissions data and emissions model predictions, Sturgess suggests that the mixing parameter can be found at least for a given combustor design. In general, it is expected that the mixing parameter relation would differ for different combustor design and/or technology. In Celis [21] model, the mixing parameter is defined as a function of the equivalence ratio based on information provided by Sturgess [31] and Allaire et al. [33] and is shown in Figure 3. It can be noted that this formulation of the mixing parameter will limit the range of acceptable mean equivalence ratio between around 0.4 and 2.1.

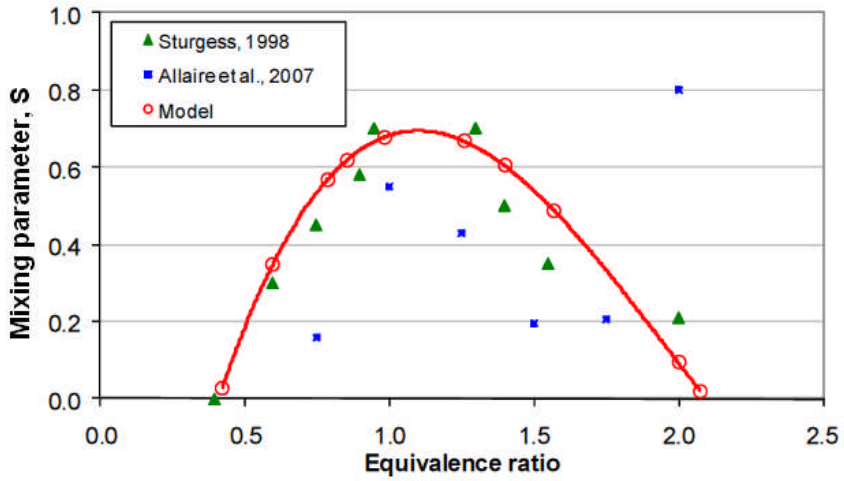

Figure 3 - Mixing parameter versus Equivalence ratio (from Celis [21])

In practice, when the PaSR is used, it receives as input the air and fuel mass flow. The mixing parameter correlation is used to retrieve S. The mean mixture fraction, f_m, is given by the

mass flow inputs and the standard deviation is therefore determined. The mean and standard deviation are subsequently used as input for the clipped Gaussian transformation.

2.1.2.4 NO_x emissions formation

In the case of NO_X emission, it is widely accepted that there are four channels for its formation. Those channels are: thermal NO_X, N_2O mechanism, prompt NO_X and fuel NO_X.

2.1.2.4.1 Thermal NO_X and N_2O mechanism

In gas turbine combustor primary zone combustion conditions, the important set of three reactions that lead to NO_X formation is called the extended Zeldovich mechanism [8, 24, 34 and 35]. These equations describe the formation of NO at high temperature in the post flame gases. Generally, NO_X is composed of NO and NO_2, but in fact the exhaust gas is almost completely composed of NO. Conversion of NO into NO_2 happens only afterward. Also NO_X detector devices require NO to be oxidised into NO_2 [24]. For this reason, only reaction in which NO is created are of real significance to the estimation of NO_X from gas turbine engines. The extended Zeldovich mechanism (or thermal NO_X) reactions are shown in equations 2.18 to 2.20.

$$O + N_2 \rightleftharpoons NO + N \quad [2.18]$$

$$N + O_2 \rightleftharpoons NO + O \quad [2.19]$$

$$N + OH \rightleftharpoons NO + H \quad [2.20]$$

Another set of equation can also be used to relate the formation of NO, using N_2O as intermediary, when primary zone temperature is lower than 2200 K. The reactions involved are shown below [24, 36].

$$H + N_2O \rightleftharpoons N_2 + OH \quad [2.21]$$

$$O + N_2O \rightleftharpoons N_2 + O_2 \quad [2.22]$$

$$O + N_2O \rightleftharpoons NO + NO \quad [2.23]$$

The change of NO mass fraction due to the thermal and N_2O mechanisms can be derived from the six reactions shown above [24]. This is assuming that (1) the reaction is mixing controlled, (2) O, O_2, OH, H and N_2 are in equilibrium and (3) N is in a steady state. The NO mass fraction rate of change is given by equation 2.24.

$$\frac{dY_{NO}}{dt} = \frac{2\bar{M}_{NO}}{\rho}(1-\alpha^2)\left\{\frac{R_1}{1+\alpha K_1} + \frac{R_6}{1+K_2}\right\} \quad [2.24]$$

Where Y_{NO} is the mass fraction of NO, $\bar{M}_{NO}$ is the molar weight of NO, ρ is the density, α is defined by $\alpha = [NO]/[NO]_{eq}$. R1, R6, K1 and K2 are constants defined as follows.

$$R_1 = k_{1f}[N]_{eq}[NO]_{eq} \quad [2.25]$$

$$R_6 = k_{6f}[O]_{eq}[N_2O]_{eq} \quad [2.26]$$

$$K_1 = \frac{R_1}{R_2+R_3} \quad [2.27]$$

$$K_2 = \frac{R_6}{R_4+R_5} \quad [2.28]$$

Where,

$$R_2 = k_{2f}[N]_{eq}[O_2]_{eq} \quad [2.29]$$

$$R_3 = k_{3f}[N]_{eq}[OH]_{eq} \quad [2.30]$$

$$R_4 = k_{4f}[H]_{eq}[N_2O]_{eq} \quad [2.31]$$

$$R_5 = k_{5f}[O]_{eq}[N_2O]_{eq} \quad [2.32]$$

k_{1f} to k_{6f} are the forward reaction constants. The bracket ([]) refers to concentrations of species.

2.1.2.4.2 Prompt NO_X

The prompt NO_X mechanism is a channel for NO_X formation at low temperature where thermal NO_X channel becomes less significant. This channel of formation is more complex and is less well understood than the thermal NO_X channel. According to [35], there are three form of prompt NO; the Fenimore prompt NO, the non-equilibrium O and OH concentrations and the reaction between O and N_2. Celis [21] provides a formula to estimate the formation of prompt NO. The formula is based from the work of De Soete [37] and using the method of [38] with Jet-A fuel modelled as $C_{12}H_{23}$.

$$\frac{dY_{NO}}{dt} = \left(\frac{\bar{M}_{NO}}{\rho}\right) f_{pr} k'_{pr} ([O_2]_e)^a [N_2]_e [C_{12}H_{23}] exp\left(\frac{-36499.507}{T}\right) \quad [2.33]$$

Where,

$$f_{pr} = 4.75 + 0.0819x - 23.2\phi + 32\phi^2 - 12.2\phi^3$$

$$k'_{pr} = 6.4 \times 10^6 \left(\frac{0.0820575.T}{P}\right)^{a+1}$$

$$a = \begin{cases} 1.0 & X_{O_2} \leq 4.1 \times 10^{-3} \\ -3.95 - 0.9 ln X_{O_2} & 4.1 \times 10^{-3} < X_{O_2} \leq 1.11 \times 10^{-2} \\ -0.35 - 0.1 ln X_{O_2} & 1.11 \times 10^{-2} < X_{O_2} < 0.03 \\ 0.0 & X_{O_2} \geq 0.03 \end{cases}$$

2.1.2.4.3 Fuel NO_X

Fuel-bounded nitrogen is present in various quantities depending on the fuel type. The fuel NO_X channel of formation corresponds to the formation of NO_X from the fuel-bounded nitrogen. When considering aviation fuel, the amount of fuel-bounded nitrogen is low, and it is often considered acceptable to neglect this channel of formation.

2.1.3 CFD MODELLING

The third way of predicting emissions from combustion, and especially NO_x, is by using full CFD simulation. In this case the cost in term of computational power is much larger than any methods described in previous sections.

In general, emissions estimation is done in two steps. The first step is to obtain the flow properties in the modelled combustor. The model combustor can either be in 2D or 3D, but for aero-gas turbine combustors it is generally accepted that 3D combustor models should be used in order to capture the flow field sufficiently well. For NO_x estimation some information are critical such as pressure and temperature in the flow. For this reason CFD solver will need to include energy terms when resolving the Navier-Stokes equations. The second step is to apply at each node of the model the chemical kinetic relationships of emissions formation. For NO_x formation, Zeldovich and prompt NO_x mechanisms can be used which have been described for the reactor based model. Other kinetic reaction mechanisms can be used as proposed within the fluent CFD package [38]. Example of emissions prediction using CFD can be found in [39-41]. Similarly to other emissions prediction methods CFD requires extensive validation so that when modelling existing combustors technology, the flow field (in term of parameter such as pressure and temperature) is representative of the actual combustor. This allows, the prediction of NO_x emissions to be representative of the process happening inside of the combustor.

Even though this method can potentially give very accurate results, it was decided not to use it in this work for several reasons.

- The CFD method requires having detailed information regarding the geometry of the combustor to model.
- The time involved with solving the flow field was deemed prohibitive (with the computational power available to the author) to be used as a tool for optimisation that requires thousands of evaluations to reach a solution.
- Requirement of data regarding the internal flow field for validation purpose not available.

2.2 INTERNATIONAL CIVIL AVIATION ORGANISATION AND EMISSIONS REGULATIONS

In order to enforce a safer and environmentally greener aviation industry on a global level, the International Civil Aviation Organisation (ICAO) was created by the United Nations (UN). This agency was created to set targets in terms of safety and emissions for aircraft and engine manufacturers. It also ensures a structured planning and development so that the industry growth does not impair safety or the environment [42].

The ICAO three main environmental objectives for the international aviation industry are as follow [43]:

- Decrease population exposure to high level of aircraft noise
- Reduce the emissions impact from aviation activities on a local level
- Reduce the emissions impact from aviation activities with respect to the large scale climate change.

The Committee on Aviation Environmental Protection (CAEP) was created by the ICAO to study aviation environmental impact and to provide recommendations for reducing identified issues. One important role devoted to the CAEP is to set a number of standards to which all aircraft have to comply to be allowed into operational service. These standards are describes in Annex 16 volume I and II [42].

The volume II – Aircraft Engine Emissions sets the standards for four different pollutants including NO_x. NOx regulations are based on a standard Landing and Take-Off cycle (LTO). The cycle is defined by four segments which are: taxi, approach, take-off and climb. Figure 4, shows a diagram of the LTO cycle. Figure 5 shows how limits on NO_x emissions have been implemented by the CAEP.

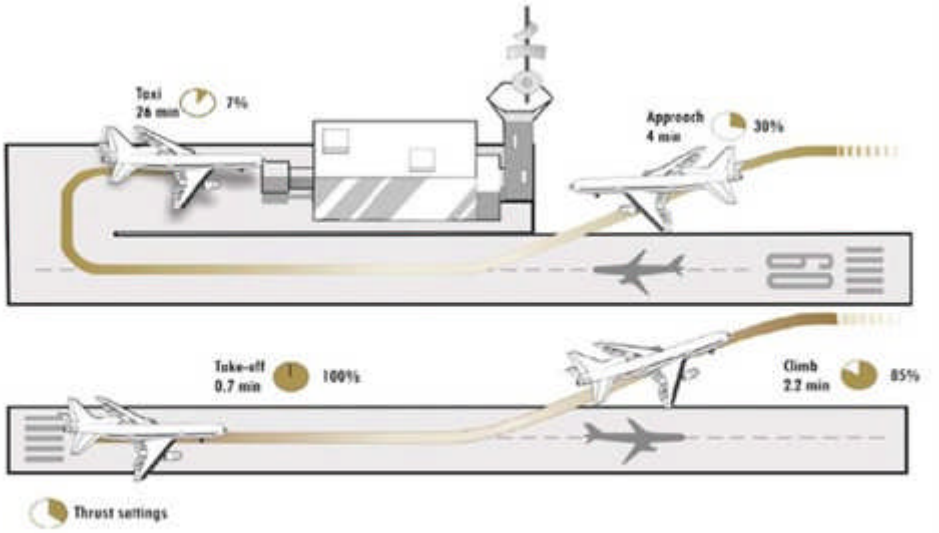

Figure 1 - Illustration of ICAO Emissions Certification Procedure LTO Cycle.
Source: ICAO.

Figure 4 - LTO cycle as defined by the ICAO [42]

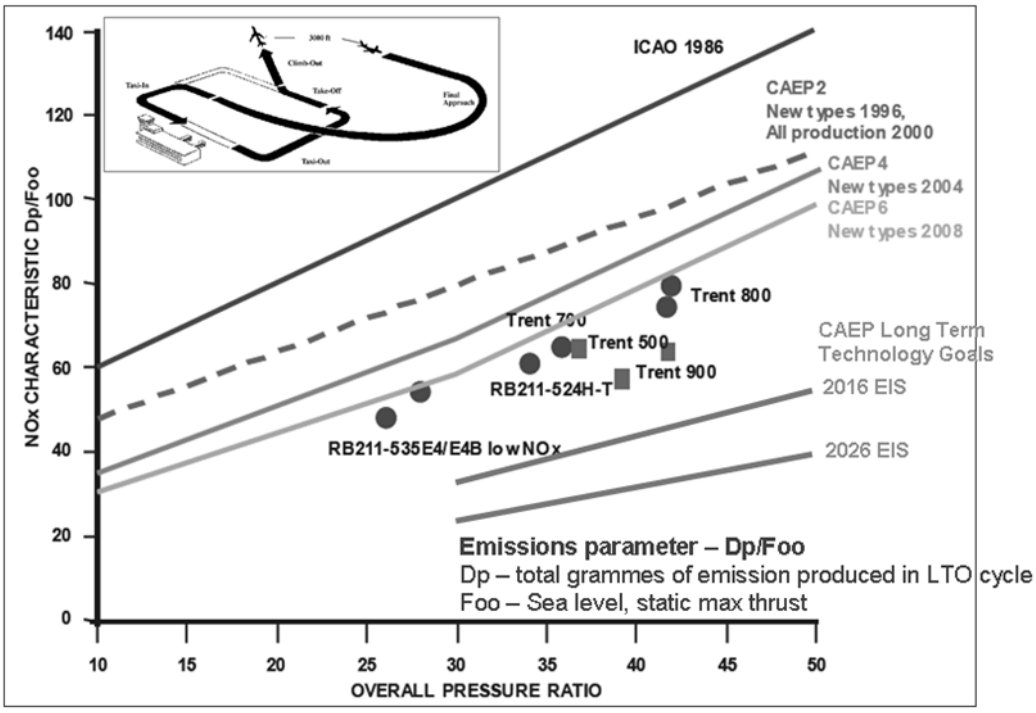

Figure 5 – LTO NO_x limits for aero-engines based on the overall pressure ratio [44]

The amount of pollutant emitted during these four segments is calculated as follows:

$$NO_x(LTO) = \sum_{i=1}^{4} \left(EINO_{x_i} * SFC_i * \frac{FN_i}{F_{00}} * t_i \right) \qquad [2.34]$$

Where i represents the segment, SFC is the specific fuel consumption, F is the net thrust, F_{00} is the rated net thrust at sea level and t is the time spent in segment i.

Different regulatory limit are set depending on the entry of service of the engine as well on the pressure ratio and static rated thrust at sea level. The reader can refer to [45 and 46] for details.

Another type of regulation comes from airport authorities directly. At this time, only few airports enforce NO_x regulations (London, Zurich and Geneva are some examples). Those regulations are simply in the form of a tax depending on the type of aircraft and thus the level of emissions. Simply put, low NO_x aircraft will pay less tax than aircraft known to emit more while also taking into account the mass of the aircraft [47].

2.3 DRY LOW NO_X (DLN) OR LEAN PRE-MIXED PRE-VAPORISED (LPP) COMBUSTOR TECHNOLOGY

DLN concept is referring to combustor design which is capable of reducing NO_x emission without requiring injection of water. Water injection is a well known technique which can reduce NO_x up to 80%. Obviously such technique is difficult to implement for aircraft application. Actually, DLN concept merely regroups all engine design that tries to reduce NO_x emission without water injection. The main thread followed by the DLN concept is to eliminate zone of high temperature by improving the fuel/air mixing prior to combustion. One particular concept that achieves this feature is the LPP design. The fuel is injected, fully vaporized and then fully mixed with air. Only then the mixture goes into the main combustion zone. As the name suggest, the combustion zone operates at low equivalence ratio. Flame temperature is relatively low and local fuel/air in-homogeneity is prevented. The outcome is a very low NO_x production. However, the LPP combustor is supposed to operate as close as possible to the lean blowout limit, therefore it is often required to add a pilot stage to ensure stable combustion. Also such concept will require some sort of variable geometry to maintain the equivalence ratio over the whole power range. Such combustor concept has not yet been applied to aircraft engine but it seems sensible to consider them as a good candidate for near future aircraft technology. Before this technology can safely be implemented for aircraft engine a number of issues need to be solved. The first issue is the relight capability at high altitude. Since the LPP principle is to burn fuel very lean, the relight at high altitude in case of engine flame out is difficult to achieve even with the presence of the pilot stage. Another issue coming from this concept is the occurrence of flashbacks that could damage the combustor components. The probability of flashback is increased due to the inherent design of the LPP concept in which fuel and air is mixed prior to the actual combustion chamber. If, for any reason, instabilities arise such a pressure drop upstream, flashback is highly likely to occur. The problem of reliability is also increased by the

additional complexity stemming from the variable geometry. Additional complex moving parts in an aircraft combustor is directly adversely impacting the overall reliability of the combustor component.

Despite the drawback listed, this method of reducing NO_x is very efficient and as such efforts are made to overcome them. It is possible that in the near future engine manufacturer will attempt to fit LPP technology to aircraft engines. In this regard, representative NO_x emissions modelling of the same would be invaluable to assess its performance once fitted on an aircraft engine.

2.4 OPTIMISATION STRATEGY

2.4.1 THE OPTIMISATION PROBLEM

The general problem of optimisation is simply trying to get the absolute minimum or maximum in one or more objectives under a certain number of equality or inequality constraints. The optimisation problem is usually stated as follows [48].

Find

$$X = \begin{Bmatrix} x_1 \\ x_2 \\ \vdots \\ x_n \end{Bmatrix} \quad [2.35]$$

That minimises (or maximises) f(X), under the set of equality and inequality constraints defined as follows.

$$g_i(X) = 0, \qquad i = 1,2, \dots, k \quad [2.36]$$

$$h_j(X) \leq 0, \qquad j = 1,2, \dots, m \quad [2.37]$$

f(X) is the objective function, with X the n-dimensional vector of optimisation variables. In practical engineering problems, optimisation variables are bounded within prescribed values that are meaningful for the problem considered. This means optimum values of f(X) can vary depending on the set of boundary selected for each optimisation variables.

2.4.2 MULTI OBJECTIVES OPTIMISATION

Literature on the subject of multi objective optimization, suggest various approaches of solving a problem. The basic methodology lies in firstly finding multiple trade-off optimal solutions with a wide range of values for objectives and to choose one of the obtained

solutions using higher level information in the second step. In the first step it is understood that each trade-off solution will correspond to a specific order of importance of the objectives. One approach of solving the problem assumes the user is aware of a preference factor among objectives. A simple method would therefore be to form a composite objective function as the weighted sum of objectives, where a weight for an objective is proportional to the preference factor/vector assigned to that objective. This method of scalarising an objective vector into a single composite objective function effectively converts a multi-objective optimisation problem into a single objective optimisation problem. This procedure is simpler but can be very subjective and will depend also on the higher level information known in the problem. At times this procedure may be used to find multiple trade-off solutions by repeatedly using the procedure using different preference vectors [39].

The main disadvantage of this method is that the process of finding a quantitative relative preference vector is highly subjective and tedious as it may require at times an analysis of non-technical, qualitative and experience driven information and therefore unless a reliable and clear preference vector is utilised, the optimal solution obtained by such methods is highly subjective to a particular user. Classical multi objective optimisation methods, which convert multiple objectives to single objectives (using a relative preference vector of objectives), use this approach.

The second approach uses the higher level information (as discussed in step 2 earlier) to evaluate and compare the set of trade off solutions. Based on this information it chooses one optimal solution and hence like in the earlier discussed approach does not use the higher level information to actually search for new solutions.

Literature therefore suggests that the second approach tends to be more methodical, more practical and less subjective, however if reliable relative preference vectors are available and no requirement of a set of trade-off solutions are needed then the first approach may be considered suitable.

Classical methods are generally classified into Direct Search Methods and Gradient Based Methods. In direct search methods only the objective functions and constraint values are used in a search process. They are usually slow and are known to require a large number of iterations to achieve convergence. Its advantage however is that it is easy to apply for different problems with little modification to the algorithm. Gradient based methods use the first and/or second order derivatives of the objectives and/or constraints to guide the search process and have the advantage of converging with lesser evaluations, and hence much faster and nearer to an optimal solution. They however have been found disadvantageous when used in discontinuous or non-differentiable problems. Classical Methods are therefore very quick and can be used to tackle specific problems, but are known to at times get stuck at local optima (or to a sub optimal solution) and may have problems in discrete search spaces.

Trajectory optimisation cases may contain non linearity, some variables used could contain complex interactions and with a design space that may have numerous undesirable local optima. Classical methods have therefore not been found entirely suitable for application.

In general trajectory optimisations are found to show the following characteristics:

- Non-linearity: model outputs are assumed to be non-linear, non-smooth and non-differentiable (black box approach).
- Real value: all variables are real value (as opposed to binary values)
- Deterministic: all models show deterministic behaviour (i.e. one set of input always leads to the same output)
- Multi-modal problem: the objective space is expected to have many local optima in which optimisers can get stuck
- Constraint: optimisation variables have a specific range and some parameters can be constrained to limit the objective space.
- Optimal control: each stage of the trajectory evolves from the preceding one.
- Multi-objective: multiple objectives can be optimised at the same time.

Thus, some of the key benefits of genetic algorithms over classical methods, as observed in literature, were as follows:

- Robustness: genetic algorithms use probabilistic rules and an initial random population to guide their search in comparison to classical methods (which use fixed transition rules), and hence can recover from early mistakes and enable them to handle a wide class of problems and specifically multi-modal problems.
- Minimal problem information required and hence can be made problem independent with a limited increase in complexity
- Parallel implementations: genetic algorithms can be easily and conveniently used in parallel systems with multiple processors to evaluate solutions in a distributed manner and hence enable reduction of computational time substantially.
- Flexibility in exploration and exploitation of the decision variable space: genetic algorithms allow better control of exploration and exploitation of the decision variable space by varying the parameters involved in genetic operators (mutation and cross-over), unlike classical methods which have fixed transition rules and hence have fixed degrees of exploration and exploitation. This therefore allows the algorithm to recover quickly out of a local optima region, if encountered.

Genetic algorithms however have one main disadvantage of being computationally expensive in comparison to classical methods. This is primarily due to the fact that they use a population of solutions and a large number of evaluations to optimize. This however can be mitigated to large extent using parallel implementation.

2.4.3 EVOLUTIONARY BASED METHOD

The basic idea of using evolutionary concepts in creating a problem solving algorithm was first conceptualised by John Holland and his colleagues of the University of Michigan [49, 50]. It basically uses the principle of 'survival of the fittest and extinction of the weaker species through natural selection'. The salient points of the theory suggest that strong individuals in a population have a greater chance of passing their genes to future generations via reproduction (cross-over) and therefore over a period of time (after many generations) species carrying the correct combination of genes become the dominant population. During the lengthy process of evolution random changes may occur in genes (mutation) thus changing characteristics of an individual chromosome and its future generations. However, if these processes provide an additional benefit/ advantage in terms of survival or fitness, new species evolve or they are duly eliminated through the process of natural selection.

At this point the reader may note that the study undertaken uses a real parameter genetic algorithm and not a binary coded genetic algorithm, the essential difference being the variables are all treated as real numbers and not binary bits. The difference is very significant and hence the reader is referred to literature for more elaborate explanations. [49]

The genetic algorithm however replicates approximately the same basic process in finding solutions. The variables used are termed as genes. A set of genes used at any instance form a chromosome. The set of chromosomes defines the population. The solutions thus calculated using the variables or genes form the raw fitness of each chromosome in the population. The genetic algorithm sorts the chromosomes out based on their fitness and based on a pre-set population count, the algorithm eliminates the least fit individuals. Finally the fit individuals selected form a new generation (see Figure 6).

Amongst the fit individuals (or chromosomes) selected, a further set is randomly selected to form a mating pool and genetic operators are utilised to cross-over (essentially reproduction where two chromosomes are used to create offspring) and mutate (wherein the operator introduces a random 'genetic change') the selected chromosome. The crossed over and mutated offspring are again merged into the population and fitness value of each chromosome is calculated. The process then continues iteratively to form new generations till prefixed criteria, such as maximum fitness possible or maximum generations are reached.

As discussed in the previous section, genetic algorithm being a population based approach, are ideal to solve multi objective optimisation problems as they effectively search the whole feasible objective space or design space. As the algorithm progresses it will try and find a set of non-dominated solutions, that is, each solution dominates another solution in at least one objective. The final non-dominated set will meet the following two conditions:

1. Any two solutions of the non-dominated set must be non-dominated with respect to each other.
2. Any solution not in this set, but in the feasible objective space, must be dominated by at least one member of the non-dominated set

This non-dominated set then forms the Pareto optimal set (Figure 7).

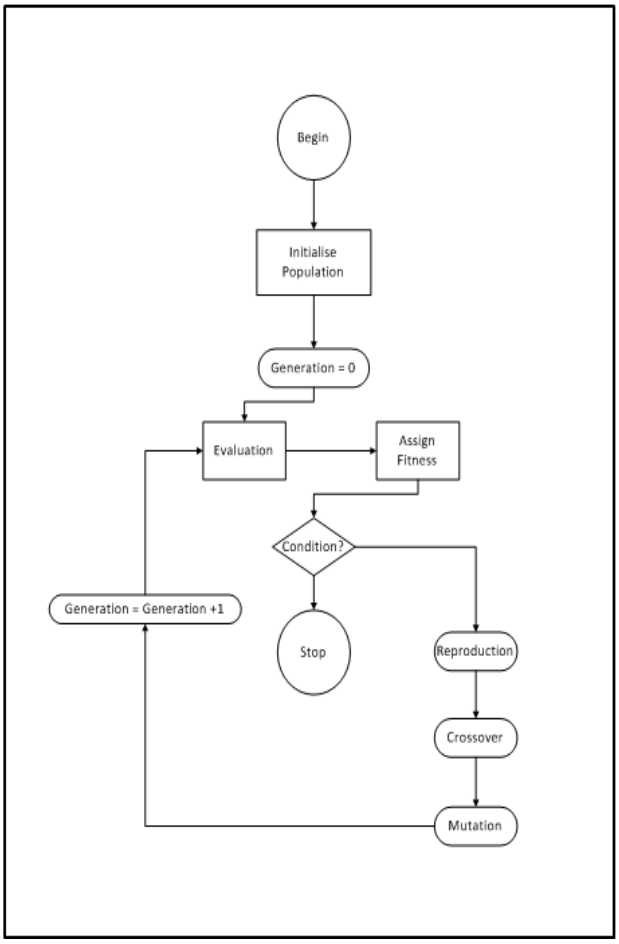

Figure 6 - A schematic describing the working principle of the GA

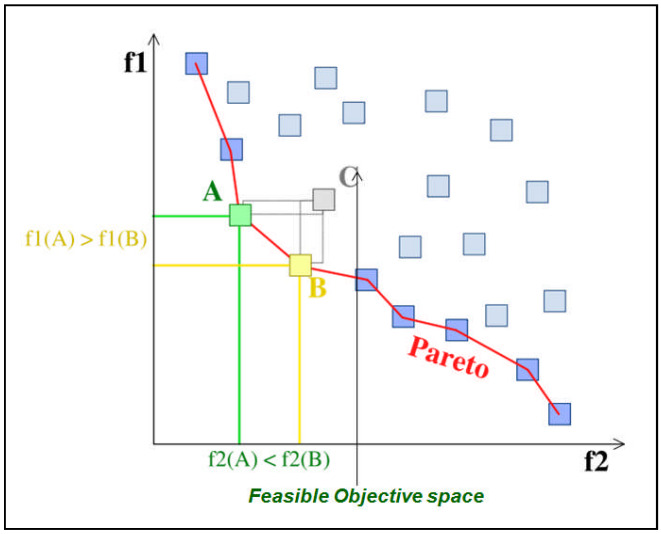

Figure 7 - Pareto optimal (non-dominated) front

2.4.4 OBJECTIVES IN MULTI OBJECTIVE OPTIMISATION

The 'objectives' of multi objective problems may be non-conflicting or conflicting. The result of the former will be that the cardinality of the Pareto optimal set may be one. However if the objectives are conflicting, which they invariably are, then the non-dominated set (or Pareto optimal set) will form a defined Pareto front with a cardinality higher than one. Therefore the main objective of a multi objective optimisation algorithm is to ensure:

a. It finds solutions as close as possible to (or preferably on) the true Pareto optimal front, which will be used as an indicator of its accuracy.
b. It finds solutions as close and as diverse as possible along the true Pareto optimal front, which provide the user with a good range of trade off solutions for its objectives (its diversity).

2.4.5 METRICS TO TEST THE PERFORMANCE OF A MULTI OBJECTIVE GENETIC ALGORITHM

To test the performance of a multi objective genetic algorithm, literature on the subject [51] has suggested two key metrics based on the objectives as discussed in the previous section.

a. γ_c –Convergence (distance) metric : this metric is an indicator of the measure of the extent of convergence an algorithm achieves, to a known set of Pareto-optimal solutions. It is primarily used when testing an algorithm using testing functions (such as ZDT functions) and the set of Pareto-optimal solutions are known.
   To calculate this metric a set of uniformly spaced solutions are selected from the true Pareto-optimal front in the objective function space (as indicated with open circles in *Figure 8*). Then for each solution obtained, with the algorithm being tested (as indicated with dark circles), the minimum Euclidean distance of it from chosen solutions on the

Pareto-optimal front is computed. The average of these distances is used as the convergence metric. The smaller the value of this metric the better the convergence to the Pareto front.

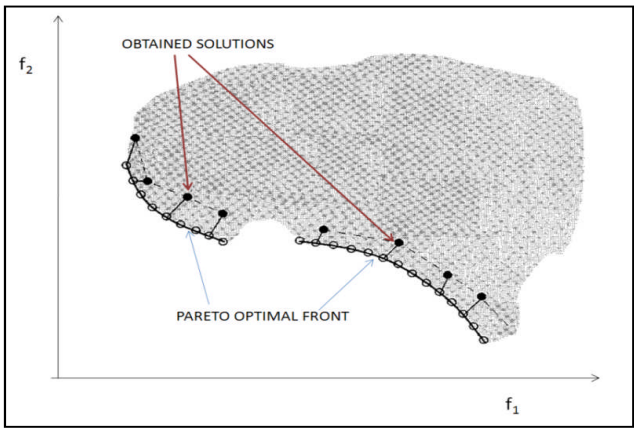

Figure 8 - Methodology to calculate the convergence metric [51]

b. Δ – Diversity metric : this metric measures the extent of spread achieved among the obtained solutions and is indicative of the extent to which a set of solutions spans the entire Pareto-optimal front (see Figure 9).
   This metric is calculated using the Euclidean distance between consecutive solutions in the obtained non-dominated set of solutions. Non-uniformity in the distribution is calculated by Eq 2.38:

$$\Delta = \frac{d_f + d_l + \sum_{i=1}^{N-1} |d_i - \bar{d}|}{d_f + d_l + (N-1)\bar{d}} \qquad [2.38]$$

Where,
d_f and d_l = Euclidian distance between the extreme solution and boundary solutions of the obtained non dominated set
= Average of all distances d_i (i= 1, 2..., n-1)
N = Number of solutions in the non-dominated front
For most widely and uniformly spread-out set of non-dominated solutions the numerator of Δ would be ideally zero and hence the value of the metric as close to zero is always considered to be the optimal performance.

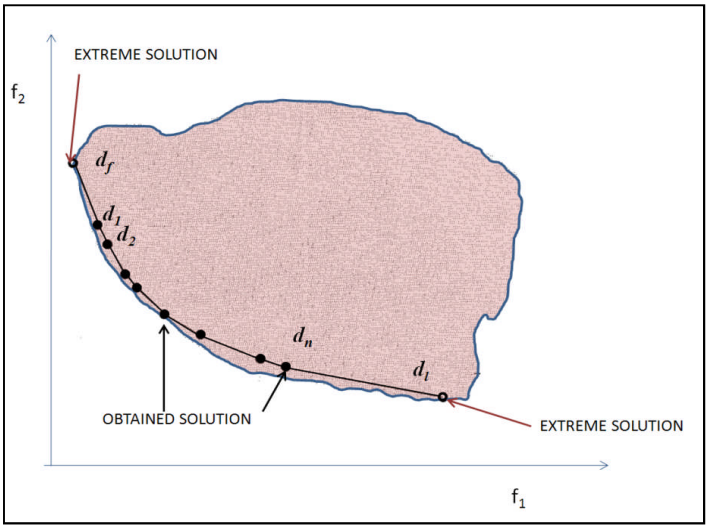

Figure 9 - Methodology to calculate the diversity metric [51]

2.5 PAST OPTIMISATION STUDIES

A number of authors published in the field of aircraft and engine optimisation. Antoine et al [52, 53], used optimisation tools to generate Pareto front applied to the design of optimised aircraft geometry. Optimisation objectives were minimum fuel consumed, minimum flight cost, minimum NO_x emitted for the LTO cycle and minimum noise generated. These optimisations were based on a twin-engine long range aircraft (6000nm trajectory). The main parameters used in their work related to aircraft geometry but also engine parameter and performance. The authors used a simple correlation based methods (similar to a P3T3 method) for the estimation of NO_x EI. Some constraints were also included to ensure the generation of realistic solutions. In term of trajectory optimisation, it was limited to only the initial and final cruise altitude and the cruise speed. Climb parameters were not varied. The main conclusions were that reduction of aircraft noise, NO_x emissions, and cost are possible by allowing trade off against fuel consumption.

Another study from Le Disloquer [54] focuses on aircraft emissions such as NO_x, CO_2 and H_2O. The main purpose of the study was to analyse simulations of aircraft trajectory and evaluate the influence of net thrust and SFC in different turbofan designs. Three models were included in the simulations, the aircraft model, the engine performance model and the emissions model. Specifically, the author was considering engine designed for low LTO cycle NO_x and overall low NO_x emissions.

Bower [55] has developed a method to design one or more aircraft so that demand is satisfied based on a pre-defined network of airports. The objective is to design the fleet of aircraft that will minimise direct operating cost, CO_2 emissions or NO_x emissions. Aircraft optimisation is performed using the NSGA II multi-objective optimiser. Pareto front of

aircraft design were generated for a network of 4 cities linked together with 8 segments. It was concluded that operating cost and NO_x are strongly dependent with little to no trade off available. It also showed that all generated aircraft design benefited from a higher by-pass ratio and thicker, higher aspect ratio wings compared to current single aisle aircraft design.

Celis [56] published a preliminary study on aircraft trajectory optimisation using a genetic algorithm. The aim of the work was to establish preliminary requirement for the effective optimisation of multivariable problem applied to trajectory. The study focused on using the GA technique on the climb phase using only 4 segments to describe it. The conclusion was that GA is a suitable tool to perform optimisation and that scaling to more complex problem would not be a major issue.

Pervier [57] published a study in continuity of Celis [56] work into proving scalability of the GA technique applied to trajectory optimisation. In this study, the objective was to assess the performance of an improved GA technique. The main improvement in term of GA capability was the introduction of multi-objective optimisation i.e. the production of Pareto fronts. It was firstly tested against mathematical test function and proved to be very efficient at finding optimum Pareto sets even when constraints were added to the problem. The second phase was designed to test the GA optimiser with an aircraft, engine and emission model to optimise trajectories and generate Pareto fronts for fuel/time and fuel NO_x objectives. As opposed to Celis [56] work, optimisation included the full trajectory (climb, cruise and descent) and was using a larger number of segments to describe it (typically 80 segments). However the NO_x estimation was derived from a simple P3T3 model. The study concluded on the satisfactory performance and good scalability of the multi-objective GA optimiser.

Based on the work found in public literature the following has been identified as the contribution to knowledge from the work undertaken in this thesis:

- Utilisation of a multi-objectives genetic algorithm optimiser to optimise aircraft trajectories. The novelty is that trajectories are defined by trajectory and engine design parameters. Optimisation objectives are to find the minimum fuel, time, NO_x and length of persistent contrails using high fidelity models.
- A hypothetical LPP combustor was specifically developed and used in aircraft trajectory optimisation to assess environmental benefits in term of NO_x emissions.

Chapter 3 Selection and testing of optimiser

The purpose of this chapter is to ensure that the optimisation technique used for the trajectory optimisation of chapter 5 will be performing sufficiently well so that 2-objectives Pareto front can be generated within an acceptable time frame. Several genetic algorithm techniques have been tested for their performance in term of ability to converge under a certain number of evaluations and diversity (spread of solutions) in the Pareto front generated.

3.1 NON DOMINATED SORTING GENETIC ALGORITHM II (NSGA II)

The optimiser for GATAC [58] is currently based on the concept of "Non-dominated Sorting Genetic Algorithm" (NSGAII) created by Deb [51]. It is considered 'the state of the art' genetic algorithm for multi objective optimisation as it has been designed for lower computational complexity of non-dominated sorting and has introduced elitism, by which apart from improving its ability to retain good solutions, once found it also speeds up the performance of genetic algorithms.
The basic sequence of the algorithm is as follows (see Figure 10):

I. The algorithm begins with an initial population of N individuals and multiplies it with an initialisation ratio for the 1st generation
II. This population is sorted based on the principle of constraint non-dominated sort to form the initial generation P_t [51]
III. If after sorting, individuals exceeds N , then N individuals are selected based on crowding distance from the final front
IV. Using constrained crowded tournament selection, a mating pool is created from P_t
V. The genetic operators (mutation and crossover) are then used to form offspring population Q_t
VI. On the merged set R_t ($=Q_t + P_t$) steps II-III are performed to form the next generation.

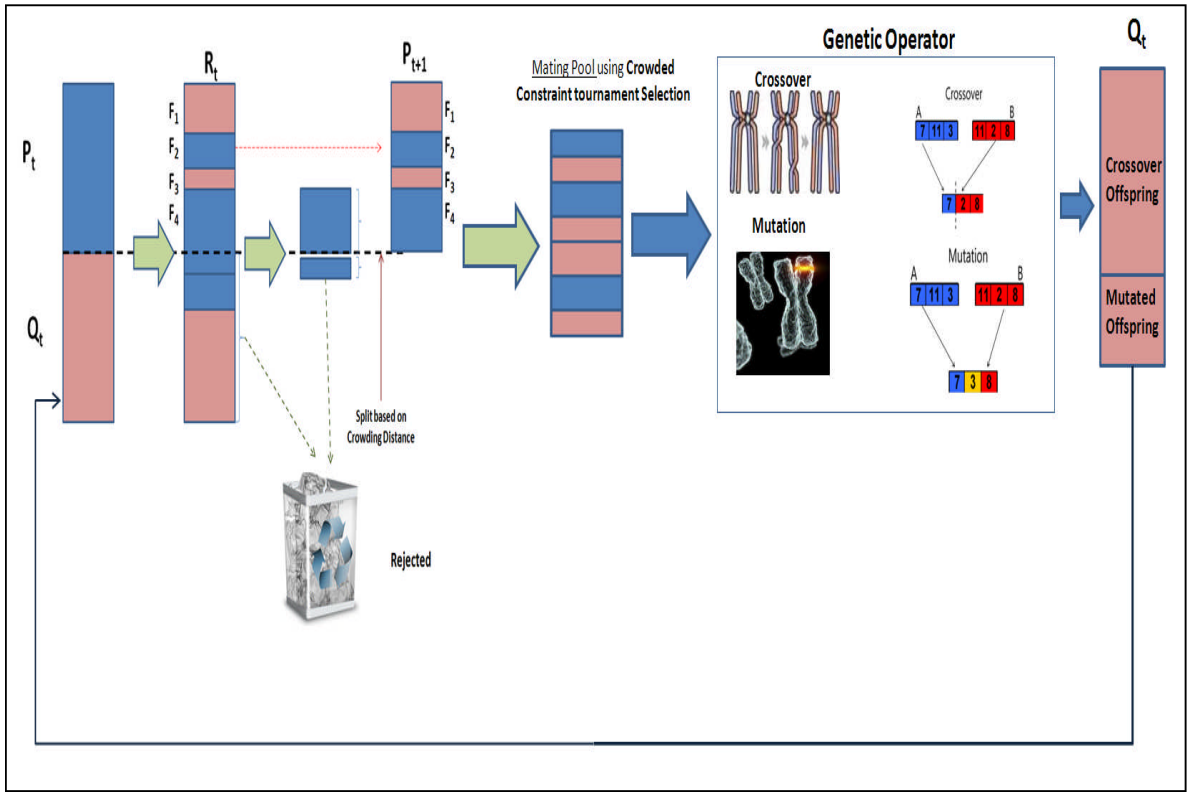

Figure 10 - NSGAII Basic principle

3.2 STRENGTH PARETO EVOLUTIONARY ALGORITHM II (SPEA II)

This is another type of algorithm based on evolutionary techniques. It basically uses an initial population and an archive (or an external set). A brief description of the algorithm is as follows, however for a more detailed description of the fitness assignment and environmental selection procedure, the reader is referred to the reference [59]:

I. The initial population P_t consists of N individuals with an empty archive P_t' of size N' individuals.
II. The population is merged (P_t +P_t') and then qualified using fitness assignment (based on strength and density information in addition to non-dominated front sorting)
III. Environmental selection. In this process all non-dominated solutions are copied into an archive P_{t+1}'. This results in the following two possible cases:
    a. If number of non-dominated elements are less than archive size N' - The remaining slots are then filled with dominated elements using crowded distance information.
    b. If number of dominated elements is larger than the number in the archive, then individuals are removed using truncation operator.
IV. The mating pool is then created using constrained crowded tournament operator,

V. The mating pool is shuffled and genetic operators (crossover and mutation) are used on the chromosomes to form the new generation.

3.3 ADAPTATION OF NSGAII FOR THE GATAC OPTIMISER- NSGA MO2

For the GATAC [0000] framework the optimiser that was built was essentially based on the NSGAII using the Object Oriented Language JAVA. The algorithm was initially developed at Cranfield University by Rogero [60] and was subsequently modified at Airbus France. The new algorithm was then tested and benchmarked at Cranfield University. The algorithm termed as NSGA MO2, essentially used the same basic process of non-dominated sorting as in NSGAII but differed in two respects:

a. It used a different selection processes to form the mating pool
b. It used an entirely different sequence of genetic operators (Dynamic Vector Mutate method for mutation and double crossover methods for Cross-over/ reproduction - Tri Linear Crossover and SBX crossover)

A brief description of the algorithm is as follows:

I. The algorithm begins with an initial population of N individuals and multiplies it with an initialisation ratio for the 1st Generation
II. This population is sorted based on constraint non-dominated sort to form the initial generation P_t
III. If after sorting individuals exceeds N , then N individuals are selected based on crowding distance from the final front
    a. The offspring population Q_t formed from P_T
    b. Using Stochastic Universal Sampling Selection individuals are selected for crossover. Using random selection individuals are selected for mutation
IV. On R_t (= Q_t + P_t) perform steps II-II to form the next generation.

3.4 FURTHER MODIFICATIONS OF NSGA MO2: NSGA MO3

After Benchmarking and testing against other available algorithms, minor modifications were made to MO2 to form MO3. These included alternative selection methods and genetic operators. The basic framework being the same, the mating pool was created using a Random Selection Process for both Genetic operators. The Genetic Operators used were Polynomial Mutation and SBX Crossover [60]. The modifications improved the performance to a certain extent as is evident in the benchmarking and testing results discussed in the next section.

3.5 BENCHMARKING AND TESTING OF MULTI OBJECTIVE ALGORITHM

During the Initial phase of the benchmarking, the optimiser used the genetic algorithm NSGA MO2 to first perform single objective optimisations. Therefore the benchmarking was initially done to compare the performance of the optimiser against commercially available optimiser in MATLAB [61]. The tests were conducted using standard mathematical test functions (for e.g. Hedgehog function and Ackley function). The performance criteria examined, included number of evaluations required for convergence, time required for evaluations and the criteria on which convergence was reached (for e.g. Maximum Fitness or stall). The results recorded after testing indicated that the NSGA MO2 had a superior performance in comparison to the MATLAB optimiser.

The next phase of the benchmarking involved the use of NSGA MO2 for multi-objective optimisation, and hence the benchmarking and testing was undertaken against the NSGA II, SPEA II and NSGA MO3 (as discussed earlier, an improved version of NSGA MO2) algorithms. It may be noted at this point that all algorithms were tested using the same parameter settings for all three phases of testing.

To validate the performance of the optimiser algorithms two phases of systematic benchmarking and testing activities were undertaken. The phases were as follows:

Phase 1: Performance testing using ZDT Functions

- Evaluations to reach the Pareto optimal front
- Convergence metric
- Diversity metric

Phase 2: Constraint handling performance

3.5.1 PHASE 1: PERFORMANCE TESTING USING ZDT TEST PROBLEMS

These test problems were conceptualized by Zitzler et al. to gauge the performance of a multi-objective optimiser algorithm for the following criteria [49]:

- Minimum number of evaluations required by the algorithm to converge to the Pareto optimal front
- Ability of the algorithm to handle complexities lateral to the Pareto Optimal Front and hence converge as close as possible to it. The convergence metric, as described earlier, is used to assess this ability.
- Ability of the algorithm to handle complexities along the Pareto optimal front and hence produce a diverse set of trade off solutions. The diversity metric, as described earlier, is used to assess this ability.
- Ability to handle different shapes of Pareto optimal front (convex, non-convex and/or discontinuous)

The functions used are as follows [49].

The rational for selecting the ZDT functions for testing the different optimisers were justified by the similitude expected with the trajectory optimisation characteristics. Similarities are the following:

- Large number of variables (trajectory optimisation will require between 20 and 30 variables)
- Multi modal test functions (Trajectory objective space is expected to feature multi-modality)
- Multi objective test functions
- Real value variables

3.5.1.1 ZDT1

This problem tests the ability of the multi-objective GA to tackle a large number of variables (30) and a convex Pareto-optimal set. All Variables of the function lie in the range [0, 1]. The optimal solutions are $x_1 \in [0, 1]$, $x_i = 0$ where i= 2,...,n. The objective functions are as follows:

$$f_1(x) = x_1 \quad [3.1]$$

$$f_2(x) = g(x)\left[1 - \sqrt{x_1/g(x)}\right] \quad [3.2]$$

$$g(x) = 1 + \frac{9(\sum_{i=2}^{n} x_i)}{(n-1)} \quad [3.3]$$

3.5.1.2 ZDT3

This problem is considered to be of a higher level of complexity. It tests the ability of the multi-objective GA to tackle a large number of variables (30) and a number of convex and disconnected Pareto optimal fronts. All variables of the function lie in the range [0, 1]. The optimal solutions are $x_1 \in [0, 1]$, $x_i = 0$ where i= 2,...,n. The objective functions are as follows:

$$f_1(x) = x_1 \quad [3.4]$$

$$f_2(x) = g(x)\left[1 - \sqrt{x_1/g(x)} - \frac{x_1}{g(x)}\sin(10\pi x_1)\right] \quad [3.5]$$

$$g(x) = 1 + \frac{9(\sum_{i=2}^{n} x_i)}{(n-1)} \quad [3.6]$$

3.5.1.3 ZDT6

This is considered a very complex problem as it tests the ability of the multi-objective GA to reach a non-convex Pareto optimal front. The additional complexity that the GA will encounter is that the density across and towards the Pareto optimal region is considered to be non-uniform and thin respectively. Most Genetic Algorithms are known to face problems converging towards the Pareto optimal front with this function. This problem uses 10 variables with variable bounds in the range [0, 1]. The optimal solutions are $x_1 \in [0, 1]$, $x_i = 0$ where i= 2,...,n. The objective functions are as follows:

$$f_1(x) = 1 - \exp(-4x_1)\sin^6(6\pi x_1) \quad [3.7]$$

$$f_2(x) = g(x)[1 - (f_1(x)/g(x))^2] \quad [3.8]$$

$$g(x) = 1 + 9\left[\frac{(\sum_{i=2}^{n} x_i)}{(n-1)}\right]^{0.25} \quad [3.9]$$

3.5.1.4 Discussion of Results

The tests were conducted using ZDT functions as discussed. The algorithms were tested against the three criteria - number of evaluations required by the algorithm to reach the Pareto optimal front, convergence and diversity characteristics. The progress of each algorithm was evaluated after 4600, 13000 and 22000 evaluations

a. Evaluations required to reach the Pareto optimal front: The progress of each algorithm are graphically represented in Figure 11 to Figure 13**.** It may be observed that ZDT1 and ZDT3 being relatively less complex functions enabled most algorithms to reach the Pareto optimal front within 13000 evaluations. However by 22000 evaluations all the algorithms had converged on the Pareto optimal front. For the ZDT6 functions, being more complex due to the non-convex front, it is observed that all algorithms were unable to reach the actual Pareto front and only achieved near optimal set of solutions.

b. Convergence towards the Pareto optimal front: The convergence metric calculated for each algorithm after the prefixed set of evaluations are as graphically represented in Figure 14**.** The algorithms displayed similar performance trends as discussed earlier. ZDT1 and ZDT3 indicated good convergence overall with all algorithms, except NSGA MO2, reaching near complete convergence by 13000 evaluations.

c. Diversity along the Pareto optimal front: The diversity metric calculated for each algorithm after the prefixed set of evaluations are as graphically represented in Figure 15**.** It may be observed that a good and close to the final diversity in solutions is reached by all algorithms within 13000 evaluations for ZDT1 and ZDT3 functions. However ZDT6 needed significantly larger number of evaluations to reach an improved diversity and that again may be attributed to the complexity of the test function.

d. In conclusion of discussion for this phase the following were the key observations

- A lower number of evaluations are required for NSGA MO3 and SPEA2
- For the complexity of ZDT6 even though the algorithms did not converge onto the true Pareto front, a set of 'near optimal' solutions were found, however the diversity achieved was very good.
- The diversity and convergence is comparable for all algorithms after Pareto optimal front is reached
- SPEA2 provides overall better diversity but was found to be computationally more expensive. This is attributable to its fine grained fitness assignment strategy which incorporates density information and the selection procedure (Environmental Selection)
- It must also be noted that all algorithms have been used with the same basic setting (i.e. genetic operator ratios, mutation and cross-over methods, population sizes etc.). The algorithms may improve in performance if optimal settings for each individual algorithm are identified for a particular case and incorporated. This however may be achieved either through extensive trial and error methods of testing or application of another genetic algorithm (or alternate control methodology) to actually monitor the settings and based on the performance, change the settings as the optimisation progresses.

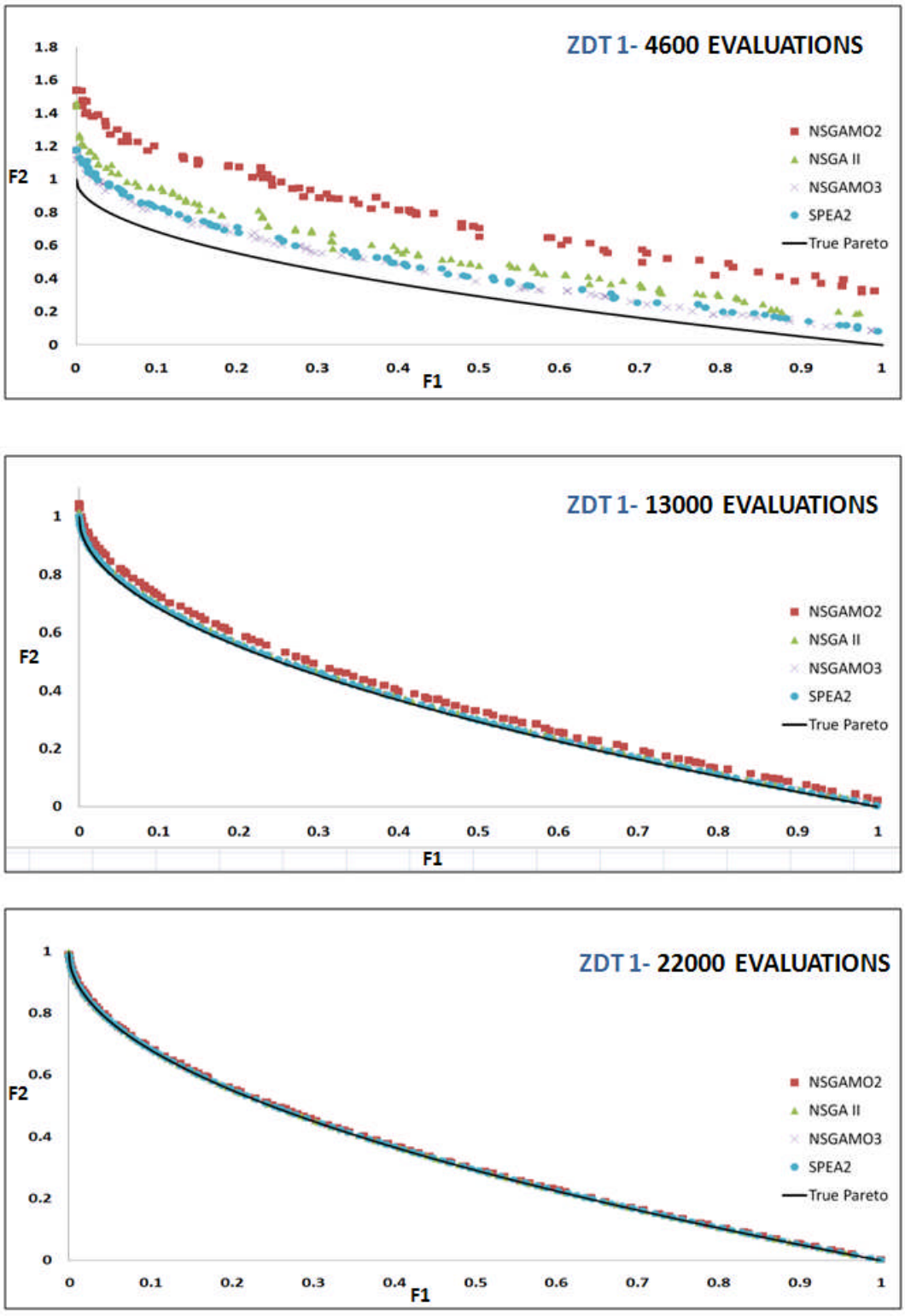

Figure 11 - Progress of Algorithms towards Pareto-Optimal Front- ZDT1

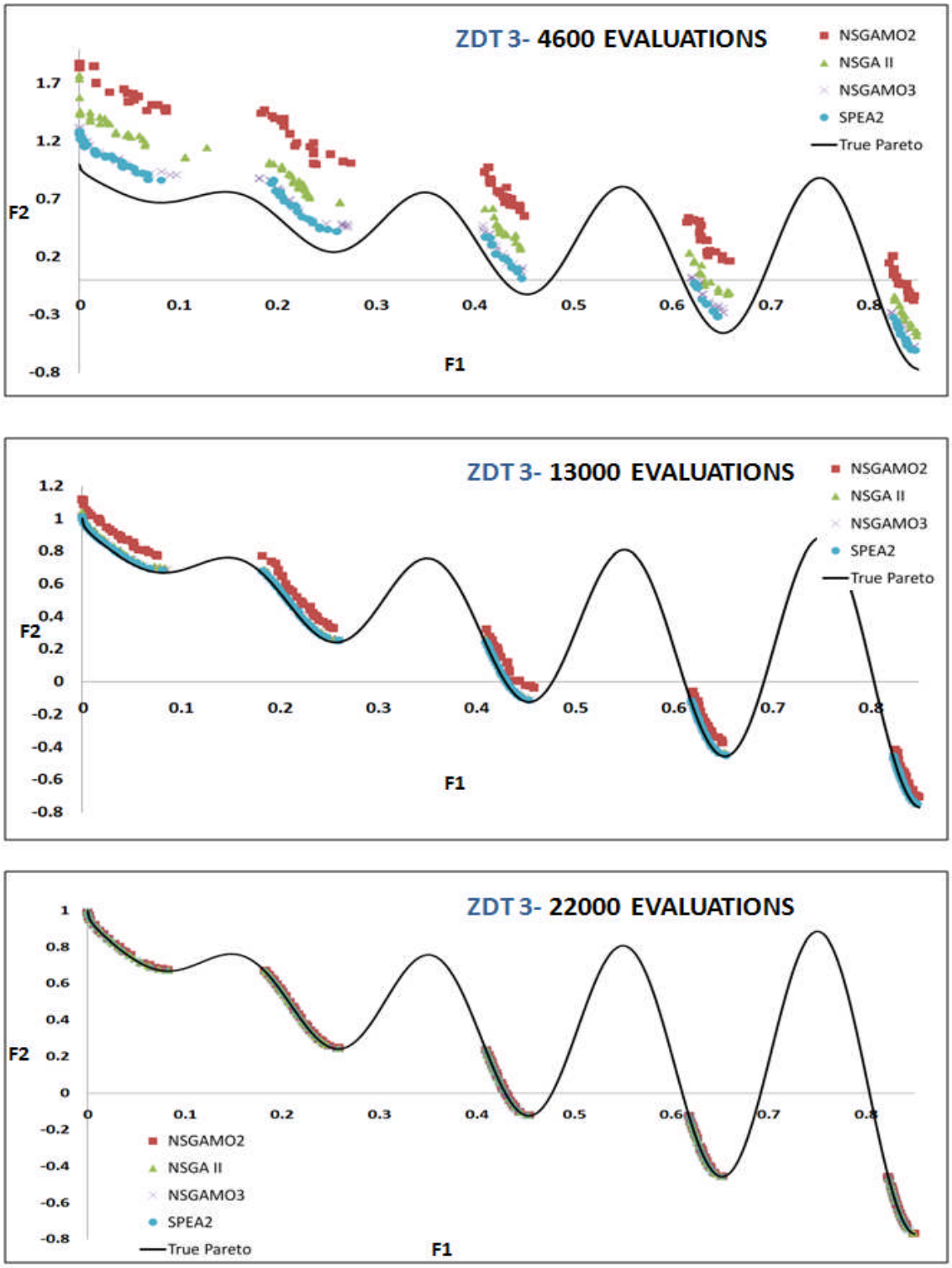

Figure 12 - Progress of Algorithms towards Pareto-Optimal Front- ZDT3

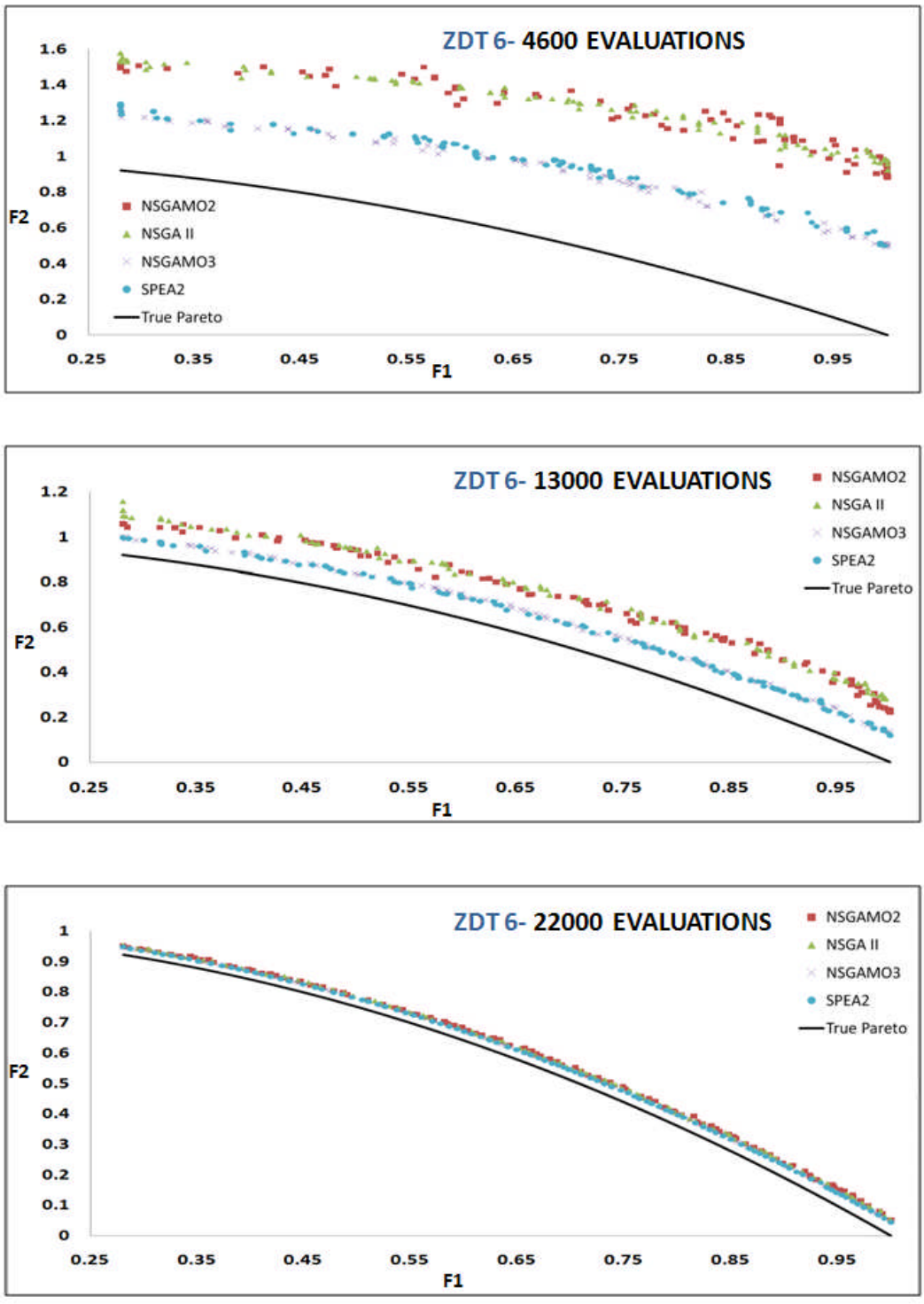

Figure 13 - Progress of Algorithms towards Pareto-Optimal Front- ZDT6

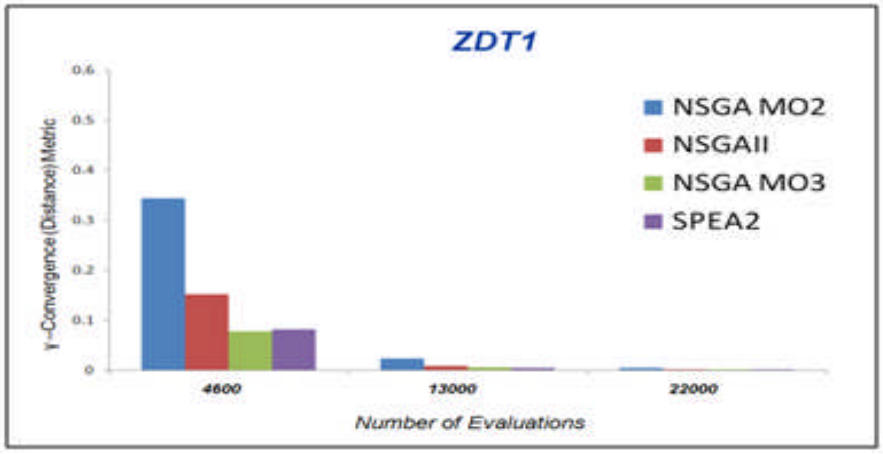

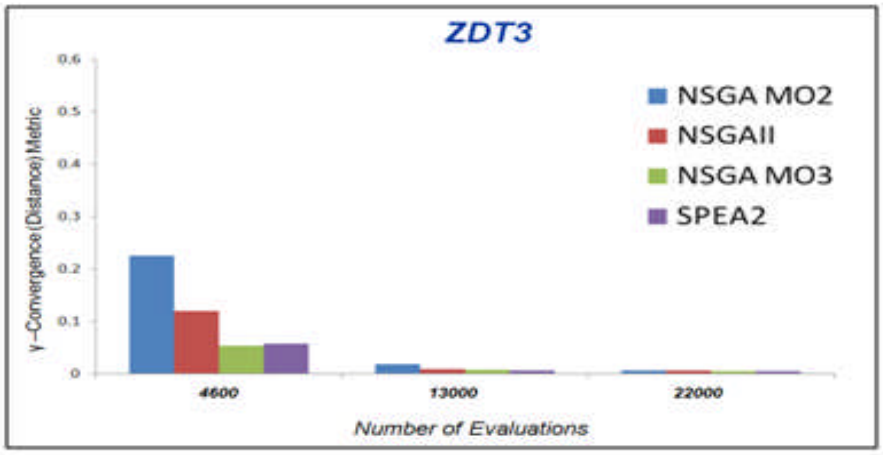

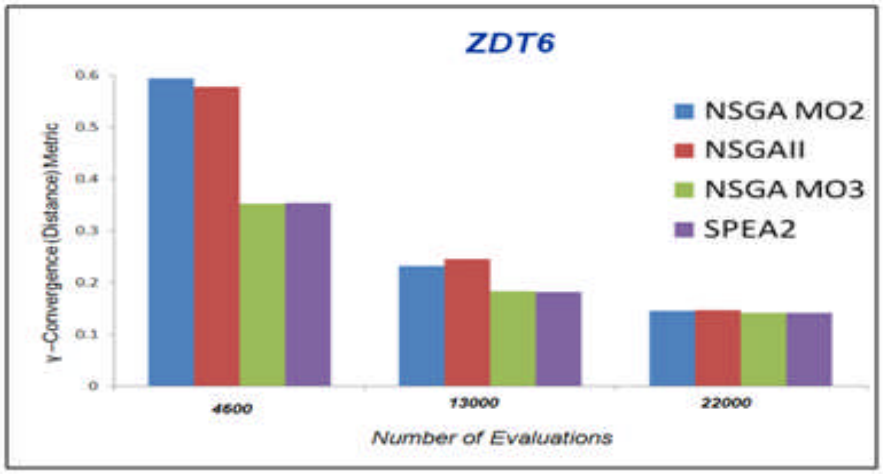

Figure 14 - Convergence metric results- ZDT1, ZDT3 & ZDT6

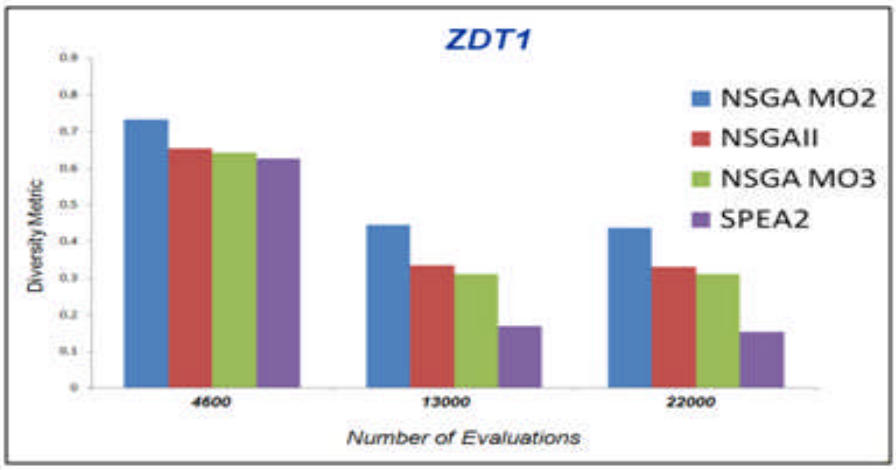

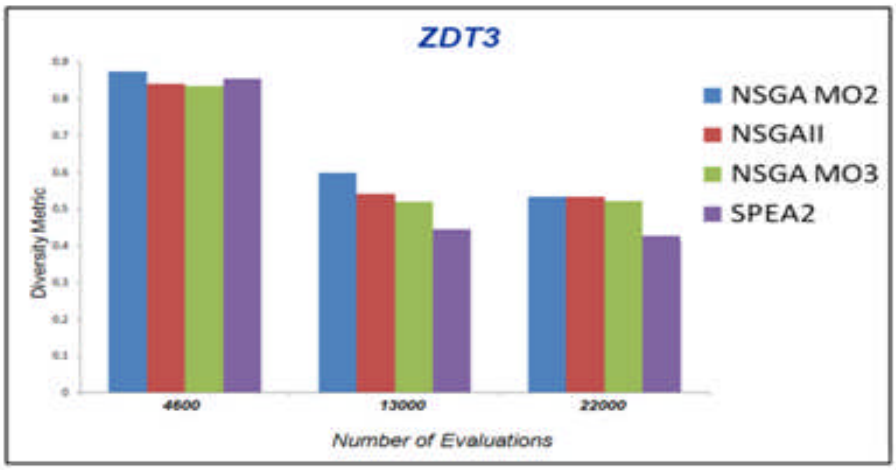

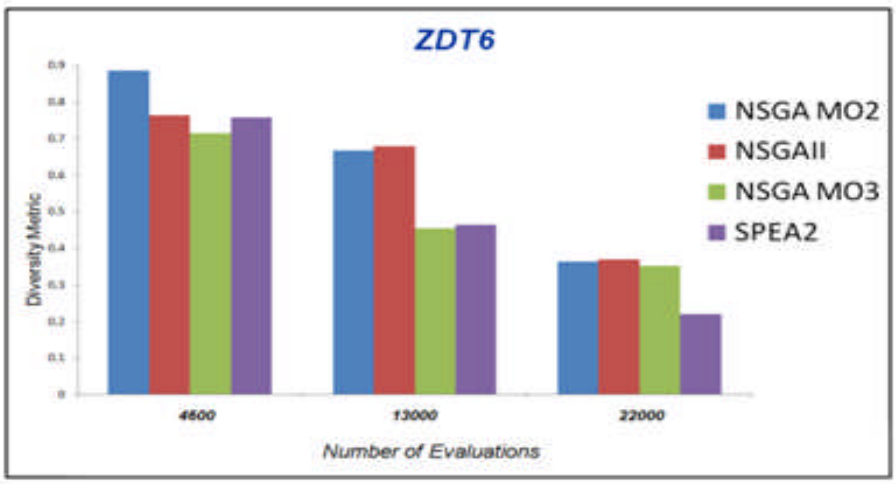

Figure 15 - Diversity metric results- ZDT1, ZDT3 & ZDT6

3.5.2 PHASE 2: PERFORMANCE TESTING FOR CONSTRAINT HANDLING

These test problems were suggested by the authors of NSGAII to gauge the constraint handling performance of a multi-objective optimisation algorithm. The functions used are as follows [51]. The reason for choosing these functions is that their objectives are easy to optimise (two objectives with only two variables). This ensure that the test only focus on handling correctly the set of constraints given to the optimiser.

3.5.2.1 CONSTR problem

This problem tests the ability of the multi-objective GA to reach the Pareto optimal front when a part of the unconstrained Pareto optimal region is not feasible. A graphical representation of the problem is as shown in Figure 16. This is a two-variable problem. The variables are $x_1 \in [0.1, 1.0]$ and $x_2 \in [0, 5]$. The objective functions and constraints are as follows:

$$f_1(x) = x_1 \tag{3.10}$$

$$f_2(x) = (1+x_2)/ x_1 \tag{3.11}$$

$$g_1(x) = x_2 + 9x_1 \geq 6 \tag{3.12}$$

$$g_2(x) = -x_2 + 9x_1 \geq 1 \tag{3.13}$$

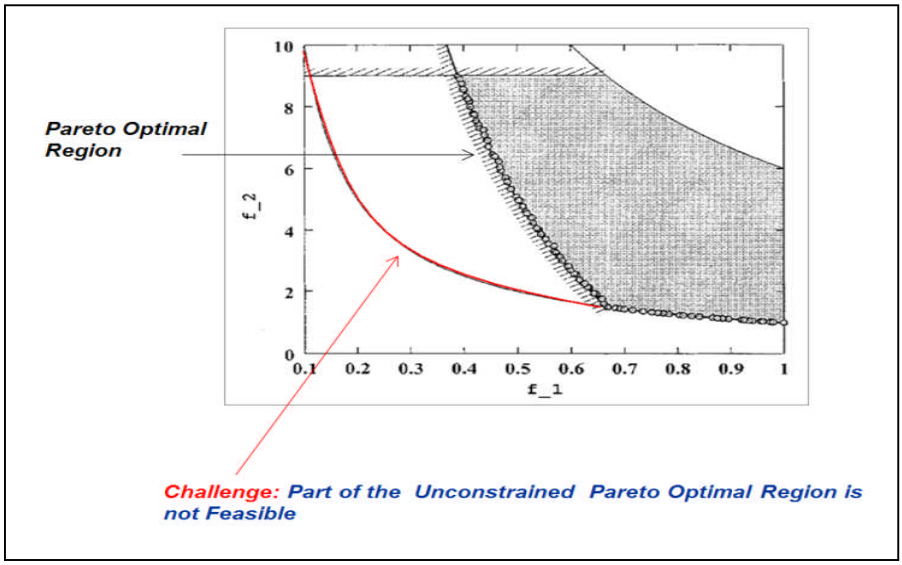

Figure 16 - Schematic of CONSTR function indicating constraint altered Pareto optimal front [51]

3.5.2.2 TNK problem

This problem suggested by Tanaka [62] is aimed at testing the ability of the multi-objective GA to reach the Pareto optimal front that is discontinuous and on application of constraints the constrained Pareto optimal region falls entirely on the first constraint boundary. A graphical representation of the problem is as shown in Figure 17. This is a two variable problem. All variables of the function lie in the range [0, π]. The objective and constraint functions are as follows:

$$f_1(x) = x_1 \tag{4.15}$$

$$f_2(x) = x_2 \tag{4.16}$$

$$g_1(x) = -x_1^2 - x_2^2 + 1 + 0.1 \cos(16 \arctan(x_1/x_2)) \leq 0 \tag{4.17}$$

$$g_2(x) = (x_1-0.5)^2 + (x_2-0.5)^2 \leq 0.5 \tag{4.18}$$

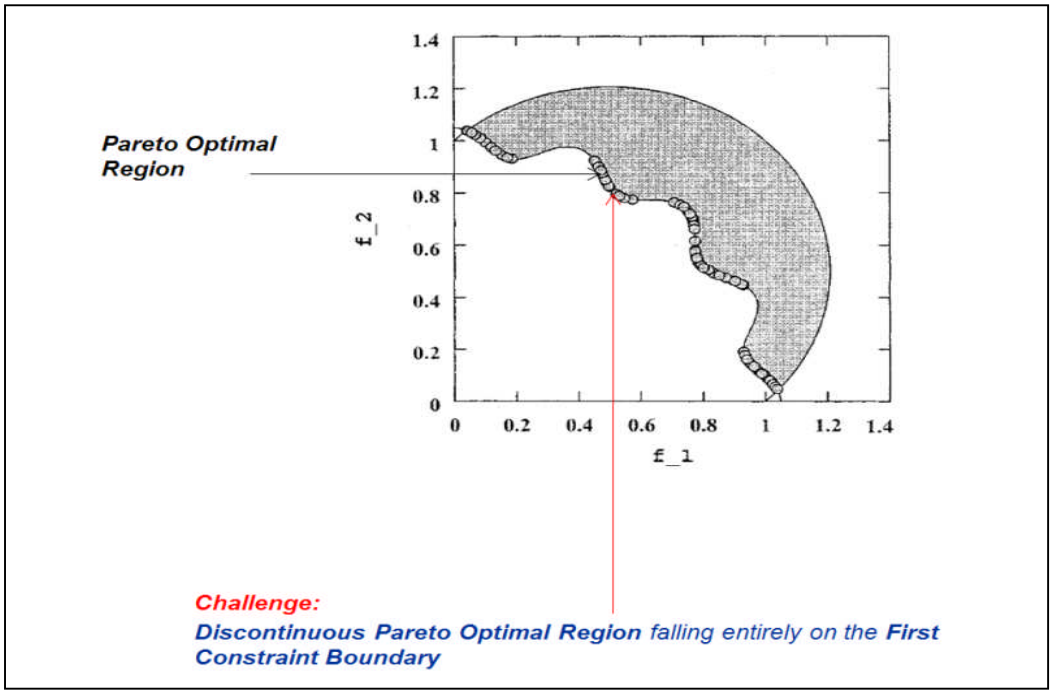

Figure 17 - Schematic of TNK function indicating constraint altered Pareto optimal front [51]

3.5.2.3 Discussion of Results

The tests were conducted using CONSTR and TNK functions as discussed. The algorithms were tested for their ability to reach the Pareto optimal front with the application of constraints. All the optimisers were used with same settings as before. Figure 18 and Figure 19 indicate plots of the converged runs for all optimisers. All algorithms successfully reached the Pareto optimal front within 10000 evaluations and hence displayed good constraint handling ability.

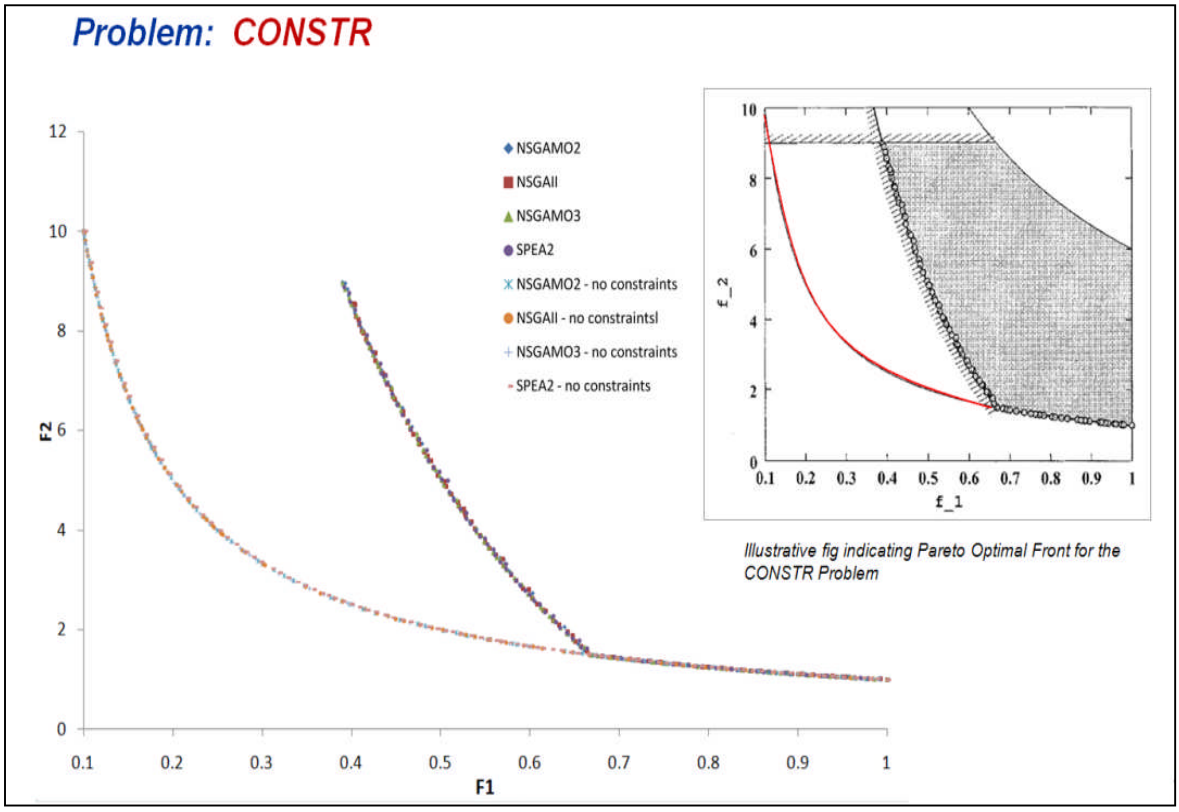

Figure 18 - Pareto Optimal Front formed by Algorithms for CONSTR Function

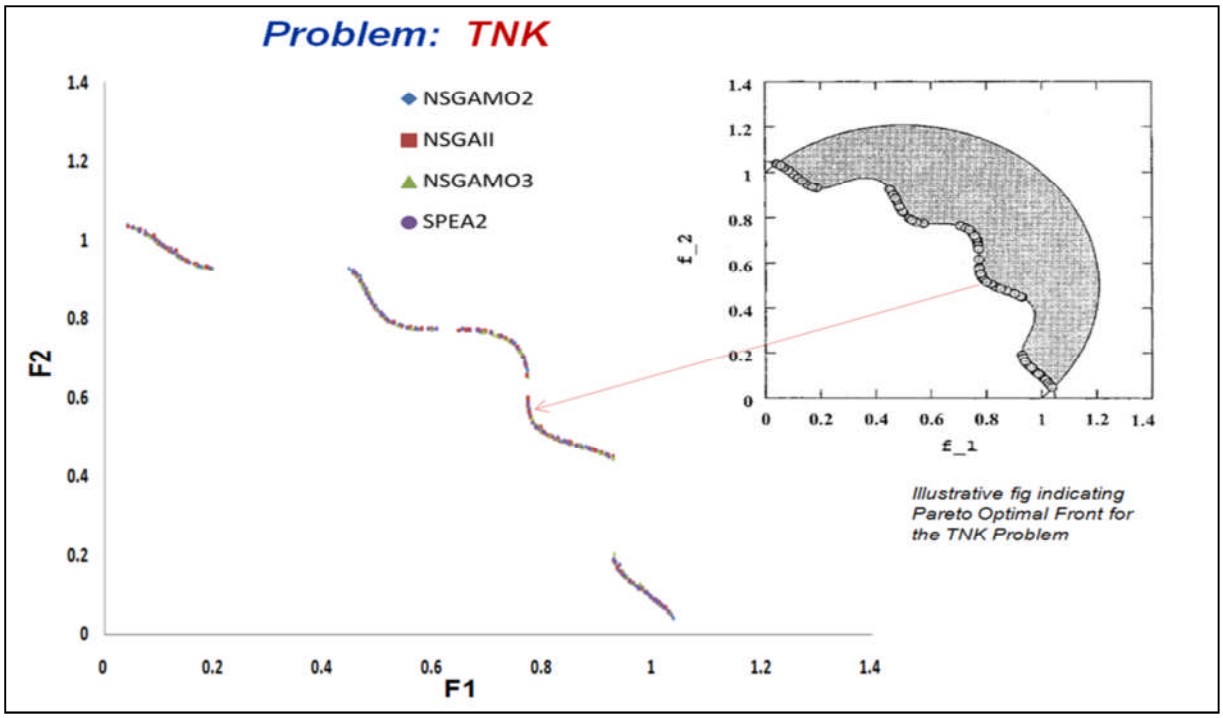

Figure 19 - Pareto Optimal Front formed by Algorithms for TNK Function

3.6 CONCLUSIONS

The benchmarking exercise has shown that all genetic algorithm tested were performing very well for all the test functions used with a small performance advantage for the SPEA2 technique. It also shown that all the optimiser tested with the constraint handling test functions were performing very well. Thus it was concluded that for the purpose of the optimisation to perform in the frame of chapter 5, any optimisation technique could be used. Even though SPEA2 was performing slightly better than the other methods, some technical issues were identified (mainly due to coding implementation) that would block the optimisation process for no apparent reason. With such reliability issues and the optimisation times expected from the use of the model integrated to the case studies of chapter 5, it was decided that NSGA MO2 would be the best suited algorithm for the rest of the study.

Chapter 4: Development of Emissions models

Chapter 4 details the emissions models to be used in chapter 5 optimisation studies. This chapter firstly focuses on the improvement made of an existing reactor based NO_x emissions model. The outcome is a comparison for different engine model on the level of NO_x emitted. The improved reactor based model indicates good agreement. The next part of the chapter describes the modelling of a hypothetical LPP combustor that could potentially fit future generation of aircraft. The combustor is modelled after a currently existing LPP combustor developed by Rizk and Mongia [6]. Finally to assess the length of persistent contrails generated by aircraft flying at cruise level, a contrails model has been developed and validated. The details are given in chapter 4.

The improved conventional combustor model was also briefly tested for a stationary gas turbine combustor in order to test the validity of the model when used with natural gas fuel.

4.1 MODEL IMPROVEMENT FOR CONVENTIONAL COMBUSTOR

4.1.1 INTRODUCTION

The original model developed by Celis [21] largely underestimated the production of NO_x at all power setting and especially at low power setting. This comparison was made based on the result of the CF6-80E1A3 engine model example. Even though other pollutants like CO, UHC and soot were fairly well predicted, in the context of trajectory and engine cycle optimisation, the better prediction of NO_x emissions is of greater interest. For this reason, improvements of the reactor based model for NO_x emissions prediction is desirable. In addition, as the model is going to be used within a framework for optimisation purpose, a lower computational time is also desirable.

The initial reactor layout modelling conventional combustors is shown on the top part of Figure 20. The modified reactor layout is shown at the bottom of the figure. The number of reactor has been reduced to focus on the NO_x prediction only. To predict NO_x emissions, the most important zones are the flame front and the primary zone where temperature is high enough to produce significant amount of NO_x. Reducing the number of reactor also significantly reduce the computational time. A clear difference between the two models lies in the amount of fuel that is entering in the different reactors. In the original model, it is assumed that 100% of the total fuel flow is entering in each combustor areas. In other words, all the fuel is entering the flame front zone (split between core and near wall region), then all the fuel is entering again the primary zone. It is the same for intermediary and

dilution zone. This way of distributing the fuel amongst the reactors is relatively inaccurate as it assumes air and fuel reaction to take place many times whereas the actual fuel and air reaction should only take place in the flame front mainly and to a lesser extent in the primary zone (depending on the engine power setting).

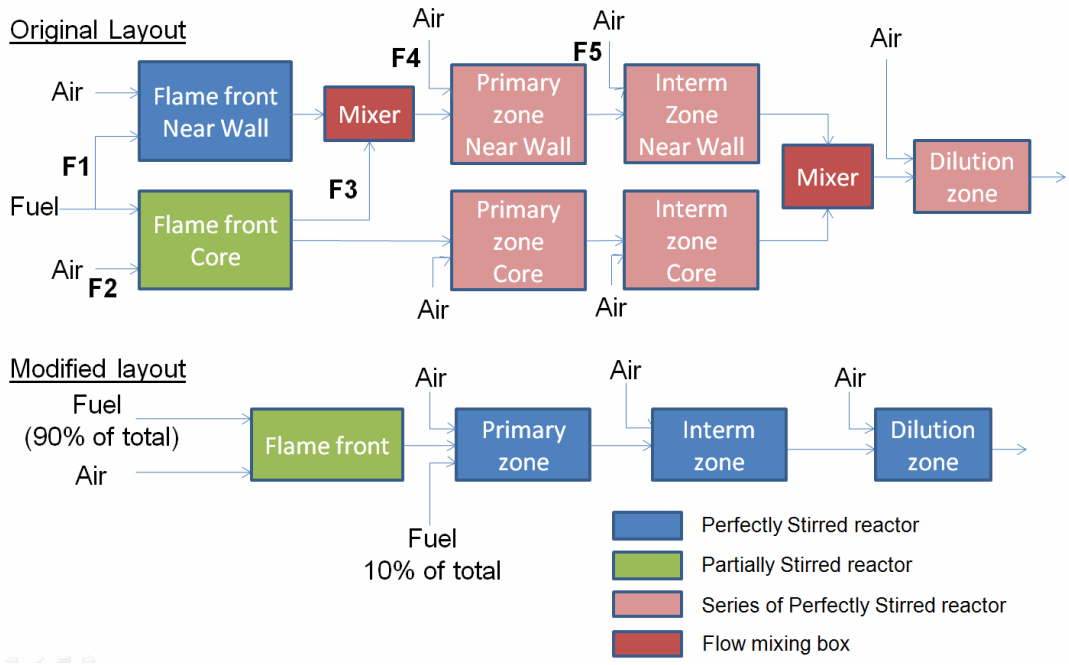

Figure 20 - Reactor layout for the original and the modified emissions model. Original layout comes from [21]

The modifications brought to the model comprise a reduction of the number of reactor by using perfectly stirred reactor models instead of series of perfectly stirred reactors to reduce calculation time. Modifications were made in the flame front partially stirred reactor to improve the computational speed. Especially the original model needed to call a Matlab program to calculate the clipped Gaussian elements. Modifications were made so that the calculation is entirely done using FORTRAN code. In the original program, the CEA program was called externally thus necessitating the use of input and output text files for each equilibrium calculation. To save computational time, the CEA program has been fully integrated within the emissions code so that arguments can quickly be sent and retrieved when calling the CEA program. Overall the original program needed about 20 seconds to calculate an emissions point while with the modifications the program has an average calculation time of one second per emissions point.

4.1.2 RESULTS

Figure 21 shows the outcome of the modifications undertaken. Four aero-engines have been modelled using Turbomatch, based on CF6-80E1A3, CFM56-7B27, Trent 982 and Trent 895. All engines were modelled using public domain information and educated guesses where necessary. The first engine is the one used by Celis [21] to validate his model; as such it was reused to compare it with the improved emissions model. The other three engines were selected to test the new model for different engine power ranges. CFM56-7B27 is for the low to medium power range and the Trent engines are selected for the high end of engine power. The NO_x emissions prediction of the four engines was compared against the ICAO databank [15]. The ICAO emission points are taken at sea level with engine power setting of 7%, 30%, 85% and 100% of engine max thrust at sea level. Also, an additional comparison was made against a P3T3 model [16 and 20] for the CFM56, Trent 892 and Trent 895 engines for the same engine conditions.

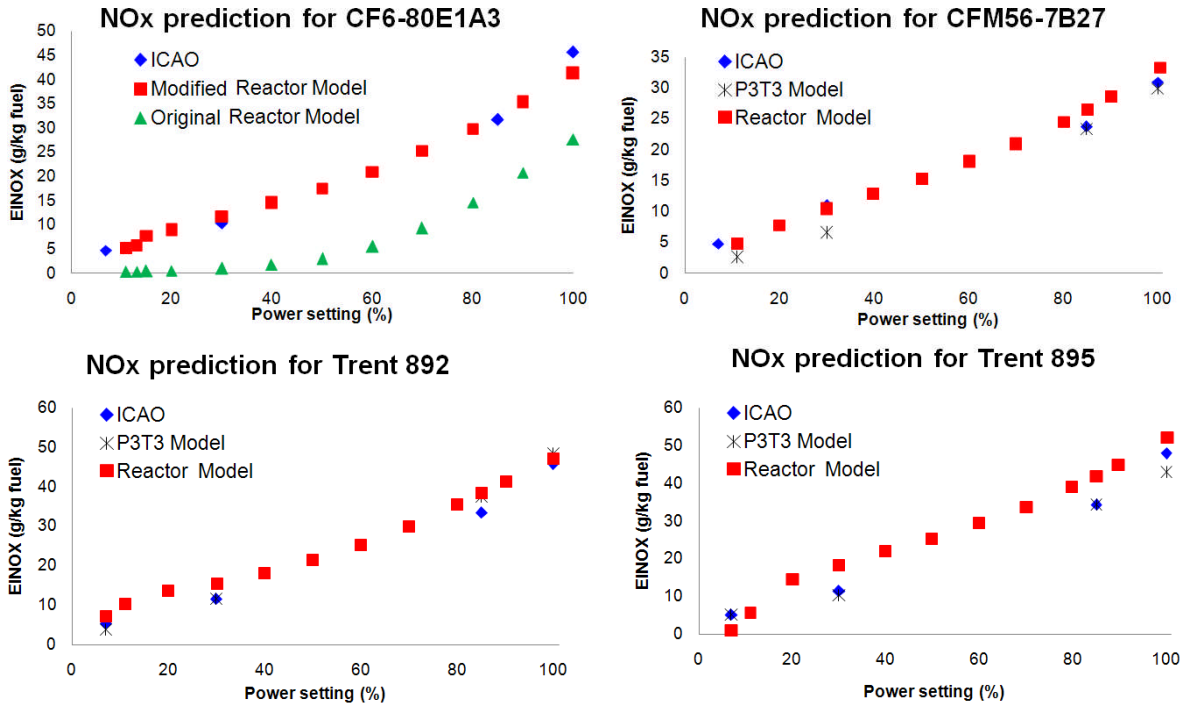

Figure 21 - Results of NO_x emission prediction for the CF6, CFM56, Trent 892 and Trent 895 engines

It can be seen that the original emissions model by Celis [21] was underestimating NO_x emission at all engine power settings. The modified emissions model is now closer to the ICAO databank. The three other engines tested also show good agreement with ICAO databank. In addition, The P3T3 model show similar results.

To ensure that the prediction of NO_x for the modified model is also valid at other conditions than sea level, a comparison was made against the P3T3 emissions model. The P3T3 method

is often used to obtain NO_x emission at high altitude [16]. Here the purpose is to qualitatively check that values obtained with the two models are similar to conclude that the modified reactor based model is capable of predicting NO_X at high altitude. The CFM56, Trent 892 and Trent 895 engine models were run at typical cruise condition (i.e. 31000 feet, Mach 0.8) and the inputs were fed into the two emissions models to obtain the emissions index of NO_x. The results are presented in Table 2.

Table 2 – Comparison of NO_x emission index at typical cruise conditions (31000 feet, 0.8 M)

	Emission Index of NO_x [g/kg of fuel]	
Engine model	**Modified reactor model**	**P3T3 model**
CFM56-5B27	8.2	10.6
Trent 892	9.7	15.7
Trent 895	15.4	15.4

From Table 2, one can see that the results obtained from both model are in close agreement. This result gives confidence in the use of the reactor based model at various engine operating conditions.

4.2 ADDITION OF NATURAL GAS FUEL FOR THE IMPROVED NO_X MODEL

The modified reactor model also includes a new fuel. This fuel is natural gas with the composition given in Table 3. According to [63] this corresponds to the natural gas used in the UK.

Table 3 - Mass fraction used for the implemented Natural gas [63]

Species	**CH_4**	**C_3H_8**	**N_2**	**CO_2**
Mass fraction (%)	86.2	10.8	2.5	0.5

The model together with the natural gas fuel was tested with the General Electric LM2500 stationary gas turbine (modelled using Turbomatch). The LM2500 engine was run from 40% to 120% of the base load (engine base load is 22.8 MW). The model validation is done using GE chart of delivery shaft power versus compressor inlet temperature [87]. The information retrieved is power turbine inlet temperature and exhaust gas discharge mass flow which can be compared with Turbomatch output. Table 4 summarises the validation at different engine loads.

Table 4 - Summary of LM2500 data used for Turbomatch model validation

		Exhaust mass flow (kg/sec)			**Power turbine inlet temperature (K)**		
Shaft Power	**% of base**	**GE**	**Model**	**% error**	**GE data**	**Model**	**% error**

(MW)	load	data[87]			[87]		
23.3	102.2	69.2	70.8	-2.31	1102	1070	2.90
22.8	100.0	68.5	70.3	-2.63	1089	1061	2.57
20.9	91.7	66.7	67.6	-1.35	1055	1035	1.90
18.3	80.3	63.1	64.0	-1.43	1016	1000	1.57
16.0	70.2	59.9	60.3	-0.67	989	965	2.43
13.8	60.5	55.8	56.6	-1.43	961	931	3.12
11.6	50.9	52.2	52.4	-0.38	930	898	3.44
9.0	39.5	46.7	47.0	-0.64	889	867	2.47

From Table 4, the difference never exceeds 3.5%. Given the number of assumptions to model the engine and the limited information available on the public domain this level of discrepancy is deemed acceptable. Thus the Turbomatch model of the LM2500 stationary gas turbine is assumed sufficiently representative of the real engine. It is now possible to use the information from the Turbomatch engine model to feed the NO_x emissions model.

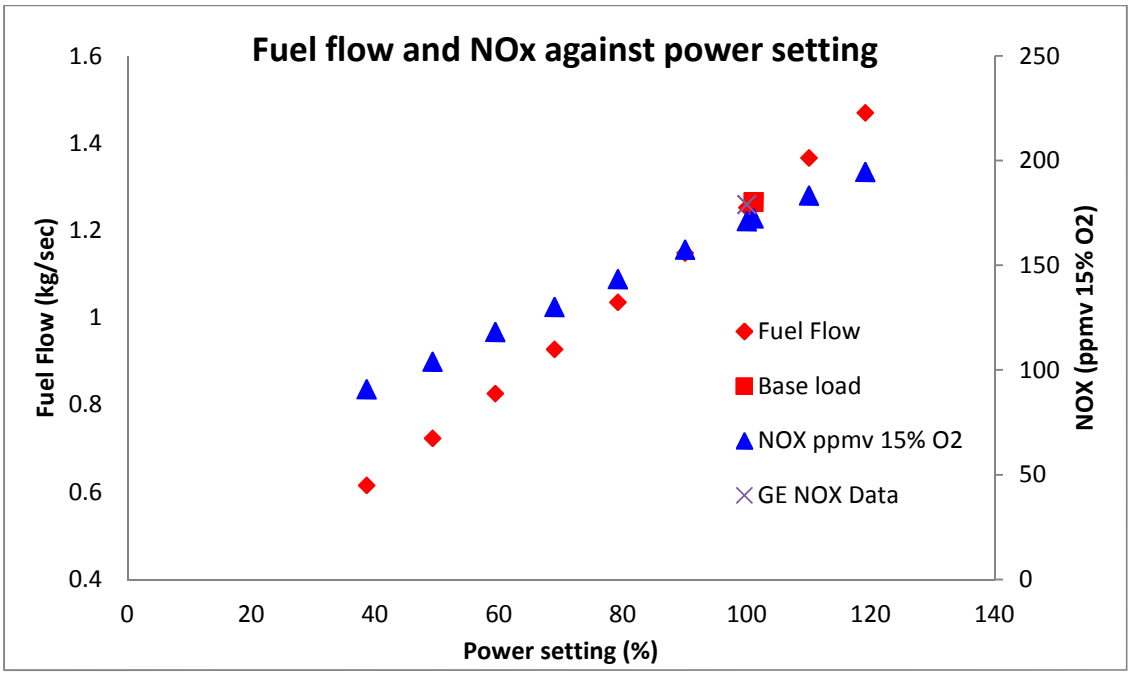

Figure 22 - Fuel flow and NO_x versus percentage of base load for the LM2500 gas turbine

Figure 22 shows the evolution of fuel flow and NO_x emissions in term of ppmvd corrected for 15% oxygen. One can see that the NO_x emissions figure provided by GE at base load falls relatively close to the figure predicted by the model. This does not provide a full validation of the model in this case, but the access to NO_x emissions information at other power loads is difficult. Additional information is required to ensure that NO_x trend is also adequately captured by the model.

4.3 LEAN PRE-MIXED PREVAPORISED COMBUSTOR MODEL

The model developed represents a lean pre-mix pre-vaporised combustor (LPP). The modelling and layout is based on a concept proposed by Rizk and Mongia [6]. Ref. [6] describes the modelling of an LLP combustor, namely AGT100 (Figure 23), which also features variable geometry to control the air flow going through the different combustor zones. The combustor comprises a pre-chamber where fuel is vaporised and mixed with air before injection in the main chamber. A pilot injector is added to ensure flame stability during low power operation. The variable geometry enables the air flow to be diverted between the premixed chamber (flame front core), the dome (flame front near wall) or the dilution zone. The flow split is shown in Figure 24 as a function of the variable geometry slider location.

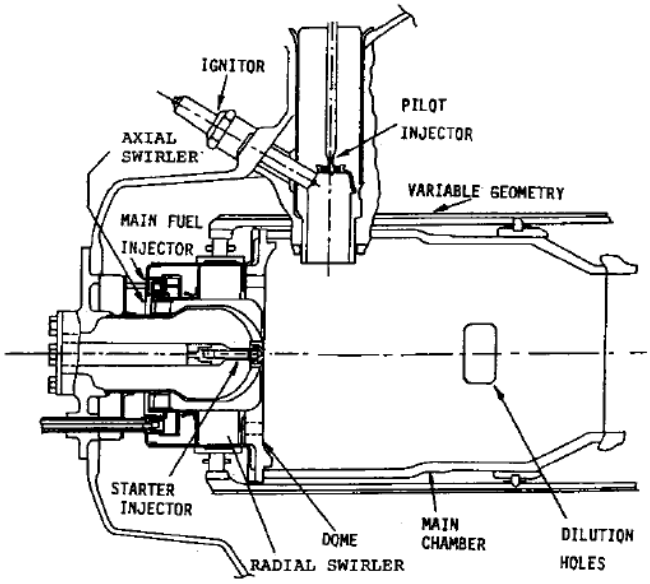

Figure 23 - AGT100 combustor [6]

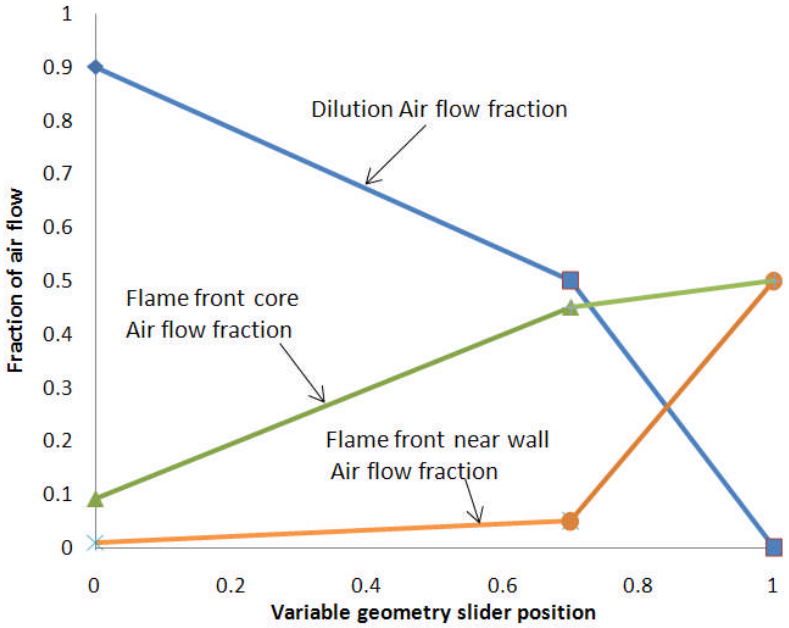

Figure 24 - Variation of air flow fraction as a function of variable geometry slider position. Adapted from [6]

4.3.1 MODEL VARIANTS

The model is essentially a modification of the reactor based model Hephaestus initially created by Celis [21]. Two variants are considered; one variant is the LPP combustor with variable geometry the other variant assumes a fixed geometry. The fixed geometry variant has been developed to make a comparison of the effect of variable geometry on the production of NO_x.

4.3.2 LPP COMBUSTOR WITH VARIABLE GEOMETRY

The reactor layout of the variable geometry LPP combustor is shown in Figure 25. As can be seen, two perfectly stirred reactors model the flame front area (Core zone and Near Wall zone). Those are selected with the assumption that fuel is vaporised and fully mixed with air, thus the use of partially stirred reactor is not necessary. A pilot zone is also modelled. It is assumed that the fuel is injected using a conventional fuel injector (swirler or other), in this case the fuel is not fully vaporised and the fuel/air mixing is heterogeneous, thus a partially stirred reactor is preferred to model this zone. Eventually the flame front and pilot flow mix and enter the primary zone reactor. It is assumed that no additional air is injected in the process. The primary zone is modelled with a perfectly stirred reactor since the flow is now assumed to be well mixed. Additional air is injected at the entry of the dilution zone.

This zone is modelled using a series of perfectly stirred reactors to take into account the gradual injection of air along this zone.

The variable geometry is modelled using the variation of the air injected in the different combustor zones (flame front core, flame front near wall and Dilution zone) given by Rizk [6]. The variation of air flow fraction as a function of the variable geometry slider is shown in Figure 24.

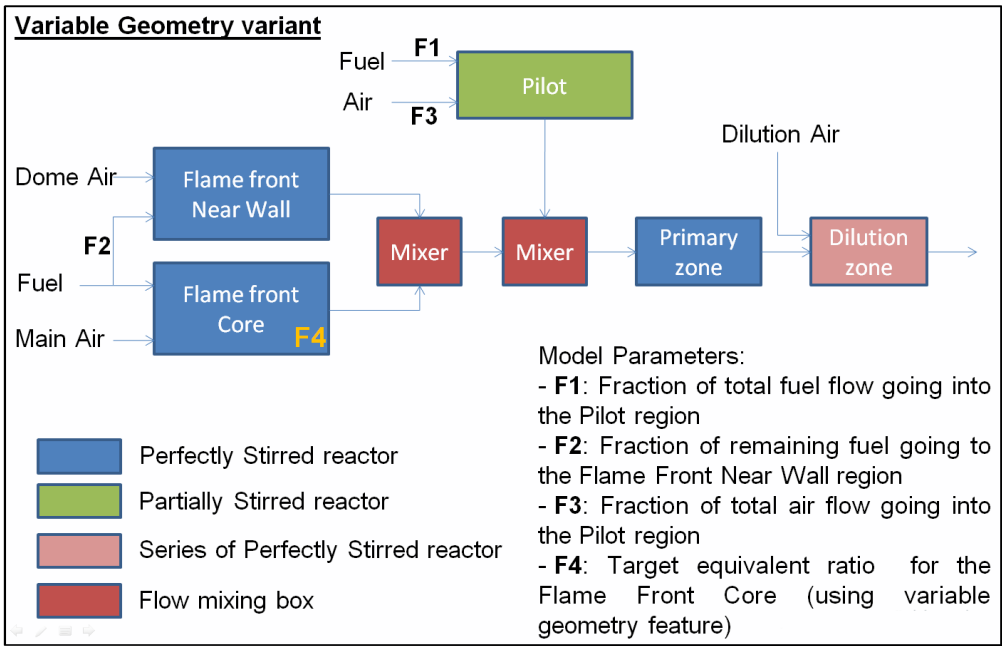

Figure 25 - Reactor layout for the LPP combustor with variable geometry

The variable geometry is used to control the equivalence ratio in the flame front core. It is effectively done by the use of sliding band that cover or uncover holes at different locations to control the air flow to the flame front core, flame front near wall and dilution zones. The user can select the target equivalence ratio at the flame front core reactor (F4 parameter on Figure 25). The variable geometry algorithm will select the slider position to achieve this equivalence ratio. This will immediately fix the fraction of air flow going into the flame front near wall zone and the dilution zone using the information shown in Figure 24. If the targeted equivalence ratio cannot be reached then the default slider position is selected (position 1 which equally distribute air between the main and dome zone). This situation mostly arises at high engine power setting.

Other parameters can be defined such as fraction of total fuel going to the pilot zone (F1), fraction of remaining fuel going to the flame front near wall zone (F2) and fraction of total air going to the pilot zone. Lastly, parameters defining the volume (area and length) of each reactor can also be set by the user.

4.3.3 LPP COMBUSTOR WITH FIXED GEOMETRY

As can be seen on Figure 26, the layout of the LPP combustor with a fixed geometry is not fundamentally changed. The main difference lies in a different approach in assigning the air flow distribution. With fixed geometry, the F4 parameter no longer exists. Instead all air flow fractions are explicitly set by the user and remain constant for any engine power setting.

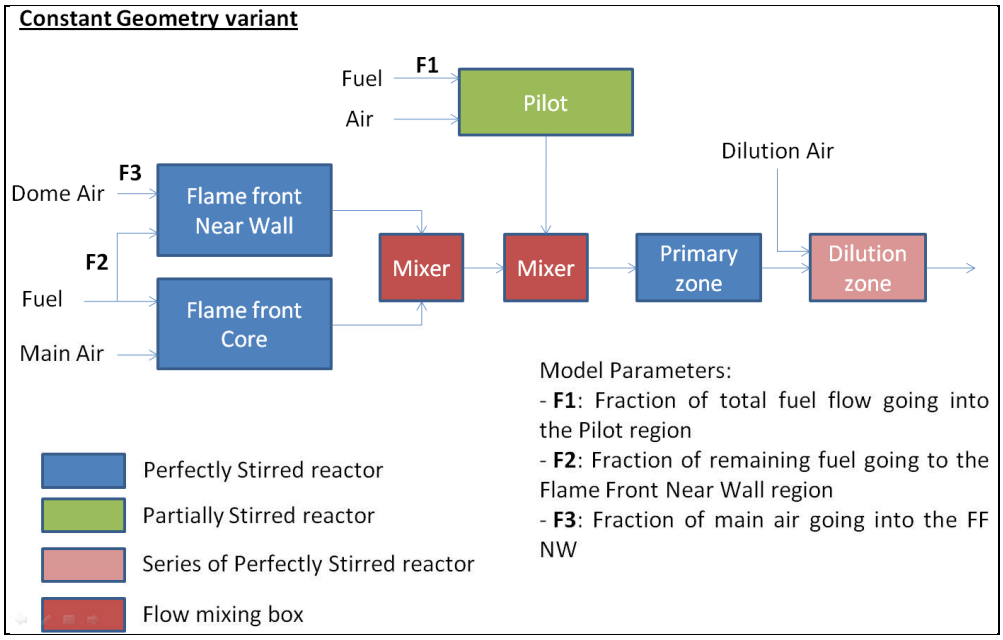

Figure 26 - Reactor layout for the LPP combustor without variable geometry

4.3.4 RESULTS

Figure 27 shows the variation of NO_x emission index as a function of power setting. Both variant of the LPP combustor were tested using inputs from a CF6-80E1A3 model (Turbomatch model) at sea level with power setting varying from 10 to 100% of the maximum take-off thrust. The targeted equivalence ratio was set at 0.5 for the variable geometry variant.

One can see the strong effect on NO_x emissions by varying the flow fractions as the power setting increases. At low power setting (below 50%) the forcing of an equivalent ratio is detrimental when compared to a simple fixed geometry. This is explained by the fact that the air flow fraction at the flame front near wall lead to an equivalence ratio closer to 1.0, thus leading to an increase in NO_x emissions. A better distribution of air is likely to avoid this shortfall, for example by diverting more air in the flame front near wall to lower the equivalence ratio. However the benefit of variable geometry is clearly visible at the highest engine power setting. The fixed geometry NO_x emission is around 16 g/kg of fuel whereas the variable geometry variant only emits about 1g/kg of fuel. This result can be explain that

in this case the air flow split is ideal in term of equivalence ratio not only in the flame front core but also in all other reactors thus leading to much lower NO_x production.

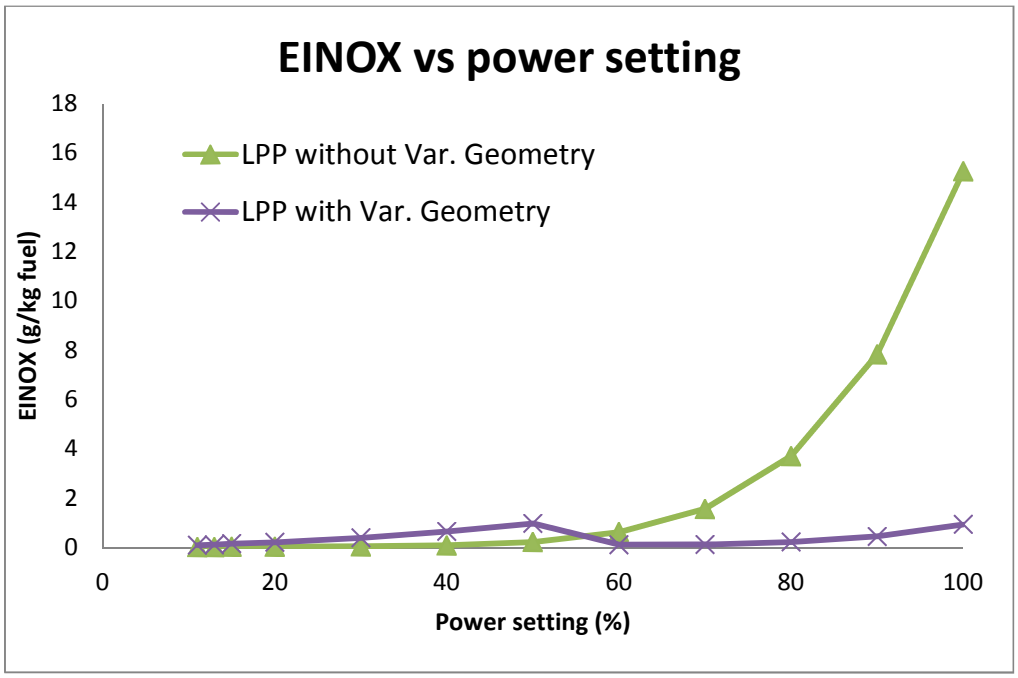

Figure 27 - $EINO_X$ variation versus power setting (CF6-80E1A3 model from Turbomatch) at sea level. Target equivalence ratio at flame front core (F4) set at 0.5

Figure 28 shows the impact on the NO_x emissions of the variation of targeted equivalence ratio at the flame front core. For higher equivalence ratio the overall NO_x emissions index increases. It can also be seen that a peak in NO_x emissions shifts towards higher engine power setting. This feature is explained by the flame front near wall equivalence ratio being the closest to 1.0 happens at higher power setting as the flame front core equivalence ratio is being increased.

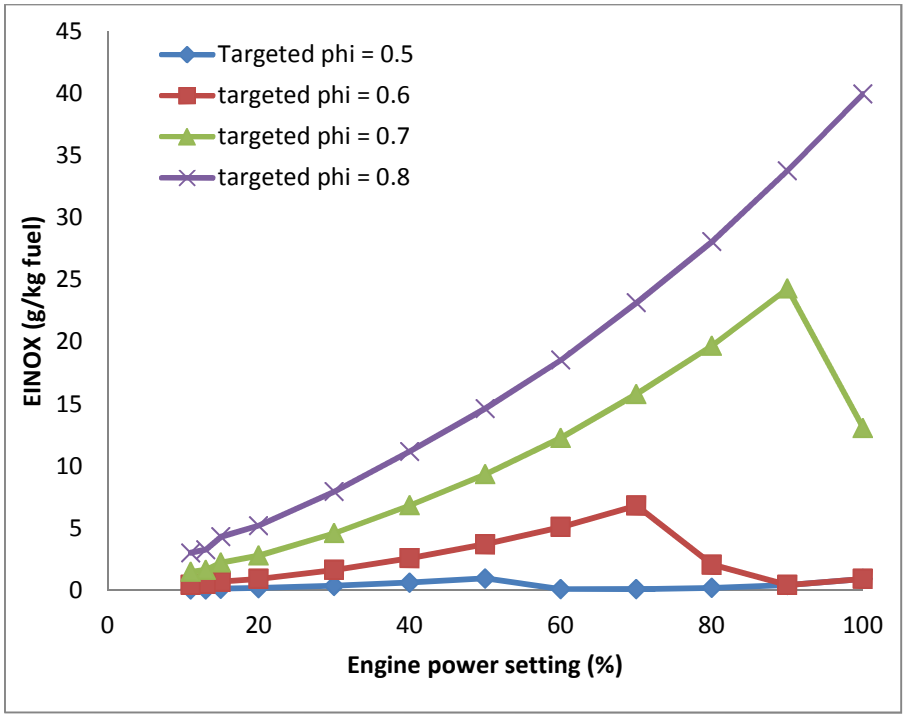

Figure 28 - NO_x emission for varying targeted Phi at flame front core versus engine power setting

4.4 CONTRAILS MODEL

Condensation trails or Contrails are a possible outcome of aircraft flying at high altitude. It has been shown by the IPCC report [64] that contrails could have a significant impact on climate change.

The contrails formation process is fairly well established and can be described as follow. The aircraft engine produce hot air at the exhaust with high water content due to the reaction of complete combustion happening in the combustor. This hot and moist air mixes with the colder and drier ambient atmospheric air. If the water partial pressure exceeds the saturation with respect to water then condensation will occur and contrails will form. Depending on the final local atmospheric conditions, two cases can arise. If the mixing between the plume and the ambient air do not lead to water saturation with respect to ice, then the water will quickly evaporate and the contrails disappear after a short period. On the other hand if saturation with respect to ice is attained, then contrails will persist. In this case they are called persistent contrails and can lasts for hours as long as atmospheric conditions remains ice saturated.

The contrails model was developed in a collaborative effort with a PhD colleague, William Camilleri, from Cranfield University in the frame of the Clean Sky project. The model is based on the methodology of Appleman [65] with modification brought by Schumann [66].

The final use of the model is to predict the formation of persistent contrails so that based on segment length; it is possible to derive a number of kilometres of persistent contrails generated by an aircraft flying a given trajectory with known atmospheric conditions (Pressure, temperature and relative humidity). This value can subsequently be used as an objective for an aircraft trajectory multidisciplinary optimisation framework.

4.4.1 CONTRAILS PREDICTION METHODOLOGY

The contrails prediction is done through the use of the water phase diagram (see Figure 29). This diagram contains two curves. The first curve corresponds to the vapour partial pressure saturation with respect to water and the second is the saturation curve with respect to ice.

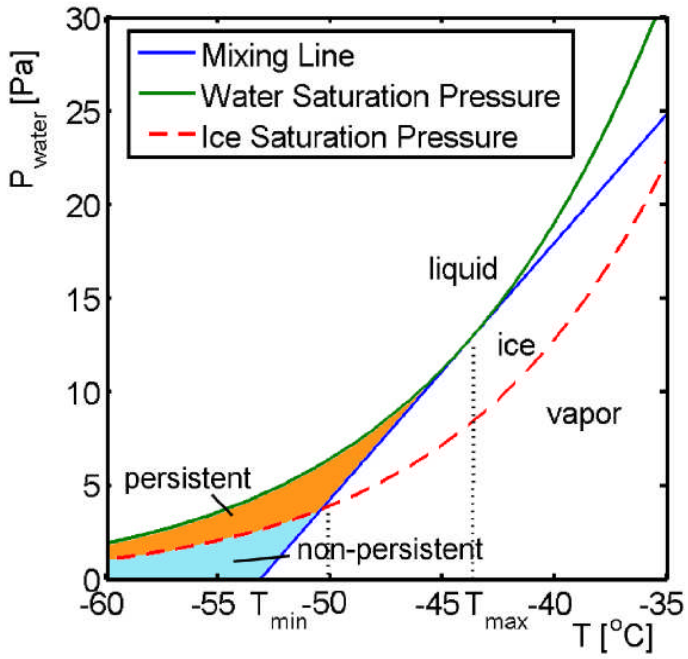

Figure 29 - Water phase diagram with critical mixing line (blue line) from Noppel [67]

By assuming that the mixing between the exhaust plume and ambient air is adiabatic and isobaric and considering equal mixing rate of heat and water, it is possible to represent the mixing process as a line on the water phase diagram (blue line in Figure 29) [67]. If the mixing line crosses the water saturation curve, contrails will form. The critical mixing line is used to find the critical temperature. The critical temperature is the maximum temperature at which contrails will form (for a given slope and final ambient conditions). The critical

mixing line is defined by the slope calculated from equation 4.1 (critical slope) given by [66] and is tangent with the water saturation curve.

$$G = \frac{EI_{H_2O}.P.c_p}{\varepsilon.LHV.(1-\eta)} \quad [4.1]$$

G is the critical slope in $Pa.K^{-1}$; EI_{H2O} is the emissions index of water in kg/kg of fuel. EI_{H2O} can be considered constant in a first approximation with a value of 1.223 kg/kg of fuel. P is the ambient pressure in Pa, c_p is the specific heat capacity of air in $J.kg^{-1}.K^{-1}$, ε is the molar mass ratio of water and air (=0.622), LHV is the combustion heat in $J.kg^{-1}$ and η is the overall engine efficiency.

Overall engine efficiency can be calculated using the following expression (this value will need to be calculated using an aircraft and an engine model).

$$\eta = \frac{FN*V_{TAS}}{\dot{m}_{ff}*LHV*10^6} \quad [4.2]$$

Where, FN is the engine net thrust in N, V_{TAS} is the aircraft true air speed in m/s and $\dot{m}_{ff}$ is the engine fuel flow in kg/s.

The next section will describe the steps followed in order predict if contrails occur and whether it is persistent.

4.4.2 MODEL STEPS

The contrails model requires a number of inputs listed in Table 5.

Table 5 - List of input parameters required for the contrails model

Parameter name	Description	Unit
Point	Calculation point	-
Tamb	Ambient temperature	K
Pamb	Ambient pressure	Pa
RHw	Relative humidity with respect to water	-
ExhaustCP	Specific heat capacity of air	$J.kg^{-1}.K^{-1}$
EngineEff	Overall engine efficiency	-
EIH2O	Emission index of water	kg/kg of fuel
LHVFuel	Combustion heat of the fuel	$J.kg^{-1}$
MMR	Molar mass ratio of water and air (constant)	-
EGT	Exhaust gas temperature	K
SegLength	Segment length	km

The first step is to calculate the critical slope using equation 4.1. Based on the critical slope value, the critical temperature is retrieved. To calculate the critical temperature, it is

necessary to find the temperature at which the critical mixing line is tangent to the water saturation curve.

One formula for water saturation can be taken from Goff and Gratch [68] (equation 4.3), however it is replaced with a simplified equation [4.4] in order to calculate the critical temperature in a quicker way.

Goff and Gratch formulation for water saturation:

$$\log_{10}(e_w) = -7.90298 \times \left(\frac{373.16}{T} - 1\right) + 5.02808 \times \log_{10}\left(\frac{373.16}{T}\right) - 1.3816 \times 10^{-7} \times \left(10^{\left(11.344 \times \left(1 - \frac{T}{373.16}\right)\right)} - 1\right) + 0.0081328 \times \left(10^{-3.49149 \times \left(\frac{373.16}{T} - 1\right)} - 1\right) + \log_{10}(1013.246) \quad [4.3]$$

Where, T is the temperature in K and e_w is the saturation pressure with respect to water in Pa.

Simplified formulation for water saturation:

$$e_w = 19.55769739 \times exp^{(0.114555811 \times T)} - 0.00069542 \quad [4.4]$$

Where, T is the temperature in °C and e_w is the saturation pressure with respect to water in Pa. The three constants were found using a least square method to approach Goff curve as closely as possible.

Figure 30 shows the results using the two formulations and shows a very good agreement for the temperature range of -85°C to -45°C.

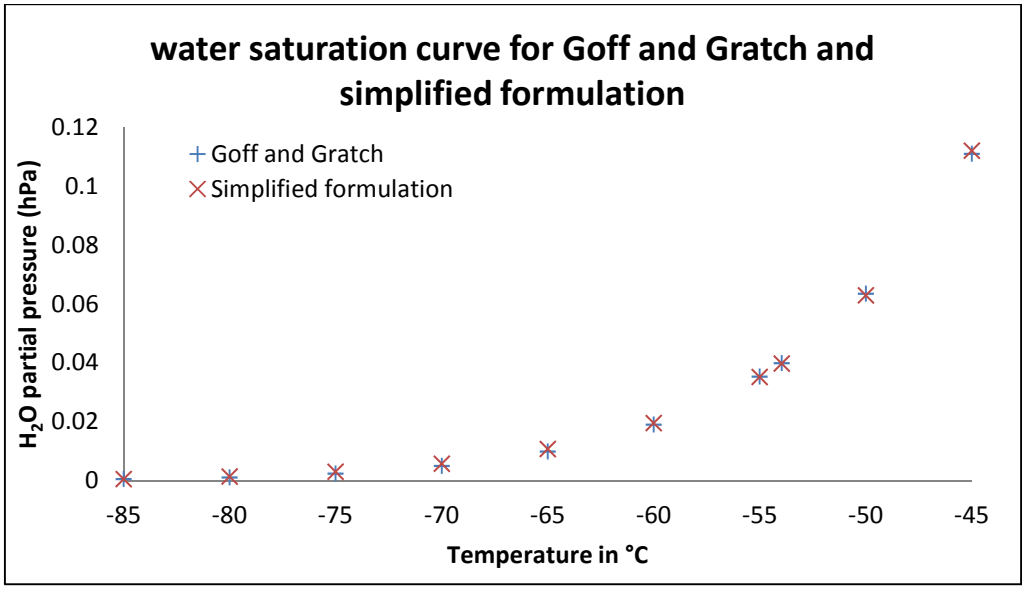

Figure 30 - comparison of Goff and Gratch water saturation formulation against simplified equation

This simplified formula is useful because it is simpler to obtain its first order derivative. Thus having access to the derivative allow for a direct calculation of the critical temperature as

opposed to using a search method to find the critical temperature using Goff formula. This is an advantage in term of computational speed.

It is now easy to calculate the saturation pressure with respect to water and ice at the critical temperature (this time using the Goff formula).

The next step is to obtain the air conditions at which the exhaust exits the engine. The exhaust vapour pressure is calculated using equation 4.5.

$$p_{v=}esw_0 + \left(G \times (EGT - T_{cr})\right) \quad [4.5]$$

Where esw_0 is the water saturation pressure at critical temperature, G is the critical slope, EGT is the exhaust gas temperature calculated as the averaged exhaust temperature of the by-pass and core flow in the case of high by-pass engine as shown in equation 4.6. Typical values for EGT are in the range 290-330 K. T_{cr} is the critical temperature.

$$EGT = \frac{T_{Exhaust,By-pass} * \dot{m}_{Exhaust,By-pass} + T_{Exhaust,Core} * \dot{m}_{Exhaust,Core}}{\dot{m}_{Exhaust,By-pass} + \dot{m}_{Exhaust,Core}} \quad [4.6]$$

The ambient vapour pressure p_{amb} (in Pa) is calculated using equation 4.7.

$$\log_{10}\left(\frac{p_{amb}}{100 * RHf}\right) = -7.90298 \times \left(\frac{373.16}{T_{amb}} - 1\right) + 5.02808 \times \log_{10}\left(\frac{373.16}{T_{amb}}\right) - 1.3816 \times 10^{-7} \times \left(10^{\left(11.344 \times \left(\frac{1 - T_{amb}}{373.16}\right)\right)} - 1\right) + 0.0081328 \times \left(10^{-3.49149 \times \left(\frac{373.16}{T_{amb}}\right)} - 1\right) + \log_{10}(1013.246) \quad [4.7]$$

Where RHf is the relative humidity relative to ice saturation and T_{amb} is the ambient temperature. It is now possible to recalculate the actual mixing slope by using equation 4.8.

$$G_{actual} = \frac{p_v - p_{amb}}{EGT - T_{amb}} \quad [4.8]$$

Contrails will form if the difference between G_{actual} and G is negative. In addition if the ambient vapour pressure (p_a) is greater than the ice saturation pressure at the ambient temperature (T_a) then the contrails is considered persistent.

4.4.3 MODEL VALIDATION

Shull [69] provides ground based contrails observation data taken at Wright Patterson Air Force Base during the month of September and October of 1997. Each day, sounding balloons were sent to obtain atmospheric conditions at aircraft flying level. Each aircraft was identified by its flight number. The information available is the flight level, the corresponding pressure altitude, the ambient temperature and relative humidity with respect to water. For each observation, it is indicated if contrails were spotted or not. Two main limitations arise in this database with respect to the contrails model developed in this work. First, it is never indicated if the contrails is persistent or not. This lack of information limits the validation of the persistent contrails prediction of the model. The second limitation comes from the fact that data is gathered within a relatively short period of time. It can be seen in the data that during the whole period of observation, the relative humidity reported was systematically very low. This limitation could also be a problem for validation purpose as the whole range of atmospheric conditions is not covered by this database.

As said, the flight level, pressure, temperature and relative humidity are known, but no information is given about the engine parameters that are required by the contrails model. In this case, it is assumed that these parameters are constant for the whole database. The values shown in Table 6 were kept constant.

Table 6 - Parameter assumed constant for the validation of the Contrails model

Parameter	Exhaust Cp [$J.kg^{-1}.K^{-1}$]	Engine overall efficiency [-]	Emission Index H2O [kg/kg of fuel]	LHV fuel [$MJ.kg^{-1}$]	Exhaust gas temperature [K]
Value	1004	0.3	1.223	43.2	300

This set of value has the effect of assuming a constant contrails factor (CF), of 0.040. This value is consistent with CF given by Schrader [70]. In his paper, he is assuming a contrails factor of 0.039 when considering high by-pass ratio engine.

Due to this assumption, only high by-pass ratio engine observations were taken into account for the validation of the contrails model.

Finally, 236 observations were compared with the model results. It appears that a hit rate (number of time the model predicts correctly divided by number of observations) is 80%. In his paper, Shull reports a hit rate of 81% for the same methodology. This gives confidence that the methodology has been correctly implemented. It is also worth noting that this methodology obtained the best hit rate in Shull study. The other two methodologies tested were Schrader and Hanson with a hit rate of 79% and 64% respectively.

4.4.4 MODEL LIMITATIONS

The only limitation comes from the simplified equation of the water saturation curve. The curve equation is only valid from -45°C to -90°C. So the contrails prediction is made only when the atmospheric temperatures lie within this boundary. Each time the atmospheric temperature is outside the boundary an error message will be displayed in the output file. This error will not affect the rest of program but will automatically assume no contrails formation for the segment.

Chapter 5: Optimisation studies

5.1 OVERVIEW

This chapter is comprised of three case studies. The first case study focuses on aircraft trajectory optimisation. It is a two-objective minimisation problem. The optimisation was run for three set of objectives: fuel/time, fuel/NO_x and fuel/contrails. The second case study is also dedicated to aircraft trajectory optimisation in which the conventional combustor has been replaced with a hypothetical advanced combustor concept (LPP combustor type) as described in section 4.3.2. The objectives set for minimisation were fuel/NO_x and NO_x/contrails. The last case study is focusing on the simultaneous optimisation of aircraft trajectory and engine cycle. It uses the conventional combustor emissions model and the optimisation was performed for three set of objectives which were: fuel/time, fuel/NO_x and fuel/contrails.

5.1.1 INTEGRATION AND OPTIMISATION FRAMEWORK

The genetic algorithm optimiser described in chapter 3 was integrated within GATAC [58] (Green Aircraft Trajectory under ATM Constraints) which is a framework software developed under the European framework program 7 (FP7). The main purpose of GATAC is to allow easy import of multiple models and easy connection with the optimiser.

For this study a global framework has been specifically developed following the concept of TERA (Techno-economic and Environmental Risk Assessment). This concept was developed at Cranfield University, and is based on a number of models link together within a framework [71-73]. The output of a TERA analysis is dependent on the type of model implemented.

The general model interaction is pictured in Figure 31. The figure shows the main models used in this study and their interactions with each other. The framework itself was programmed in FORTRAN 90, and directly uses model through executable by means of standard input and output text files. The models used for this study were either developed using FORTRAN or Matlab.

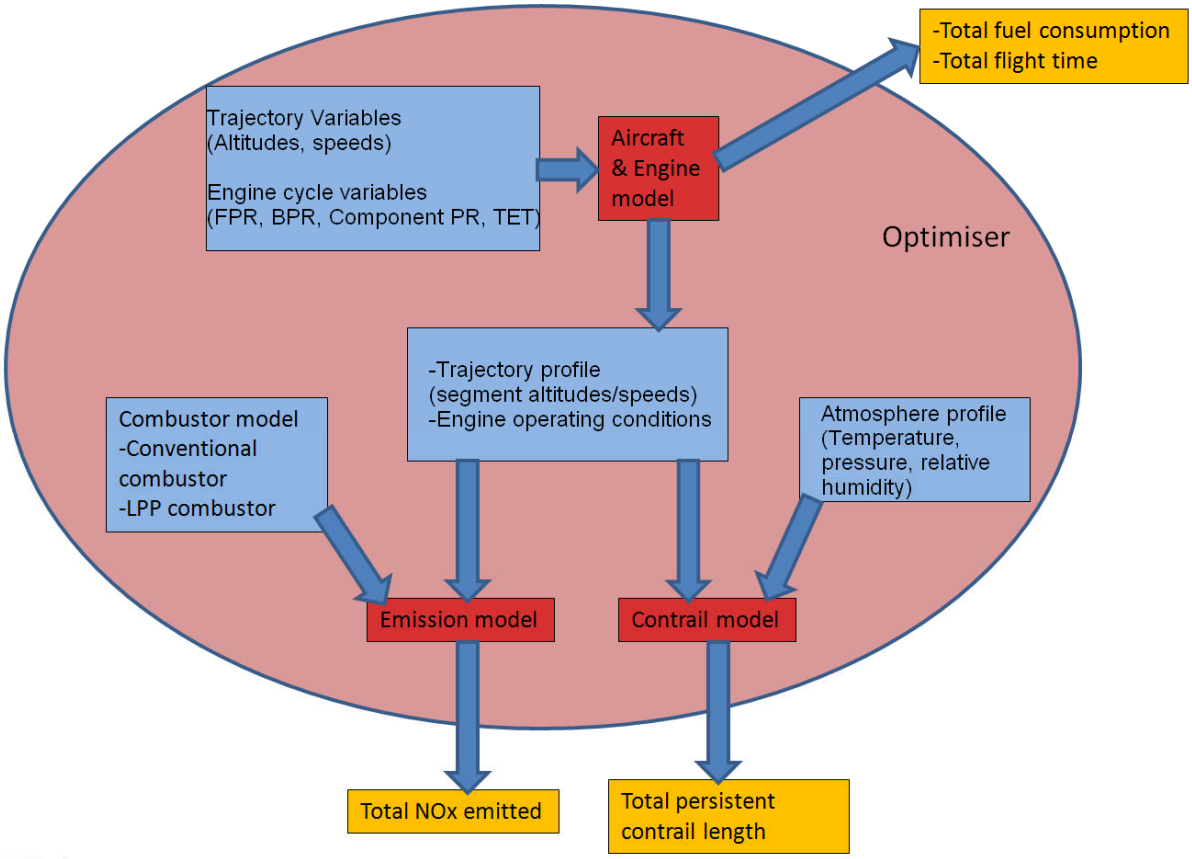

Figure 31 - Optimisation framework and model interactions for various objectives

The following section first describes the set of models used for the optimisation runs undertaken.

5.1.2 MODEL SELECTION

5.1.2.1 Aircraft and engine models

The aircraft model has been developed by Nalianda [74]. This model is able to compute full trajectories from take-off to landing. It uses first principles to derive the general behaviour of the aircraft. Aircraft drag and lift characteristics are taken from BADA [75] to ensure a certain level of fidelity. The aircraft/engine models used for this study represent a single aisle with twin-spool turbofan similar to a Boeing B737-800 fitted with CFM56-7B27 engines (see appendices A and B for full model descriptions). The integration of the engine is made through the use of Turbomatch [76]. Basically for each segment the aircraft model will request either a specified thrust or TET depending on the flight phase. Turbomatch is run and any parameters of interest can be retrieved for use in subsequent models.

A number of features make this model particularly interesting for the type of optimisation undertaken.

The model is global in the sense it is possible to retrieve global information such as fuel consumed or flight time. This information may be directly used as objectives for optimisation.

Trajectory range can be specified, this means optimisation can be easily made since all trajectories are compared on the same basis.

The model includes a limited amount of variable even though numerous segments can be computed for high fidelity results. As an example, the climb phase is defined with only 6 variables (3 altitudes and 3 speeds) whereas the aircraft and engine parameter are computed for a number of segments defined by the user (typically 30 segments). This allows potentially easier optimisation without the issue of large averaging between segments which can impair result accuracy.

The model uses a live version of Turbomatch (no database or meta-model). This implies that the engine operating point is calculated for each segment of the trajectory and thus any change in the engine design point will be taken into account for the trajectory calculation. This feature is of prime importance when optimisation includes engine design variable such as FPR, BPR, etc...

The main drawback identified is the computational time necessary to perform the trajectory simulation. In term of optimisation this can pose a problem since a large number of evaluations will be required to converge to a set of Pareto optimal solutions (estimation of 10000 evaluations). Thanks to the development of the optimiser it is possible to distribute the load on multiple computers thereby limiting the effect of this drawback. Another solution to further reduce the computational time is to lower the number of segment but this will have an impact on the accuracy of the model.

Another drawback of the model is the lack of engine weight model. Even though this aspect can be detrimental to the model accuracy when considering engine cycle optimisation, a number of constraints on the engine design have been included to insure an acceptable level of consistency. More details are given in section 5.3.2.

Aircraft model limitation:

The model is a point based method. As such, it reduces the aircraft to a single point for force calculations. This implies that side forces or structural bending and stresses are not included in the trajectory calculation. Also banking of aircraft is not included. In addition, speeds change are assumed to occur instantaneously which mean that fuel spent during acceleration phases are not included. This is justified from the fact that acceleration phase

times are negligible compared to the time of flight of the entire trajectory. Indeed it was found that the difference was less than 1 kg of fuel for trajectory of 3000 km.

Engine model limitations:

The engine model is based on thermodynamic relationships in order to compute the main values of interest such as net thrust, SFC, temperatures and pressures at all stations of the engine. In order to build the engine model the first assumption is the selection of the engine design point (altitude and Mach design point) which is unknown a priori. Other assumptions relate to the specific layout defined for the engine to model which again is not fully publicly available to the author. The same remark goes for the estimation of the turbo machinery efficiencies at design point. Overall the main limitation for the engine design point comes from incomplete knowledge. Another limitation is that transient effects such as shaft acceleration or deceleration are neglected. The rationale for such simplification is similar to that of the aircraft acceleration simplification.

In term of off design calculation, main limitations come from the use of generic compressor and turbine maps. The maps in the Turbomatch program are not necessarily the one that corresponds to the engine to model. In order to ensure the correct mass flow and pressure change relationships, those maps have to be scaled (see ref [76] for more details of Turbomatch scaling procedure) but they do not accurately replicate the actual turbo-machinery behaviour.

5.1.2.2 Atmospheric model

An atmospheric model has been developed as part of this project so that information about the atmospheric vertical profile can be generated and sent to the contrails model. One profile was selected in order to form contrails at around 34400 feet. The vertical profile was taken from [77]. It is evident that this profile represents only one atmospheric condition. However the scope of this thesis is not to exhaustively test all atmospheric conditions with respect to contrails formation optimisation.

5.1.2.3 NO_x Emissions model

The NO_x emissions model used is the one developed in this work and described in chapter 4. The amount of NO_x produced is integrated for the whole trajectory. Thus it includes the NO_x generated during the LTO cycle but also the NO_x emitted at cruise level. Current legislation does not impose limits on NO_x produced during the cruise phase, however it is interesting to assess how much of the NO_x is emitted during this phase as its impact on climate change could be severe. For case study 1 and 3, the conventional combustor model is used. In case

study 2, the conventional combustor is replaced with the LPP combustor. Here, the objective is not to see the reduction of NO_x because such reduction is an obvious outcome. From results obtained from both types of combustor, one can see that the LPP has about 90% reduction in NO_x, but no formal validation could be performed for the LPP combustor. Quantitative results from this LPP combustor must then be taken with care. Even though direct comparison between combustors is not possible, it is still interesting to observe the potential change in optimal trajectory mainly due to the effect of variable geometry included in the LPP combustor.

5.1.2.4 Contrails model

Again the model used is the one developed in this work and described in chapter 4.

5.2 TRAJECTORY OPTIMISATION

5.2.1 PROBLEM SETUP

The trajectory is composed of five phases; the phases are the take-off, climb, cruise, descent and approach and landing.

The take-off phase starts from brake release and terminates when the aircraft altitude reached 1500 ft above ground level. At this stage the aircraft is in clean configuration with a speed of V_2+10 knot.

The following climb phase starts from the end of the take-off phase and finishes when cruise altitude is reached.

Once the aircraft is in cruise phase, it continues until the top of descent is reached. The cruise phase is segmented into five. Each segment is defined by its altitude and Mach speed setting.

At the top of descent point, the aircraft enters the descent phase. In this phase the engine setting selected is idle descent until the aircraft altitude drops below 10000ft. From top of descent to 10000ft, the descent speed is initially at constant Mach number until transition altitude is crossed. Below transition altitude the descent speed switches to a constant CAS speed of 250 kt.

The approach and landing phase starts from 10000 ft and ends when the aircraft altitude reaches 0 ft. During the final approach, the flight path angle is set at 3 degrees.

Regarding the aircraft model, a number of parameters had to be set and those have been kept constant for all the subsequent case studies performed in the following sections. The main parameters selected are as follow:

- For all trajectories, it is assumed that the aircraft is at 100% load factor. This corresponds to fly with 162 passengers assuming the widely used two class configuration. This leads to a payload mass of 14696kg.
- The take-off weight was set to 68602kg for all trajectories.

5.2.2 CASE 1: FUEL/TIME/NO_X/CONTRAILS OBJECTIVES USING CONVENTIONAL COMBUSTOR

The first case study will use the aircraft and engine models that represent the Boeing 737-800 with CFM56-7B27 engines fitted. The trajectory range is set at 2990 km. This distance is derived from the great circle distance using Stockholm and Lisbon as the departure and arrival respectively. The choice of this particular city pair was driven by the range capability of the aircraft chosen used in a typical trajectory scenario. The emissions of NO_x are estimated using the conventional combustor model (single annular combustor). For this scenario only the trajectory parameters are varied. In other words, the engine design parameters are left constant.

In this scenario, the optimisation of variables will concern only two phases of the flight. The climb and cruise phases have their variables optimised whereas the take-off, descent and landing phases variable will not be optimised. This essentially means that the take-off phase will be the same for all trajectories computed. The descent and landing phases however will not be unchanged since they depend largely on the final state of the cruise phase in term of altitude, speed and also aircraft mass.

The different flight phase are defined as shown in Figure 32

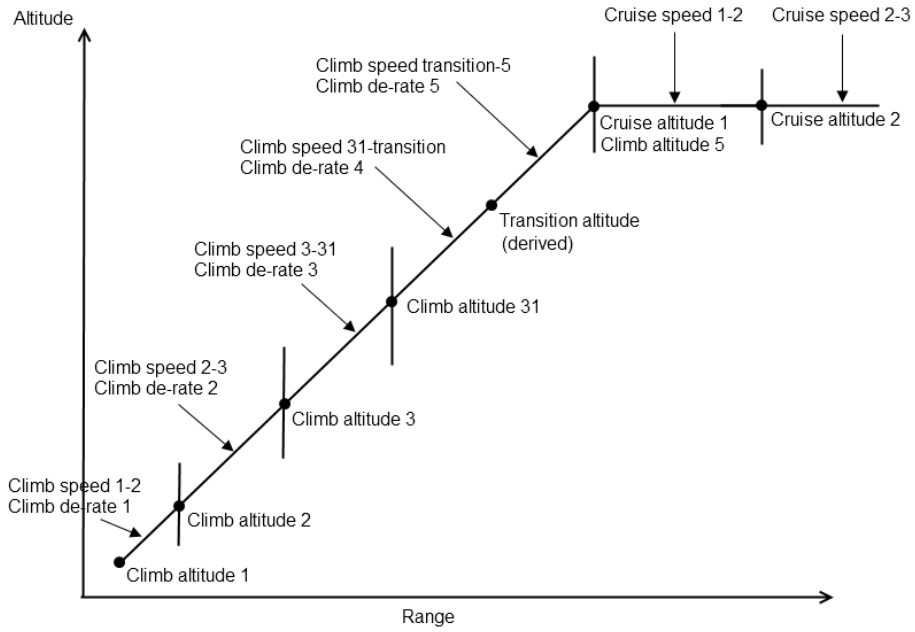

Figure 32 - Climb and early cruise parameter definition

The list of variables and their ranges is shown in Table 7.

Table 7 – List of variables and associated ranges

Variable name	Unit	Range (min - max)
Climb speed 2 – 3 (CAS)	knot	200-275
Climb speed 3 – 31 (CAS)	knot	250-300
Climb speed 31 – transition (CAS)	knot	250-300
Climb speed after transition (Mach)	-	0.65-0.78
Climb Altitude 2	feet	2000-4000
Climb Altitude 3	feet	8000-12000
Climb Altitude 31	feet	13000-27000
Climb de-rate thrust 1 (%)	-	90-100
Climb de-rate thrust 2 (%)	-	90-100
Climb de-rate thrust 3 (%)	-	90-100
Climb de-rate thrust 4 (%)	-	90-100
Climb de-rate thrust 5 (%)	-	90-100
Cruise altitude 1	feet	25000-35000
Cruise altitude 2	feet	25000-35000
Cruise altitude 3	feet	25000-35000
Cruise altitude 4	feet	25000-35000
Cruise altitude 5	feet	25000-35000
Cruise speed 1-2 (Mach)	-	0.65-0.82
Cruise speed 2-3 (Mach)	-	0.65-0.82
Cruise speed 3-4 (Mach)	-	0.65-0.82
Cruise speed 4-5 (Mach)	-	0.65-0.82

The rationale behind the choice of ranges is as follows:

- The climb speed maximum values were selected so that they do not exceed limits imposed by ATM.
- Climb altitude ranges do not corresponds to anything in particular since the range flown is determined by the speed and thrust setting, the altitude is only a “beacon” indicating a change of segment.
- The de-rate thrust ranges allow the optimiser to modify the power setting of the engine during the climb. A minimum of 90% of max climb thrust is to ensure, the climb segment does not extend more than 300 nm. The reason is that ATM controllers will usually request an aircraft to climb quickly to its assigned cruise altitude.
- Cruise altitudes ranges have been set to represent typical medium range aircraft cruise altitude. It is technically possible to fly higher (up to 39000 ft) but the range chosen are deemed sufficient to obtain representative and varied cruise profiles.
- Cruise Mach speed ranges were selected with aircraft limitation in mind. M=0.82 is near the maximum speed of this type of aircraft. M = 0.65 is still above the stall speed at 35000 ft.

Two-objective optimisations have been performed. The objectives for the run were selected as follow: Fuel/Time, Fuel/NO_x and Fuel/Contrails. All objectives were to be minimised. The next section describes the results obtained.

5.2.2.1 Optimisation results

As mentioned, three optimisations were performed for this case study: fuel/time, fuel/NO_x and fuel/contrails.

For the fuel/NO_x and fuel/contrails optimisation, the optimiser was setup for 50 generations, a population size of 200 and an initial population ratio of 10. The number of evaluations was about 11000. For the fuel/time, the optimiser setup was for 70 generations, same population size and initial population ratio. The resulting Pareto fronts obtained for each optimisation run are shown in Figure 33 to Figure 35.

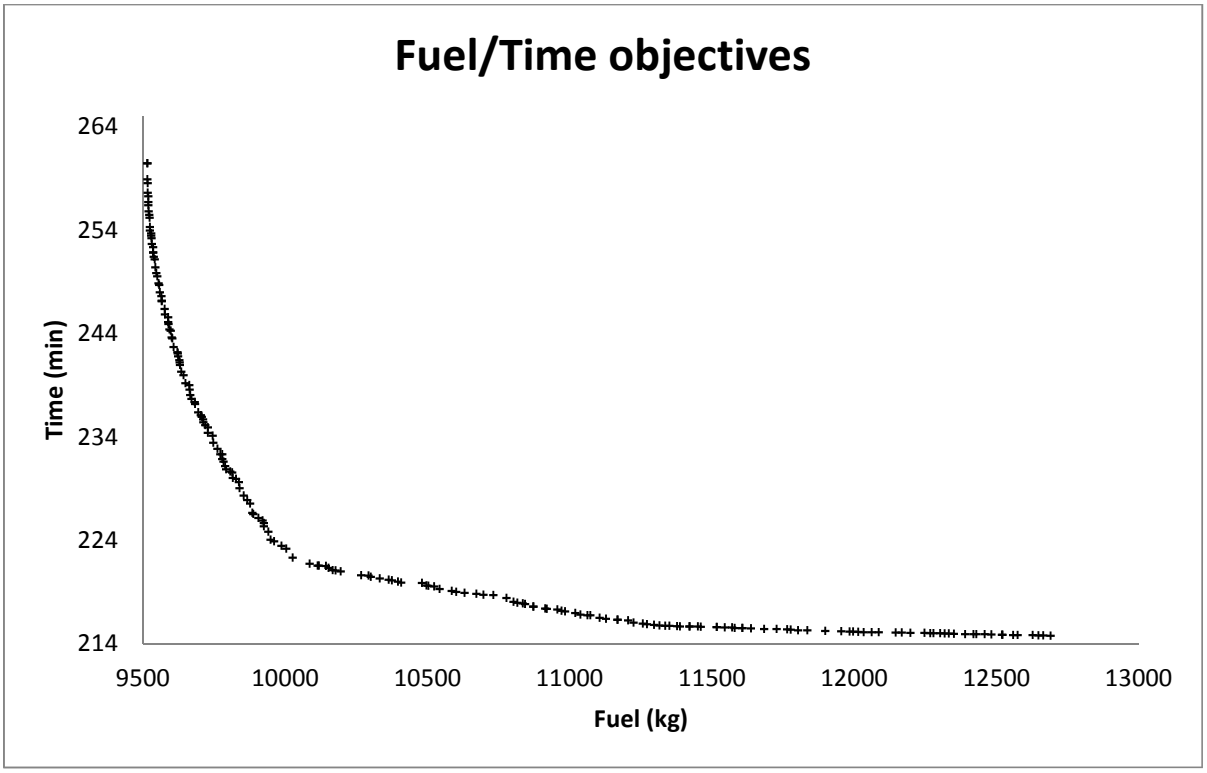

Figure 33 - Pareto front results for the fuel and time objectives

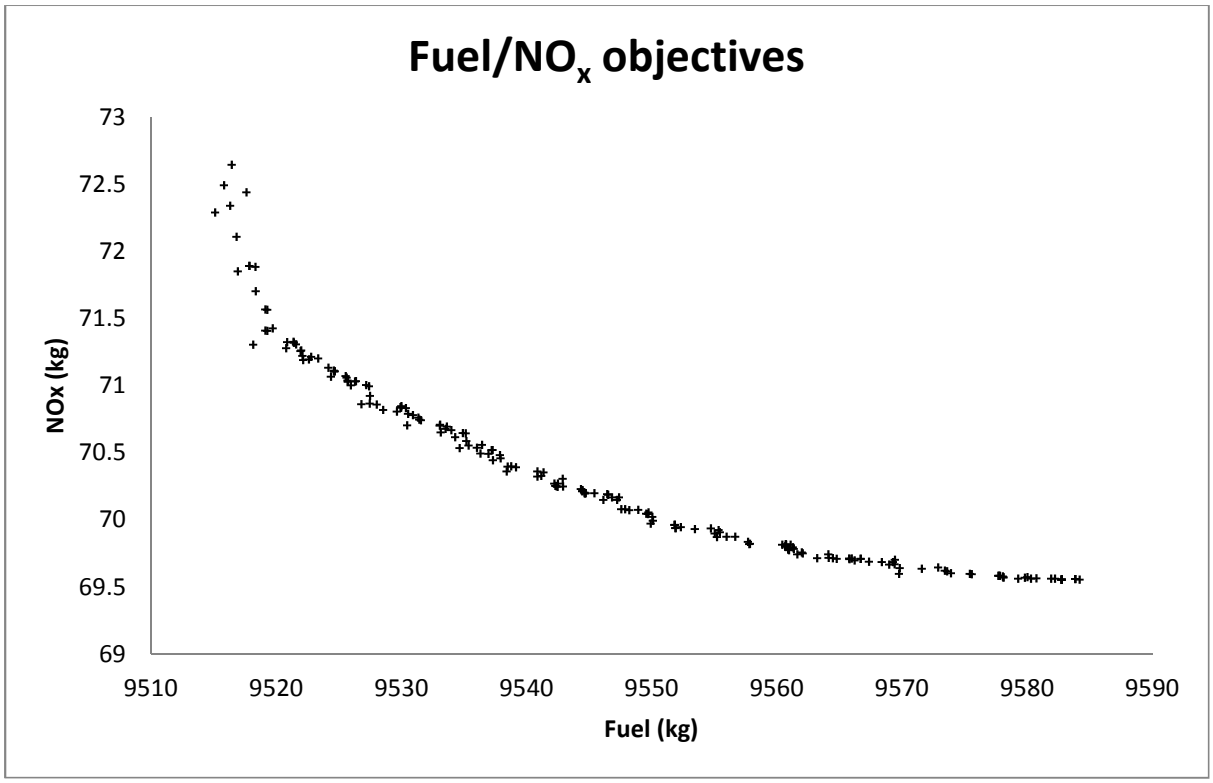

Figure 34 - Pareto front results for the fuel and NO_x objectives

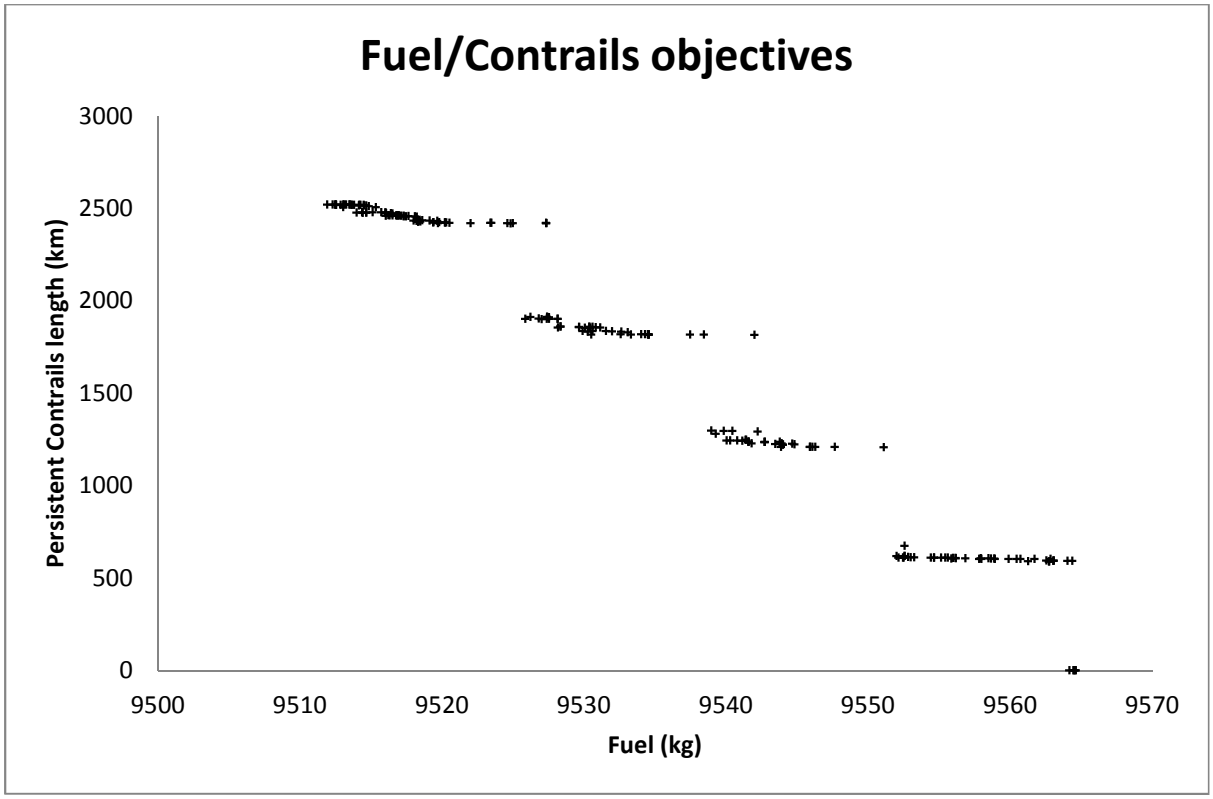

Figure 35 - Pareto front results for the fuel and contrails objectives

As it can be seen from Figure 33 the Pareto front of the fuel and time objective minimisation has settled to a smooth Pareto line after 70 generations. Based on visual inspection of the Pareto front, the diversity of the results appears to be reasonable (i.e. absence of pack of solutions). From Figure 34, the fuel and NO_x objectives show a slightly less smooth Pareto front. This small scatter of results (mainly towards the minimised fuel objective) is likely due to the reduced number of generations. In the case of the fuel and contrails Pareto result, the shape is different. The step-wise shape of this Pareto can easily be explained by the binary nature of the contrails model output (either contrails or no contrails for a given segment). Since the cruise is divided into five segments only and that the cruise phase is where a large majority of contrails may form, the step-wise shape of the Pareto was expected. The small variations of the length of contrails produced within each steps are attributed to the variation in last stages of climb and early descent.

Table 8 to Table 10 summarize the variables selected by the optimiser for the two extreme solutions (e.g. minimum fuel and minimum time solutions) for the three optimisation runs.

Table 8 – Variables selected for the minimum fuel and minimum time solutions

	Minimum fuel solution	Minimum time solution
Variable name	Value	Value
Climb speed 2 – 3 (CAS)	242	275
Climb speed 3 – 31 (CAS)	251	264
Climb speed 31 - transition	300	300
Climb speed after transition (Mach)	0.65	0.65
Climb Altitude 2	2150	2000
Climb Altitude 3	11524	12000
Climb Altitude 31	19662	19877
Climb de-rate thrust 1 (%)	95	100
Climb de-rate thrust 2 (%)	99	100
Climb de-rate thrust 3 (%)	100	100
Climb de-rate thrust 4 (%)	100	100
Climb de-rate thrust 5 (%)	100	100
Cruise altitude 1	34686	25000
Cruise altitude 2	35000	25000
Cruise altitude 3	34999	25000
Cruise altitude 4	35000	25000
Cruise altitude 5	34993	25000
Cruise speed 1-2 (Mach)	0.67	0.82
Cruise speed 2-3 (Mach)	0.69	0.82
Cruise speed 3-4 (Mach)	0.67	0.82
Cruise speed 4-5 (Mach)	0.67	0.82

Table 9 – Variables selected for the minimum fuel and minimum NO_x solutions

	Minimum fuel solution	Minimum NO_x solution
Variable name	Value	Value
Climb speed 2 – 3 (CAS)	241	250
Climb speed 3 – 31 (CAS)	251	251
Climb speed 31 - transition	300	296
Climb speed after transition (Mach)	0.65	0.65
Climb Altitude 2	2000	2000
Climb Altitude 3	10349	12000
Climb Altitude 31	20128	20569
Climb de-rate thrust 1 (%)	94	93
Climb de-rate thrust 2 (%)	100	90
Climb de-rate thrust 3 (%)	100	90
Climb de-rate thrust 4 (%)	100	98
Climb de-rate thrust 5 (%)	96	90
Cruise altitude 1	35000	35000
Cruise altitude 2	34980	35000
Cruise altitude 3	34989	35000
Cruise altitude 4	35000	34983
Cruise altitude 5	35000	35000
Cruise speed 1-2 (Mach)	0.70	0.65
Cruise speed 2-3 (Mach)	0.69	0.65
Cruise speed 3-4 (Mach)	0.69	0.65
Cruise speed 4-5 (Mach)	0.66	0.65

Table 10 – Variables selected for the minimum fuel and minimum contrails solutions

	Minimum fuel solution	Minimum contrails solution
Variable name	Value	Value
Climb speed 2 – 3 (CAS)	243	247
Climb speed 3 – 31 (CAS)	250	251
Climb speed 31 - transition	300	300
Climb speed after transition (Mach)	0.65	0.65
Climb Altitude 2	2000	2147
Climb Altitude 3	8040	8265
Climb Altitude 31	19931	19863
Climb de-rate thrust 1 (%)	90	92
Climb de-rate thrust 2 (%)	99	98
Climb de-rate thrust 3 (%)	100	99
Climb de-rate thrust 4 (%)	97	96
Climb de-rate thrust 5 (%)	100	93
Cruise altitude 1	35000	33636
Cruise altitude 2	35000	34404
Cruise altitude 3	35000	34404
Cruise altitude 4	35000	34419
Cruise altitude 5	35000	34362
Cruise speed 1-2 (Mach)	0.70	0.69
Cruise speed 2-3 (Mach)	0.68	0.68
Cruise speed 3-4 (Mach)	0.68	0.67
Cruise speed 4-5 (Mach)	0.67	0.66

Table 11 summarises the objectives achieved for each of the three runs.

Table 11 – Summary of results obtained for the 3 optimisation runs

	Fuel/time run		Fuel/NO_x run		Fuel/Contrails run	
	minimum fuel	minimum time	minimum fuel	minimum NO_x	minimum fuel	minimum contrails
Fuel (kg)	**9516**	12690	**9515**	9578	**9512**	9564
Time (min)	260	**215**	259	270	259	262
NO_x (kg)	72	160	72	**70**	72	72
Contrails (km)	2524	0	2508	2464	2521	**0**

One aspect of the optimisation was to test for repeatability of results. The optimisation for the minimum fuel was effectively repeated three times. The main remark is that the best

solution obtained was for the fuel/contrails minimisation run (9511.9 kg), whereas the two other solutions were very close. It is believed that the problem could come from a lack of generation or from a possible convergence into a non-global optima. Despite this scatter in fuel optimum, the relative difference is only 0.034%. For comparison purpose, the minimum fuel solution will be taken from the fuel/contrails run. A remark can be made on the limitation of the optimiser to reach the true optimum. As can be seen in Table 8 and Table 9, the cruise altitude of the minimum fuel solution are not always 35000 ft, which should be the case. The maximum discrepancy on the optimum cruise altitude selection in the case of the minimum fuel solution is 0.9%.

From Table 11, a number of results can be pointed out.

- The fuel consumed by the minimum fuel solution is 25% lower compared to the minimum time solution but takes 20.6% more time to fly the same distance. The NO_x emitted by the minimum time solution is significantly higher than any other solutions (about 120% increase on average)
- The NO_x emitted by the minimum NO_x solution is 3.1% lower than the minimum fuel solution, and leads to a fuel and time penalty of 0.7% and 4.1% respectively. On the other hand, the contrails produced are reduced by 1.8%.
- The minimum contrails solution increases the fuel consumed by 0.5%, the time by 1%. The NO_x emitted has not seen any significant changes.
- The change of slope observed for the fuel/time objective Pareto front (Figure 33) can be mostly attributed to two set of variables. The first set is the cruise altitude and the second is the cruise speed. In the steeper part of the Pareto front, cruise altitudes remain at their maximum allowed and time is gained by increasing the cruise speeds. Once cruise speed has been increased to its maximum (M = 0.82 is this case study), the only way to significantly decrease the time of flight is to reduce the cruise flight altitude. This drop in altitude has a higher cost in term of fuel consumption, hence the change in slope of the Pareto front.

5.2.2.2 Discussion of the results

In order to understand the rationale behind the selection of the variables, it is best to compare the evolution of some important variable for each minimised objectives. Figure 36 shows the altitude against the range for the climb phase for each solution.

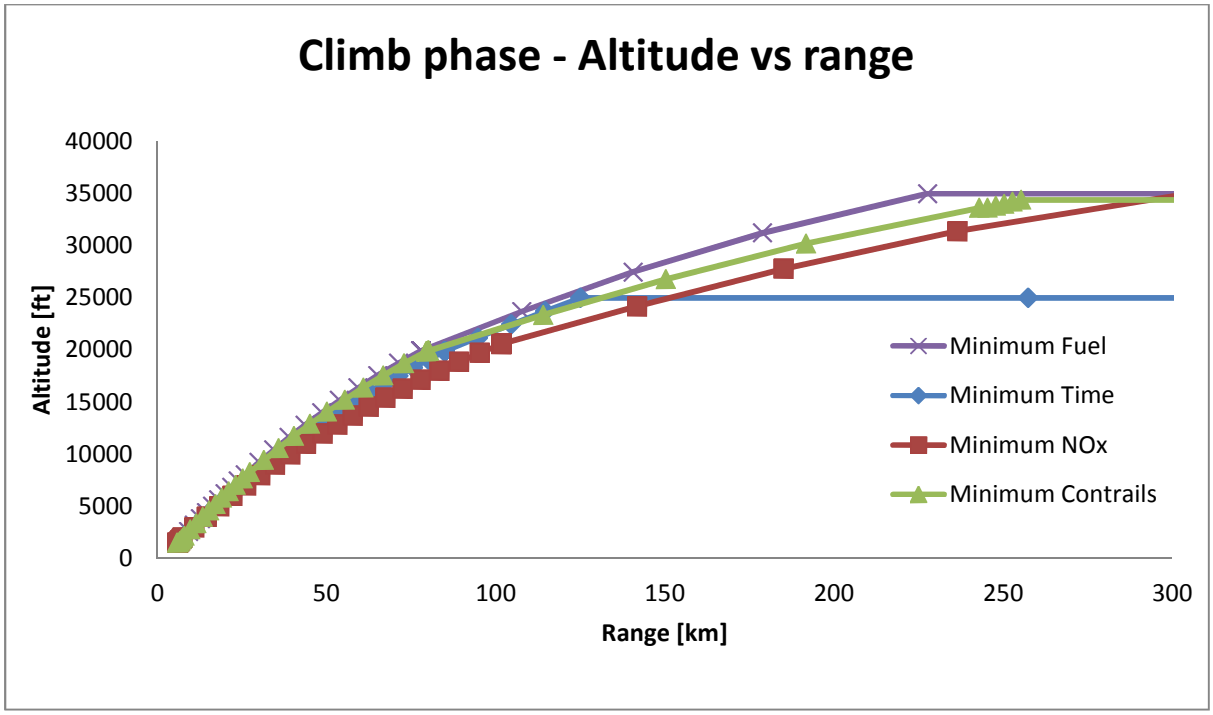

Figure 36 - Altitude vs. range for the minimum fuel, minimum time, minimum NOx and minimum Contrails solutions

It can be seen in Figure 36 that for minimum fuel, minimum time and minimum contrails, the initial climb phase (until 120km) is very similar. The minimum NO_x solution, on the other hand tends to use a lower climb rate. The reason is that the minimum NO_x solution is reducing as much as possible the thrust setting, so that TET remains low thereby limiting NO_x emissions compared to the other solutions. Due to this lower power setting, the rate of climb is lower.

For the minimum time solution, the cruise speed selected is 25000ft, for the obvious reason that since cruise speed is flown using Mach number as the variable. The highest Mach speed available (max M = 0.82) will correspond to a higher true speed if the altitude is lower. In this case the true speed at 25000ft is 494nm/h.

For the minimum fuel solution, the optimiser is selecting the altitude that will correspond to the highest SFC during the cruise phase. This corresponds to the highest available cruising altitude (35000ft).

Regarding the minimum contrails solution, the aim is simply to avoid the contrails formation zone. In these particular atmospheric conditions, flying below about 34300ft is enough to totally avoid contrails. As part of driving the Pareto front to optimality, this solution has also minimised the fuel consumed while avoiding the contrails formation. It can be seen that, depending on given atmospheric conditions, it is possible to avoid contrails with very little fuel consumption penalty.

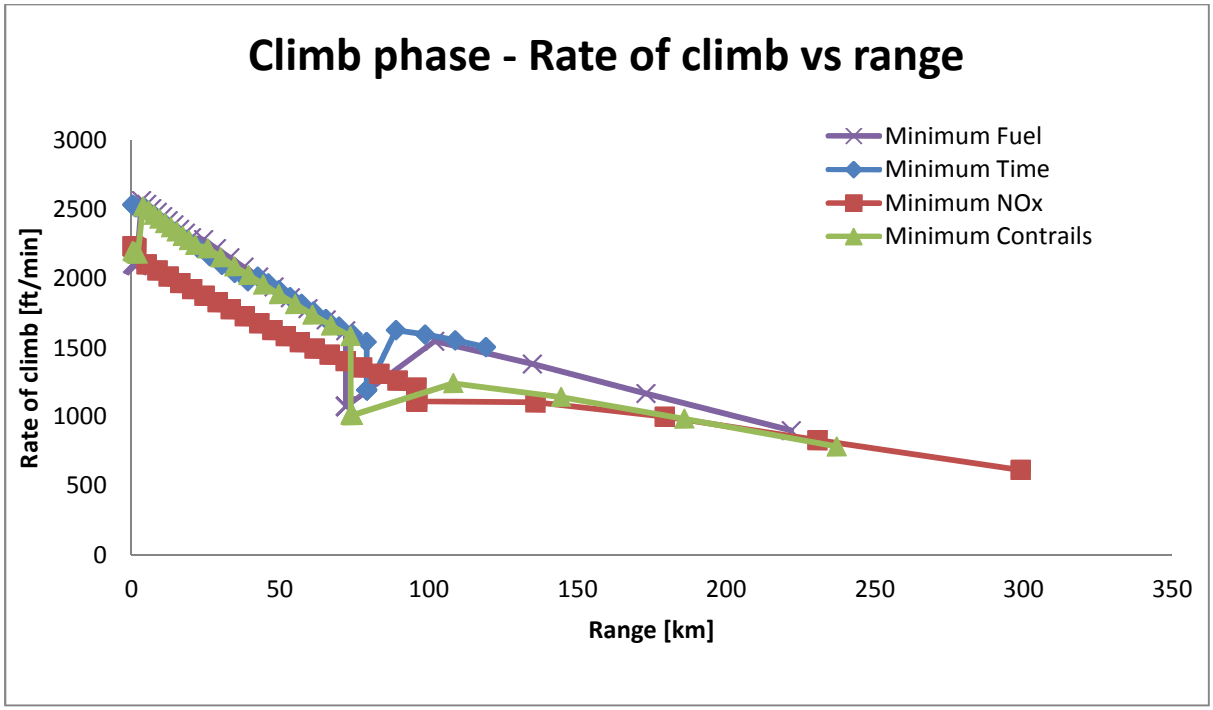

Figure 37 – Rate of climb vs. range for the minimum fuel, minimum time, minimum NO_x and minimum contrails solutions during the climb phase

In Figure 37, the rate of climb is plotted against the range. Apart from the minimum NO_x solution, the other solutions tend to maximise the rate of climb during the early climb phase. At about 70 km range, there are dips in the rate of climb for the minimum fuel, time and contrails solutions. By analysing the data, it was found that the optimiser selected Altitude 3-1 as close as possible to the transition height calculated for each case. This means that the segment 3-1 to transition is effectively reduced to a very small length (typically 1km or less). The most likely reason is that the optimiser selects the highest CAS speed for segment 3-1 to transition and the lowest Mach number after transition (in this case M = 0.65). This leads to the derivation of the lowest possible transition height. Essentially the reason is to switch as early as possible into a cruise climb mode using Mach number as the speed variable. Since the cruise climb speed selected is 0.65 (minimum speed available), the optimiser has effectively chosen to maximise the rate of climb. The rationale behind this choice, is simply to maximise the time spend at cruise where the engine can operate at its maximum efficiency.

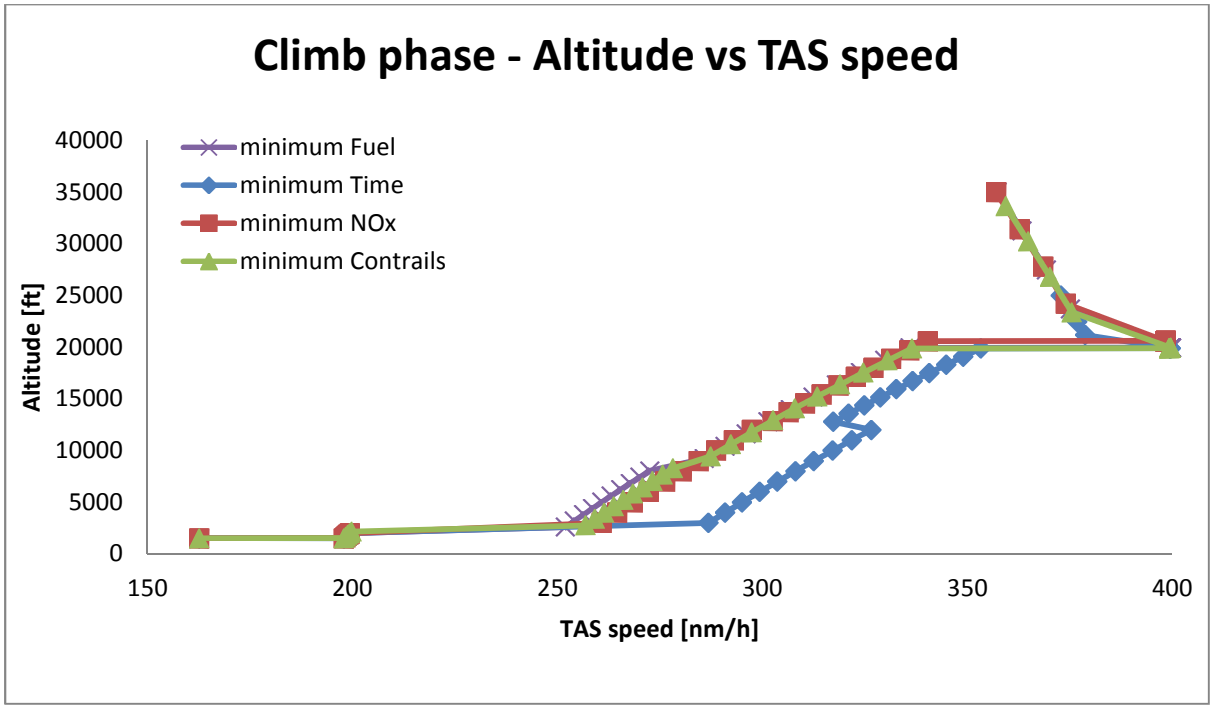

Figure 38 – Altitude vs. TAS for the minimum fuel, minimum time, minimum NO_x and minimum contrails solutions during the climb phase

The altitude against TAS is plotted on Figure 38. The peak speed at around 19000ft is what is expected even from current practice climb profile. Usually, cruise Mach and altitude are set by the air traffic controller. Typically during the climb the aircraft will fly at constant CAS until it reaches the designated Mach speed. From this point the pilot will switch for a constant Mach climb phase. This however rarely happens at the top of climb. As the aircraft continues to climb at constant Mach, the TAS or CAS will logically decrease. This is what we can see on Figure 38.

Apart from the minimum time solution, the other three solutions very closely follow the same TAS evolution with respect to altitude.

Figure 39, shows the variation of TAS against range for the cruise phase. As mentioned, this phase contains five variable altitudes and four Mach speed settings. As expected the minimum time solution simply opts for the highest speed available (M = 0.82 which corresponds to 494nm/h TAS). The minimum fuel solution shows a gradual decrease in speed along the trajectory. In order to optimise fuel during cruise phase, the selection of an optimum Mach speed is crucial. At each cruise segment, the optimiser tries to find the optimum Mach number in order to maximise the specific air range. The specific air range is given by [74]:

$$R_{ac} = -\int_{m1}^{m2} \frac{V}{SFC\beta W} \frac{dm}{m} \qquad [5.1]$$

Where, R_{ac} is the specific air range, V is the speed, SFC is the specific fuel consumption, β is the drag to lift coefficient ratio, W is the aircraft weight. Minimising the term in the integral effectively maximise the specific air range. At each cruise segment, the aircraft mass is reduced by the amount of fuel used during the last segment. To keep the specific air range to its maximum the air speed has to be re-adjusted to slower speed for each cruise segment. The minimum contrails solution speed during cruise is very close to the minimum fuel solution since this solution is essentially the same but with slightly lower cruise altitude to avoid the contrails formation zone. As such, an overall decrease of the speed along the cruise phase can be seen.

The minimum NO_x solution flies the cruise at the minimum Mach number with the aim of reducing the TET during the cruise phase to a minimum.

The small dips seen at around 250, 800, 1500 and 2100km are actually transition from one cruise segment to the next one. The transition happens only when the optimiser selects altitudes that are different between two segments. For example, if the altitude of segment 2 is lower than segment 3, the aircraft model needs to create a climbing section so that the aircraft can reach its next cruising altitude. This generates small variations in aircraft speeds. Again those segments are very short and do not significantly affect the final results of complete trajectories.

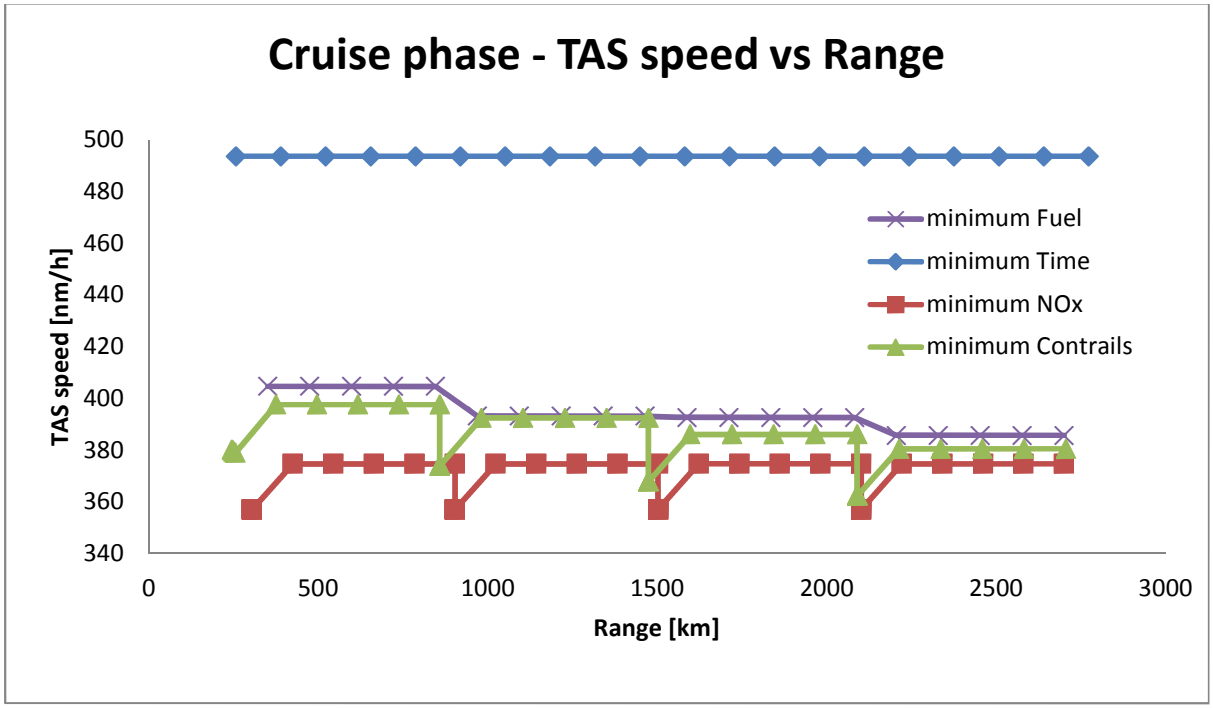

Figure 39 - Rate of climb vs. range for the minimum fuel, minimum time, minimum NO_x and minimum contrails solutions during the cruise phase

Figure 40, shows the TET against range for the climb segment. It is clear that only the best NO_x solution needs to minimise the TET. The TET peak at 100 km comes from the same reason that was described from Figure 37. The range flown during this TET peak is less than 1 km. It also aims at deriving the lowest transition height, so that the constant Mach phase starts as early as possible. A similar dip can be seen for the minimum fuel solution.

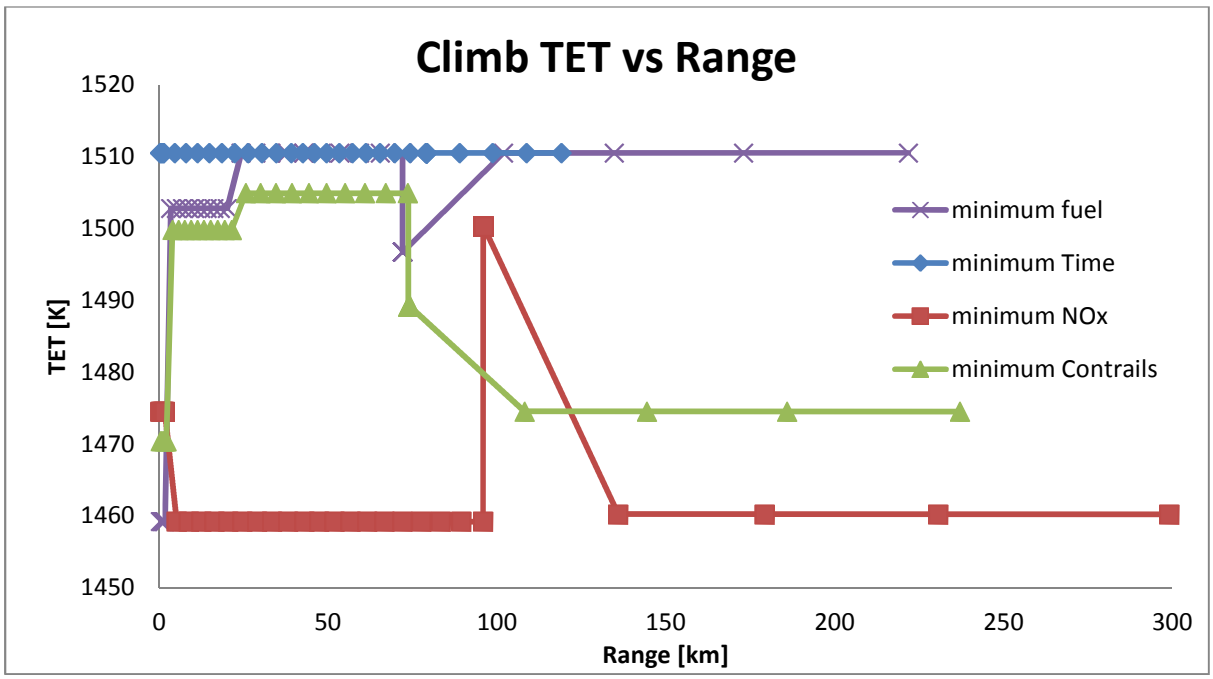

Figure 40 – TET vs. range for the minimum fuel, minimum time, minimum NO_x and minimum contrails solutions during the climb phase

5.2.2.3 Conclusion and further work

This first case study focused on the description of a trajectory optimisation problem involving the minimisation of 2 competing objectives. The optimisation was run for 3 sets of objectives: fuel/time, fuel/NO_x and Fuel/contrails minimisations. Overall, the optimiser has shown good repeatability (less than 0.04%) in convergence when comparing the 3 minimum fuel solutions of each case. It can be noted that even though little difference were found, the overall minimum fuel solution was found for the fuel/contrails objectives run. This solution has the particularity of having the smallest objective range for the final Pareto front. A conclusion that can be drawn is that the range of the objectives plays a role in the ability of the optimiser to find the extremum solutions. It implicitly implies that the search space of the optimiser is stretched thus limiting its ability to find optimum solutions. It is believed that this feature would be worsened if optimisation with 3 or more objectives is attempted. One way of alleviating this issue would be to increase the population size and number of generation but the cost in term of computing time would be significant. From the analysis of the extreme solutions of each optimisation it has been found that the variable

values selected by the optimiser were supported by first principle physics. Some additional conclusions are as follows:

- The Pareto front for the fuel/time and fuel/NO_x generated using the optimiser are showing a smooth continuous evolution. Trajectory trade off can be easily identified for each particular objectives.
- Alternative trajectories have been identified that reduces NO_x emissions without strong fuel penalty. However, the extent of NO_x emissions reduction is rather limited with a fixed engine and/or combustor technology. If seen from the point of view of the ACARE goals, an 80% reduction in NO_x emissions appears difficult to achieve with only trajectory optimisation. It is thus confirmed that technology (in aircraft and/or engine development) improvement needs to be incorporated to achieve the ACARE target.
- Given the flight range for this case study, the climb speeds, climb altitudes, and climb de-rate thrusts have a limited impact on the final objective value. This can be seen in the scatter of optimal value found for the solutions obtained. Only the minimum NO_x solution show a strong tendency at reducing as much as possible the climb de-rate thrust. This seems to indicate some difficulties for the optimiser to find optimum parameters when the global impact is very marginal to the final objective value. It is expected that doing the optimisation with a very short range would strengthen the impact of this set of variable and thus would allow the optimiser to better choose the most optimum set of climb parameters.

Further work might include the following:

- Improving the aircraft model or revising the variable boundaries to avoid the generation of segments for which the length is less than a kilometre while showing large parameter variations. Even though, such segments do not impact significantly on final objectives values, those are still unlikely to happen in a real life aircraft trajectory and should be avoided.
- It is expected that increasing the number of variables during the climb phase will lead to better optimised trajectory.
- The methodology used to obtain the results can be easily expanded to other type of objective such as flight cost or noise estimation by using additional models.

5.2.3 CASE 2: FUEL/NO_X/CONTRAILS OBJECTIVES USING LPP COMBUSTOR

The second test case is essentially based on the same set of models and optimisation setup. The aircraft and engine models remains the same, the variable set is the same as in Case 1 with the same boundaries. Thus in this case, only the emissions model is replaced. In case 1, the emissions model was representing a conventional combustor (annular type). In case 2, the model is a potential development of Lean Premixed Pre-vaporised combustor that could be fitted on future engines. The model used in this case has been described in section 4.3. One important feature of the modelled LPP is that it includes variable geometry. This essentially means that temperature at the flame front can be controlled to a certain extent. Is this case study the equivalence ratio at the flame front was set at 0.6. Using such a low equivalence ratio will inevitably lead to low NO_x formation rate at the flame front. On the other hand the LPP combustor also comprises a pilot zone which is assumed to operate throughout the flight. This zone is burning fuel similar to conventional combustors flame front region (close to stoichiometry, not fully mixed and vaporised). Even though the air and fuel mass flow rate is set to low values for this region, it will lead to NO_x formation.

Two optimisation runs were performed; a fuel/NO_x and NO_x/contrails minimisation objectives. The Pareto fronts that have been obtained are shown in Figure 41 and Figure 42.

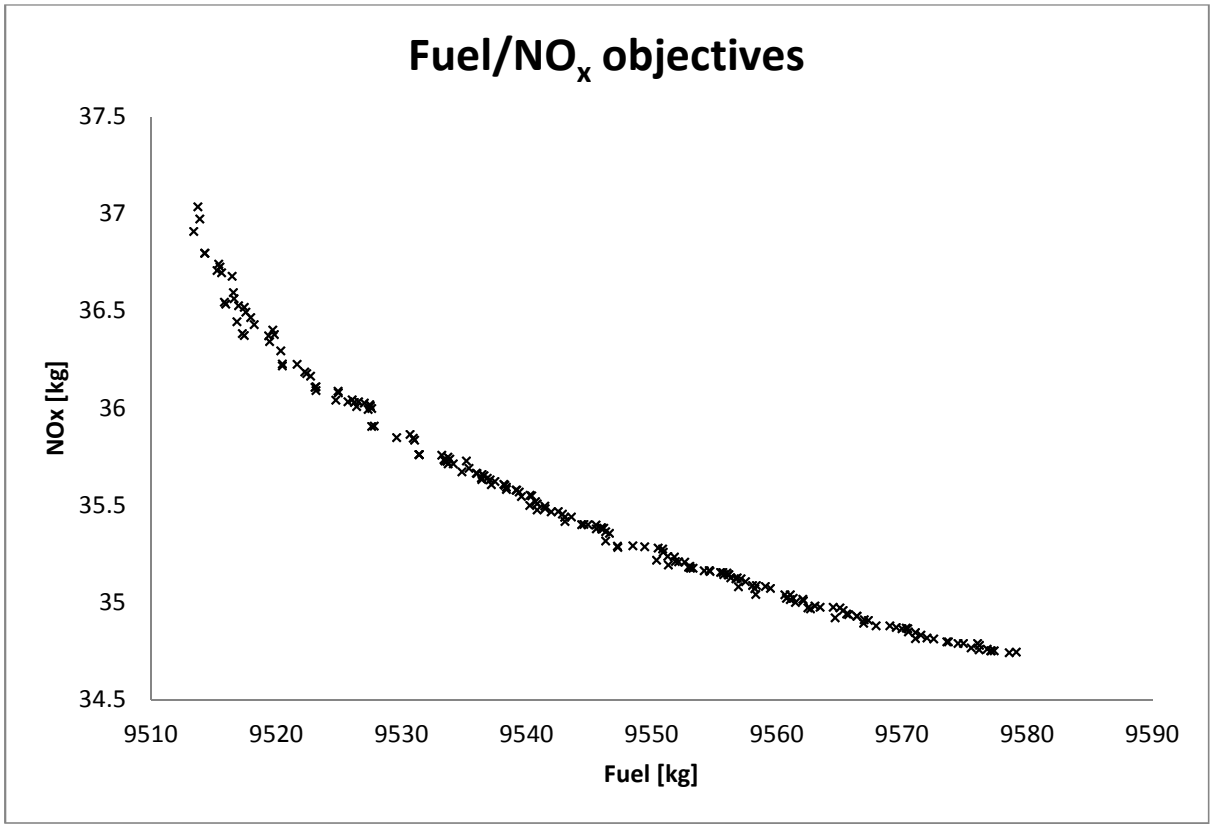

Figure 41 - Pareto front results for the fuel and NO_x objectives

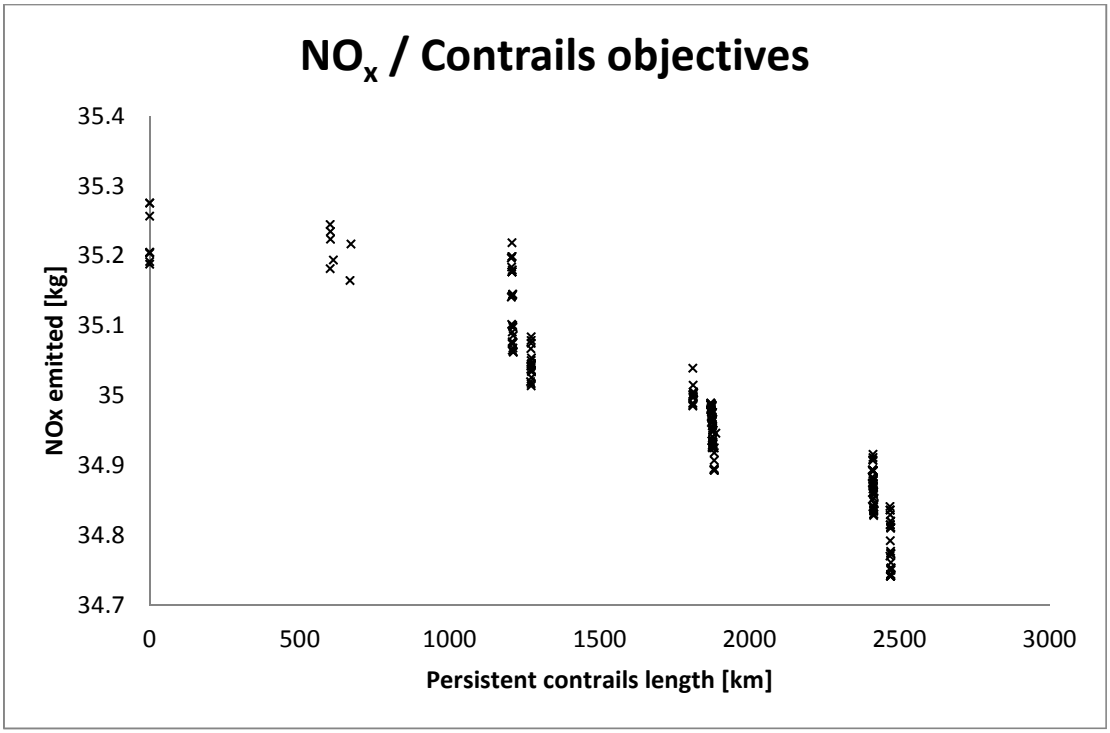

Figure 42 - Pareto front results for the NO_x and contrails objectives

Table 12 – Variables selected for the fuel/NO_x optimisations

	Fuel / NO_x objectives	
Variable name	Minimum fuel solution	Minimum NO_x solution
Climb speed 2 – 3 (CAS)	238	212
Climb speed 3 – 31 (CAS)	250	251
Climb speed 31 - transition	300	299
Climb speed after transition (Mach)	0.65	0.65
Climb Altitude 2	2017	2010
Climb Altitude 3	9058	11961
Climb Altitude 31	19900	20089
Climb de-rate thrust 1 (%)	100	91
Climb de-rate thrust 2 (%)	99	90
Climb de-rate thrust 3 (%)	100	90
Climb de-rate thrust 4 (%)	100	100
Climb de-rate thrust 5 (%)	95	90
Cruise altitude 1	35000	35000
Cruise altitude 2	35000	34986
Cruise altitude 3	34997	34998
Cruise altitude 4	34975	34984
Cruise altitude 5	34981	34996
Cruise speed 1-2 (Mach)	0.70	0.65
Cruise speed 2-3 (Mach)	0.69	0.65
Cruise speed 3-4 (Mach)	0.67	0.65
Cruise speed 4-5 (Mach)	0.67	0.65

Table 13 - Variables selected for the NO_x/contrails optimisations

	NO_x / Contrails objectives	
Variable name	Minimum NO_x solution	Minimum Contrails solution
Climb speed 2 – 3 (CAS)	217	204
Climb speed 3 – 31 (CAS)	251	250
Climb speed 31 - transition	298	287
Climb speed after transition (Mach)	0.65	0.65
Climb Altitude 2	2000	2063
Climb Altitude 3	12000	11961
Climb Altitude 31	20294	21728
Climb de-rate thrust 1 (%)	90	93
Climb de-rate thrust 2 (%)	90	90
Climb de-rate thrust 3 (%)	90	91
Climb de-rate thrust 4 (%)	100	100
Climb de-rate thrust 5 (%)	90	90
Cruise altitude 1	35000	34310
Cruise altitude 2	34999	34372
Cruise altitude 3	34999	34352
Cruise altitude 4	34998	34403
Cruise altitude 5	34999	34405
Cruise speed 1-2 (Mach)	0.65	0.65
Cruise speed 2-3 (Mach)	0.65	0.65
Cruise speed 3-4 (Mach)	0.65	0.65
Cruise speed 4-5 (Mach)	0.65	0.65

Table 14 – Summary of results for both optimisations

	Fuel/NO_x run		NO_x/Contrails run	
	Minimum Fuel	Minimum NO_x	Minimum NO_x	Minimum Contrails
Fuel (kg)	**9513**	9579	9577	9631
Time (min)	259	270	270	270
NO_x (kg)	36.9	**34.7**	**34.7**	**35.2**
Contrails (km)	2505	2469	2469	0

In term of solution found, Table 12, Table 13 and Table 14 show that in both optimisation run, the same minimum NO_x solution has been found. This gives good confidence that the solution obtained is very close to the global optimum. Also, the minimum fuel solution is very close to the solution found in case 1, which indicates that convergence was reached.

5.2.3.1 Result discussion

It is evident from the results of this case study that the NO_x emitted is less than in case study 1. However such comparison cannot be done mainly because the LPP combustor does not exist and as such it was not possible the fit the emissions model to actual measurement (as it is done for conventional engine using conventional combustor with the help of ICAO emissions databank). However, it is interesting to see that the Pareto front formed is very similar in shape. As expected the range of value for the fuel consumed for the fuel/NO_x case is very close to the one found in case 1. It appears that even though the combustor model has a specific variable geometry feature, the best solution obtained for the minimum NO_x has still the same characteristic of the one found in case 1. Those main characteristics are flying the climb segment at low power settings, cruise at the highest altitude of 35000 ft and the slowest cruise speed available i.e. M=0.65. This means that all the reduction of NO_x seen in this case is directly stemming from the LPP combustor. If such combustor was to be developed the advantage in NO_x reduction would be of about 50% compared to the minimum NO_x solution found in case 1. Such type of technology improvement would therefore be extremely valuable to reach the goal of 80% reduction in NO_x emissions.

Figure 43 shows the amount of NO_x emitted per kilometre flown for the 3 extreme solutions. One can see that the solution for minimum NO_x and minimum contrails formation are extremely close. This by itself can explain why the difference between both solutions in term of NO_x emitted is only 1.4%. Even though for the minimum NO_x solution, the amount of NO_x emitted per kilometre is constantly lower than the other 2 solutions.

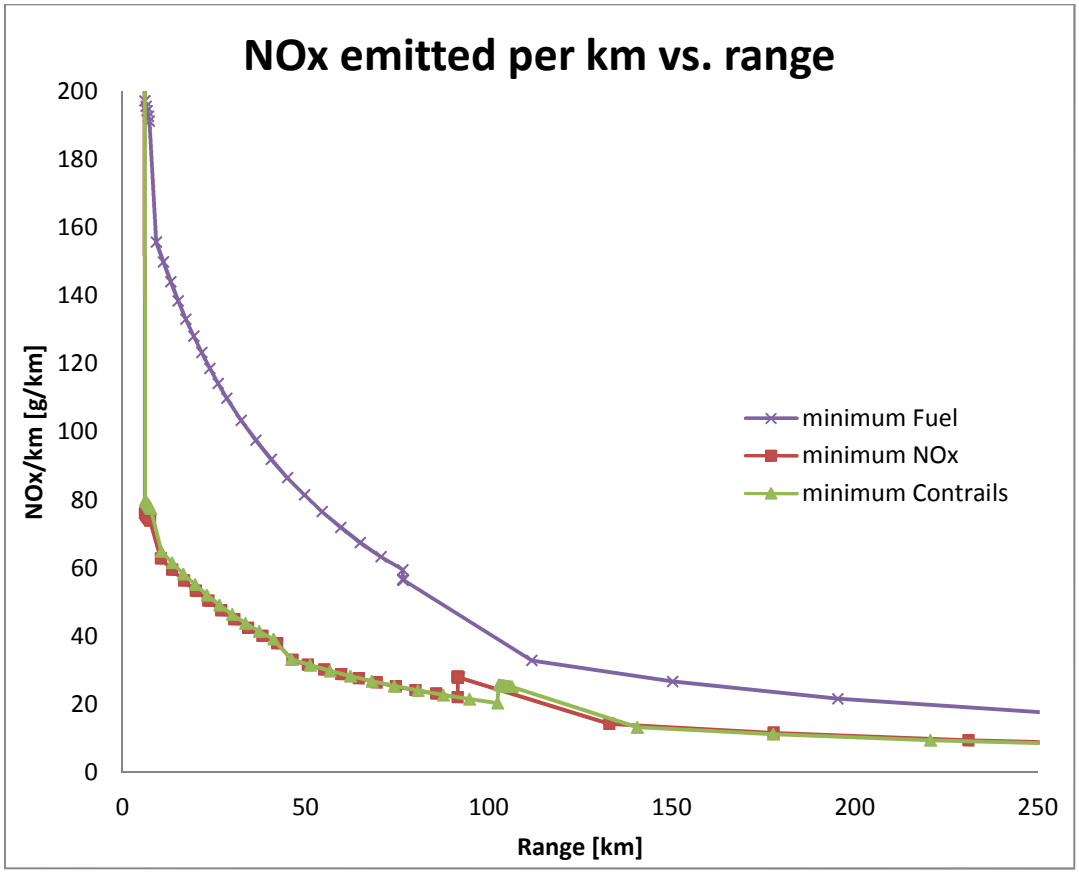

Figure 43 – NO_x emitted per kilometre flown for the minimum fuel, minimum NO_x and minimum contrails solutions during the climb phase.

5.2.3.2 Conclusions/Further work

The conclusion of the case 2 is that changing the combustor to a hypothetical LPP combustor fitted on a high by-pass engine does not modify the optimum trajectory parameter such as climb thrust settings, cruise altitude and cruise Mach speed. As the LPP has inherent lower NO_x emissions index than a conventional combustor, the final NO_x emitted from such trajectory was about half that of the conventional combustor. On the other hand the range of trade off with fuel that is available to the LPP combustor is very similar to the one found in case 1.

Further work includes looking at finding relevant data that could enable a validation of the NO_x prediction of the LPP combustor emissions model. The use of CFD analysis could add valuable information if no other data is available. Modelling of other type of advanced combustors, if properly validated, could provide a powerful way of comparing various combustor technologies in term of NO_x reduction based on optimum trajectories.

5.3 SIMULTANEOUS TRAJECTORY AND ENGINE CYCLE OPTIMISATION

5.3.1 OVERVIEW

The following case studies have been designed to optimise trajectory parameters and engine related parameters within the same optimisation run. The objective of this case study is to demonstrate the capabilities offered by the framework and associated models in term of comparison and ranking of numerous possible solutions using only a few optimisation runs. The reader must be aware that those test cases may not be representative of real life operation due to the assumptions made and that will be described in the following section. A number of constraints have been imposed on the engine design parameter so as to ensure the highest level of fidelity with the available models. This also ensures that comparison can be made on a consistent basis. The rational for simultaneous trajectory and engine cycle optimisation can be seen from the early design point of view. One benefit is shortening the early design phase since both engine and trajectory are taken into account to obtain general design trends with respect to fuel consumption and any other important objectives to achieve. The purpose of this case study is to validate the concept by checking the range of optimised solutions. It is expected that given different objectives, different group of solutions will be identified through the optimisation process. Also, from the operator point of view, who has limited flexibility over aircraft and engine design, this type of simultaneous optimisation can be useful to determine a best possible aircraft/engine/trajectory design and from the obtain solutions derive a so called ideal case. From these ideal cases an operator can then compare by how far a given design is against the ideal case.

5.3.2 PROBLEM SETUP

The case studies comprise the same models as in case 1 and 2. Case 3 uses the conventional combustor emissions model. As mentioned the variable used are trajectory and engine cycle related. Table 16 details the 28 variables used for this case study with their associated boundaries. All variables related to the trajectory part are the same as in case 1 and 2. The 7 additional variables all relate to engine design point parameters. The engine model used is the one from case 1 and 2, that is, a two-spool turbofan engine similar to the CFM56-7B27. The original engine design parameters are summarised in Table 15.

Table 15 – Original engine model (model of a CFM56 7B27) parameters as used in case 1 and 2

Design point at Top of climb (35000ft, M0.80, ISA conditions)		
Parameter name	Unit	Value
BPR	-	5.2

FPR	-	1.77
LPC PR	-	1.88
HPC PR	-	9.83
OPR	-	32.7
$\dot{m}_A$	kg/s	140
TET	K	1510
FN	kN	26.5
SFC	mg/(N.s)	16.2
Off-design performance (Take-off, SLS, ISA conditions)		
TET	K	1682
FN	kN	121.4
$\dot{m}_A$	Kg/s	350

Table 16 – List of variables and associated ranges

Variable name	Unit	Range (min - max)
Climb speed 2 – 3 (CAS)	knot	200-275
Climb speed 3 – 31 (CAS)	knot	250-300
Climb speed 31 – transition (CAS)	knot	250-300
Climb speed after transition (Mach)	-	0.65-0.78
Climb Altitude 2	feet	2000-4000
Climb Altitude 3	feet	8000-12000
Climb Altitude 31	feet	13000-27000
Climb de-rate thrust 1 (%)	-	90-100
Climb de-rate thrust 2 (%)	-	90-100
Climb de-rate thrust 3 (%)	-	90-100
Climb de-rate thrust 4 (%)	-	90-100
Climb de-rate thrust 5 (%)	-	90-100
Cruise altitude 1	feet	25000-35000
Cruise altitude 2	feet	25000-35000
Cruise altitude 3	feet	25000-35000
Cruise altitude 4	feet	25000-35000
Cruise altitude 5	feet	25000-35000
Cruise speed 1-2 (Mach)	-	0.65-0.82
Cruise speed 2-3 (Mach)	-	0.65-0.82
Cruise speed 3-4 (Mach)	-	0.65-0.82
Cruise speed 4-5 (Mach)	-	0.65-0.82
By-pass ratio	-	4.5-6.0
Fan pressure ratio	-	1.6-1.85
High pressure compressor pressure ratio	-	8.0-11.0
Low pressure compressor pressure ratio	-	1.5-2.5
Mach design point @ top of climb	-	0.75-0.85
TET design point @ top of climb	K	1450-1600
Altitude design point @ top of climb	feet	32808-39370

It can be seen from Table 16 that the boundaries selected for the engine design point parameter do not allow for very large design modification. For example, the pressure ratios for the compressor elements allow for a minimum overall pressure ratio (OPR) of around 20 and a maximum of around 50. These figures are within the range of today's engine OPRs. It is assumed that compressor and turbine have the same efficiency and that the number of stages remains constant.

The reason of allowing the altitude design point of the engine to vary is that since the trajectory parameter are varying (especially the cruise altitude), it is necessary to allow the engine design point altitude to also vary to reach the best design point selection.

In addition to new engine related variables, constraints needs to be added in order to ensure realistic engine sizing. Table 17, shows the list of constraints added.

Table 17 – List of constraints used in case study 3

Constraint name	Constraint type	Value	unit
Compressor delivery temperature @ take-off (off-design)	Less than	950	K
Compressor delivery temperature @ top of climb (design point)	Less than	950	K
Specific thrust @ top of climb	Greater than	180	N/(kg/s) or m/s
Blade height	Greater than	16	mm

The compressor delivery temperature at take-off has been selected as a constraint to reflect the strength limit of material used in current turbo fan technology. A limit of 950K was selected. For the same reasons, a limit of 950 K has been set for the compressor delivery temperature at top of climb. This ensures that the engine is not running hotter than the take-off operating point.

In order to force any potential engine design to be realistic, the blade height of the last stage of the high pressure compressor has to show a minimum of 16 mm. This value was set, so that loss due to blade tip clearance does not become unrealistically high. It is also expected that blade smaller than 16 mm will become increasingly difficult to manufacture, and would result in poor aerodynamic performance. The blade height is estimated using equation 5.2 [21], assuming a flow Mach number of 0.3 and a compressor hub/tip ratio of 0.9 at the outlet of the high pressure compressor.

$$\frac{\dot{m}_A\sqrt{T}}{AP} = M\sqrt{\frac{\gamma}{R}}\left\{1+\frac{\gamma-1}{2}M^2\right\}^{\frac{-(\gamma+1)}{2(\gamma-1)}} \qquad [5.2]$$

Where $\dot{m}_A$ is the air mass flow rate, T is the total temperature, A is the flow area, P is the pressure, M the Mach number, R is the specific gas constant and γ the ratio of specific heat of air. This method is a simplification, for more accurate calculation of blade height a fully regressed method as presented in [78] would be necessary.

The last constraint, i.e. the specific thrust, is necessary to force any design to have similar overall mass flow rate. This ensures that all engine designs require similar intake area (which would lead to similar engine drag component) and that globally different engine designs will end up with similar weight. This constraint was absolutely necessary since the model suite does not include a weight model for the engine and does not recalculate engine drag at every iteration. Thus, the framework is unable to update the total aircraft mass and drag for each engine design. A minimum specific thrust of 180 N/(kg/s) was selected since it is the value found for the original engine model.

To ensure that the engine is able to provide enough thrust for the aircraft, two design constants have been fixed. Take-off net thrust is set at 121440 N (sea level, static) and top of climb net thrust is set at 26511 N (at 32000 feet and 0.8 Mach). Those constants are essentially the one used by the original engine model as seen in cases 1 and 2. This ensures that every new engine designs meet the baseline engine in term of thrust performance.

5.3.3 CASE 3: FUEL/TIME/NO_X/CONTRAILS OBJECTIVES USING CONVENTIONAL COMBUSTOR

In this case study, a series of three optimisation runs was performed, each optimisation being a two-objective optimisation. Similar to case one, the objectives to minimise were fuel/time, fuel/NO_x and fuel/contrails. As mentioned in the previous section, the aim is to optimise aircraft trajectory and engine design parameters simultaneously. Since the trajectory parameters and their boundaries are the same as in case 1, it will be possible to compare the benefits of varying engine design parameters.

Figure 44 to Figure 46 show the Pareto front obtained for each of the three optimisation runs.

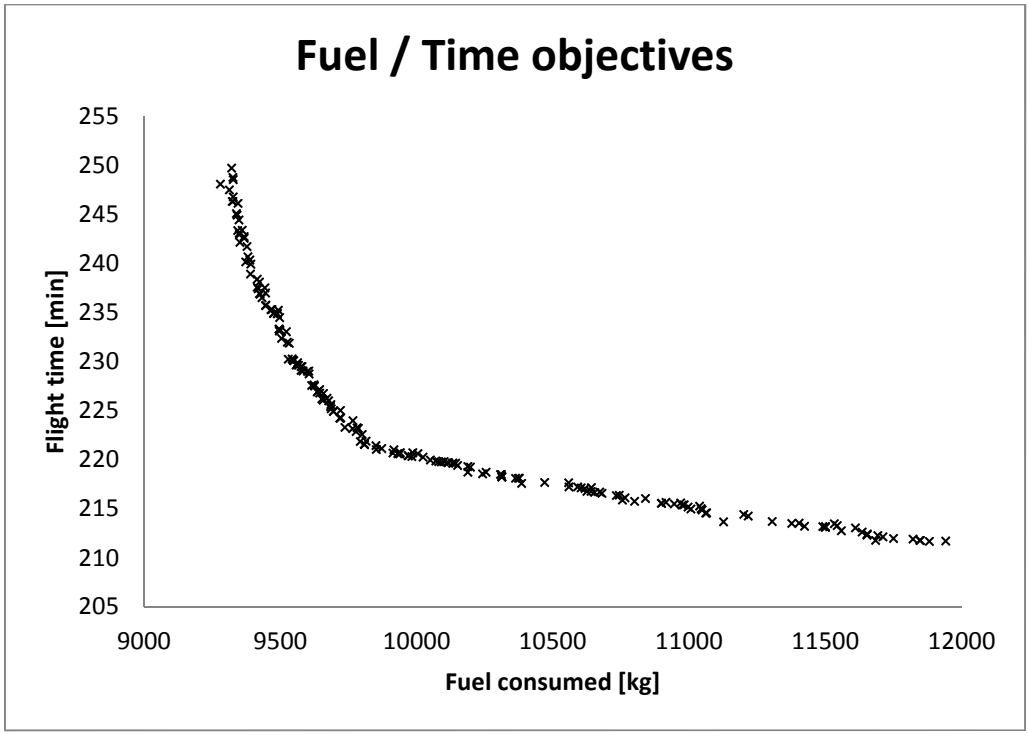

Figure 44 - Pareto front results for the fuel and time objectives

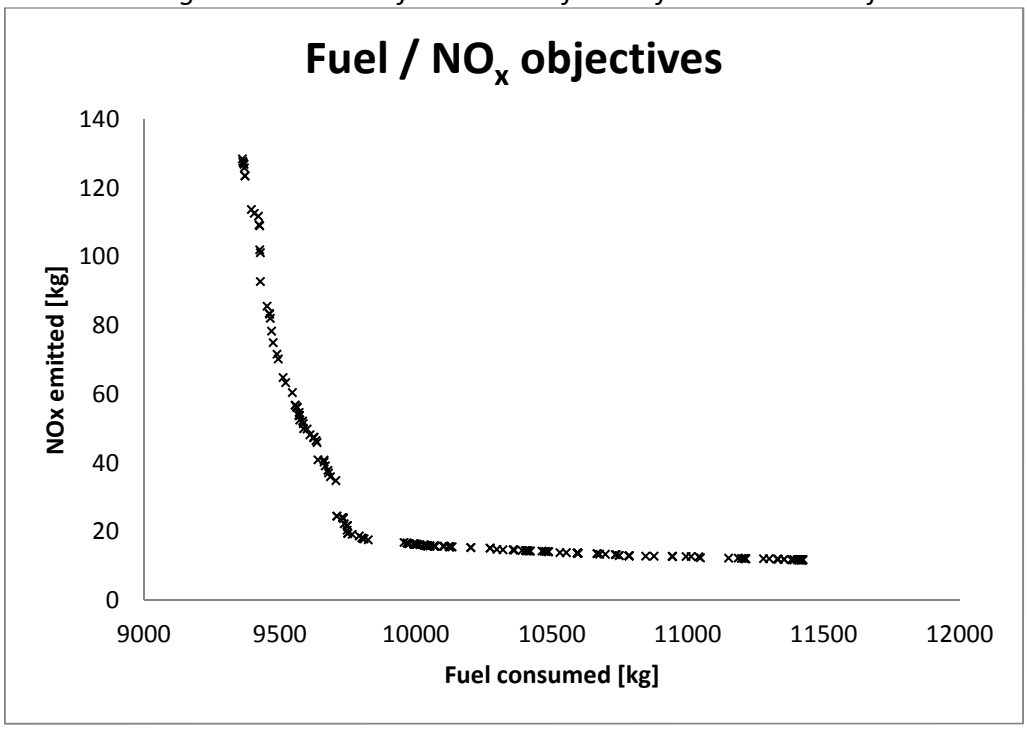

Figure 45 - Pareto front results for the fuel and NO_x objectives

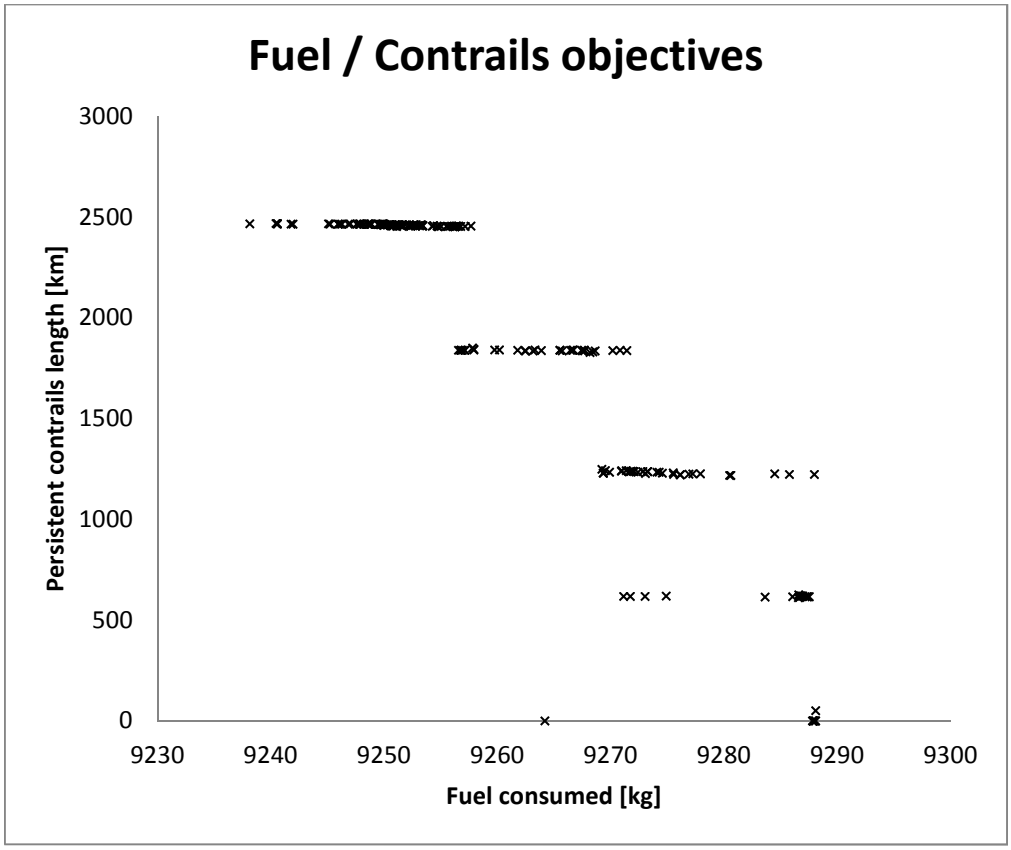

Figure 46 - Pareto front results for the fuel and contrails objectives

It can be seen that overall, those three Pareto front have a very similar shape as the one from case 1. The main differences lies with the global position of the Pareto fronts obtained. For example, in the fuel/time optimisation the Pareto obtained in shifted toward slightly lower fuel consumed. Also in the fuel/NO_x optimisation, the minimum NO_x solution is globally reduced compared to case 1. In addition, the range of solution is largely increased compared to case 1.

Table 18, Table 19 and Table 20 summarise the parameters selected by the optimiser for the extremum obtained for each optimisation run.

Table 18 – Variables selected for the minimum fuel and minimum time solutions

	Fuel / time objectives	
Variable name	Minimum fuel solution	Minimum time solution
Climb speed 2 – 3 (CAS)	252	275
Climb speed 3 – 31 (CAS)	250	280
Climb speed 31 – transition (CAS)	292	300
Climb speed after transition (Mach)	0.65	0.65
Climb Altitude 2	2235	2000
Climb Altitude 3	8177	8003
Climb Altitude 31	18581	13000
Climb de-rate thrust 1 (%)	95	92

Climb de-rate thrust 2 (%)	100	100
Climb de-rate thrust 3 (%)	97	94
Climb de-rate thrust 4 (%)	100	99
Climb de-rate thrust 5 (%)	100	100
Cruise altitude 1	28519	25000
Cruise altitude 2	34750	34797
Cruise altitude 3	35000	25012
Cruise altitude 4	35000	29835
Cruise altitude 5	34875	25000
Cruise speed 1-2 (Mach)	0.78	0.82
Cruise speed 2-3 (Mach)	0.72	0.82
Cruise speed 3-4 (Mach)	0.69	0.82
Cruise speed 4-5 (Mach)	0.68	0.82
By-pass ratio	5.91	6.00
Fan pressure ratio	1.67	1.60
High pressure compressor pressure ratio	10.83	10.91
Low pressure compressor pressure ratio	2.25	2.19
Overall pressure ratio	40.7	38.2
Mach design point @ top of climb	0.75	0.77
TET design point @ top of climb	1588	1599
Altitude design point @ top of climb	32808	37749

Table 19 - Variables selected for the minimum fuel and minimum NO_x solutions

	Fuel / NO_x objectives	
Variable name	Minimum fuel solution	Minimum NO_x solution
Climb speed 2 – 3 (CAS)	247	211
Climb speed 3 – 31 (CAS)	255	255
Climb speed 31 – transition (CAS)	251	250
Climb speed after transition (Mach)	0.65	0.65
Climb Altitude 2	3760	4000
Climb Altitude 3	10165	11996
Climb Altitude 31	13659	13001
Climb de-rate thrust 1 (%)	95	97
Climb de-rate thrust 2 (%)	99	91
Climb de-rate thrust 3 (%)	98	100
Climb de-rate thrust 4 (%)	100	100
Climb de-rate thrust 5 (%)	94	100
Cruise altitude 1	25000	34970
Cruise altitude 2	34822	34999
Cruise altitude 3	34972	35000
Cruise altitude 4	35000	34920
Cruise altitude 5	34856	35000
Cruise speed 1-2 (Mach)	0.66	0.65

Cruise speed 2-3 (Mach)	0.69	0.65
Cruise speed 3-4 (Mach)	0.67	0.65
Cruise speed 4-5 (Mach)	0.67	0.65
By-pass ratio	6.00	4.52
Fan pressure ratio	1.69	1.61
High pressure compressor pressure ratio	8.98	8.00
Low pressure compressor pressure ratio	2.5	1.5
Overall pressure ratio	37.9	19.3
Mach design point @ top of climb	0.75	0.75
TET design point @ top of climb	1590	1600
Altitude design point @ top of climb	32808	36003

Table 20 – Variables selected for the minimum fuel and minimum contrails solutions

	Fuel / contrails objectives	
Variable name	Minimum fuel solution	Minimum contrails solution
Climb speed 2 – 3 (CAS)	241	248
Climb speed 3 – 31 (CAS)	252	253
Climb speed 31 – transition (CAS)	282	277
Climb speed after transition (Mach)	0.65	0.65
Climb Altitude 2	2053	2000
Climb Altitude 3	9451	9730
Climb Altitude 31	22977	23231
Climb de-rate thrust 1 (%)	91	93
Climb de-rate thrust 2 (%)	96	95
Climb de-rate thrust 3 (%)	99	98
Climb de-rate thrust 4 (%)	94	95
Climb de-rate thrust 5 (%)	92	92
Cruise altitude 1	32872	33650
Cruise altitude 2	35000	34368
Cruise altitude 3	34954	34234
Cruise altitude 4	34856	34417
Cruise altitude 5	35000	34363
Cruise speed 1-2 (Mach)	0.69	0.67
Cruise speed 2-3 (Mach)	0.68	0.68
Cruise speed 3-4 (Mach)	0.67	0.67

Cruise speed 4-5 (Mach)	0.67	0.67
By-pass ratio	5.49	5.50
Fan pressure ratio	1.70	1.70
High pressure compressor pressure ratio	10.71	10.86
Low pressure compressor pressure ratio	2.32	2.31
Overall pressure ratio	42.2	42.6
Mach design point @ top of climb	0.75	0.77
TET design point @ top of climb	1559	1562
Altitude design point @ top of climb	33470	33470

Table 21 provides the results obtained for each optimisation run.

Table 21 – Summary of results for the 3 optimisation runs

	Fuel/time run		Fuel/NO_x run		Fuel/Contrails run	
	Minimum Fuel	Minimum Time	Minimum Fuel	Minimum NO_x	Minimum Fuel	Minimum Contrails
Fuel (kg)	**9280**	11880	**9362**	11422	**9238**	9264
Time (min)	248	**212**	262	272	261	261
NO_x (kg)	167	155	129	**12**	165	176
Contrails (km)	2438	103	2493	2477	2467	**0**

A number of remarks can be pointed out from Table 21:

- As with case 1, the minimum fuel solution obtained has been found for the fuel/contrails objectives optimisation. One reason that can explain this result is that the optimiser has more difficulties at finding extremum solutions when objectives range is larger. In the case of fuel/contrails, the differences between the two extremum solution is very small, this is due to the fact that generally the only difference between a minimum fuel solution and a minimum

contrails solution comes from the cruise altitude at which the aircraft is flying. In other word the most important parameter to avoid contrails is altitude. This feature allows the optimiser to use more evaluations at exploring a smaller search space, and thus allowing it to find better solutions.

- When compared to case 1, the fuel burned for the minimum fuel solution has been reduced by 274kg (2.9%) and can be attributed to the additional engine parameter variations.
- The minimum NO_x solution has been significantly reduced compared to the minimum NO_x solution from case 1. It can be seen that from all the solutions obtained in this case study, the minimum NO_x solution is where the largest change in engine design parameter occurs. The reduction of NOx compared to case study 1 is 83% but with a 19% extra fuel cost.
- The fuel consumed for the minimum fuel solution is 22.2% lower than the minimum time solution.
- As opposed to case study 1, the NO_x emitted for the minimum time solution remains similar but all other solutions give higher NO_x emission (apart from the minimum NO_x solution for obvious reasons). This indicate that the engine parameter have been changed in order to gain reductions but at the expense of degrading other objective figures.
- In term of fuel consumed, the difference between the minimum fuel and the minimum contrails produced solution is very small with only 0.3% fuel penalty.

5.3.3.1 Discussion of the results

Figure 47 shows the climb phase altitude variation against the range and Figure 48 is a plot of the altitude against TAS also for the climb phase. These figures clearly show that the climb phase does not change radically when compared to the case study 1. The minimum time solution is still defined by the selection of the highest speeds available and the lowest cruise altitude. This solution was expected since time is completely defined by the trajectory parameter, whereas engine design parameter would not bear impact on the time calculated to fly a given trajectory.

However some changes can be seen for the minimum NO_x solution. In this case, the minimum NO_x solution shows the fastest climb to cruise level. Figure 49 also shows an overall higher rate of climb during most of the climb phase. This was not the case in case study 1.

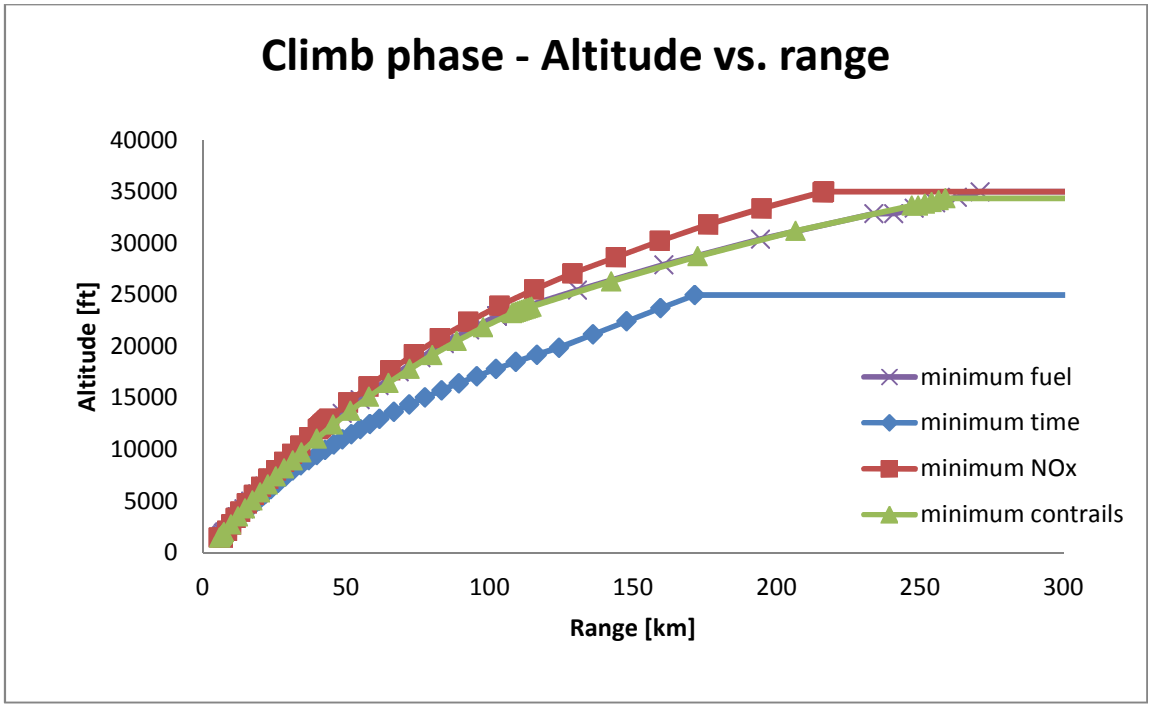

Figure 47 - Altitude vs. range for the minimum fuel, minimum time, minimum NO_x and minimum contrails for the climb phase

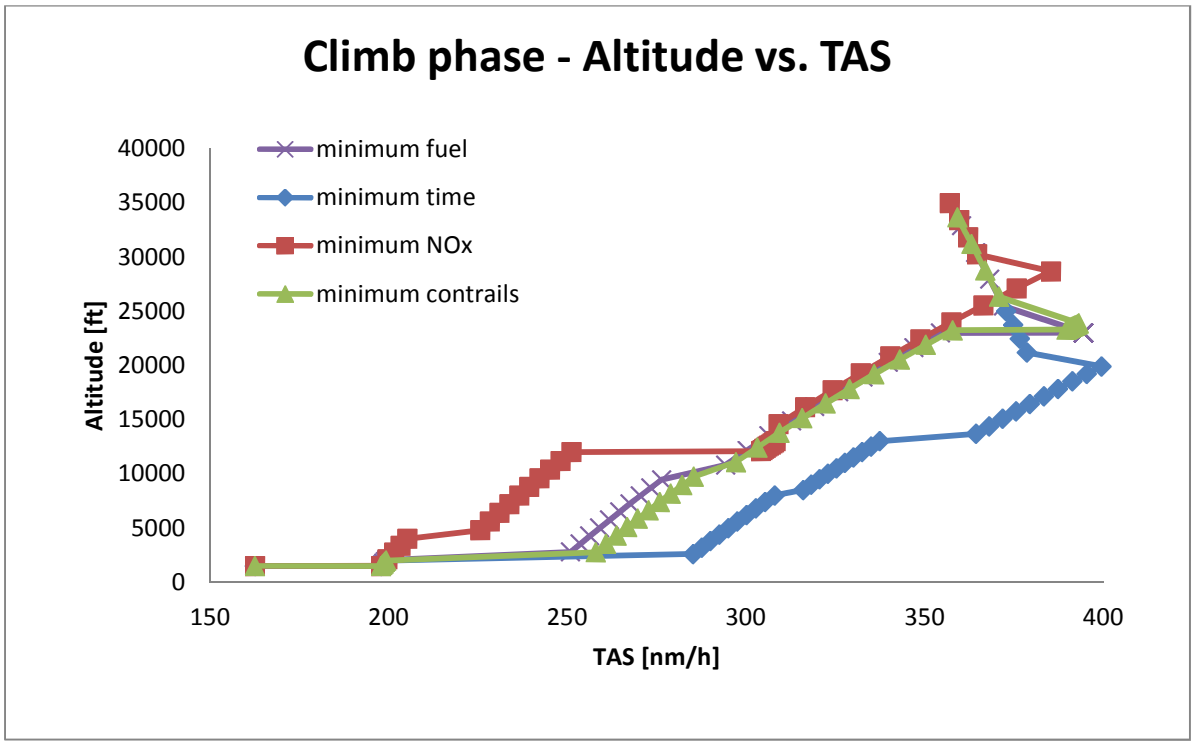

Figure 48 – Altitude vs. TAS for the minimum fuel, minimum time, minimum NO_x and minimum contrails for the climb phase

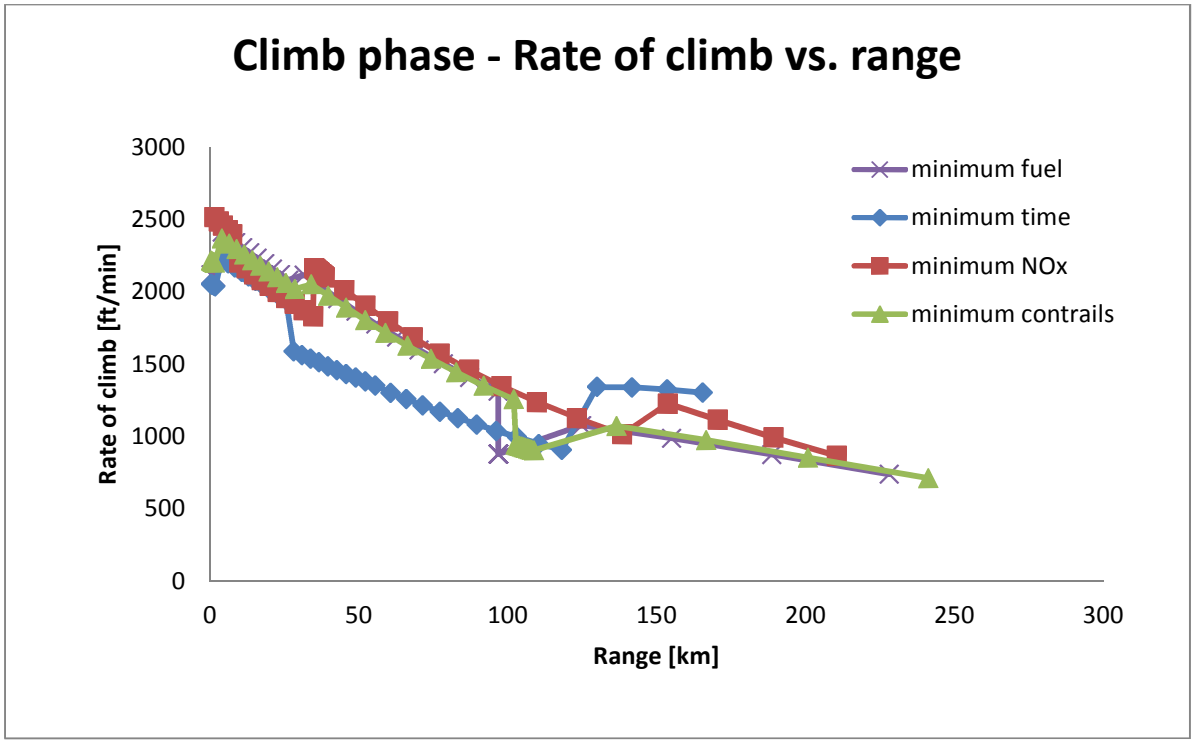

Figure 49 – Rate of climb vs. range for the minimum fuel, minimum time, minimum NO_x and minimum contrails for the climb phase

Figure 50 and Figure 51 are plots of the TET versus range and $EINO_x$ versus range respectively. Both figures show the evolution of the climb phase. The main point of Figure 50 is that the TET values for the minimum NO_x solution are unexpectedly higher than the other three solutions. This appears as a paradox, since it is well known that usually higher TET leads to high NO_x emissions. However, even though the TET along the climb is high, the $EINO_x$ calculated by the emissions model remains consistently low for the whole climb phase. Figure 52 shows the emitted NO_x per kilometre flown against the range. This also shows smaller emissions for the low NO_x solution.

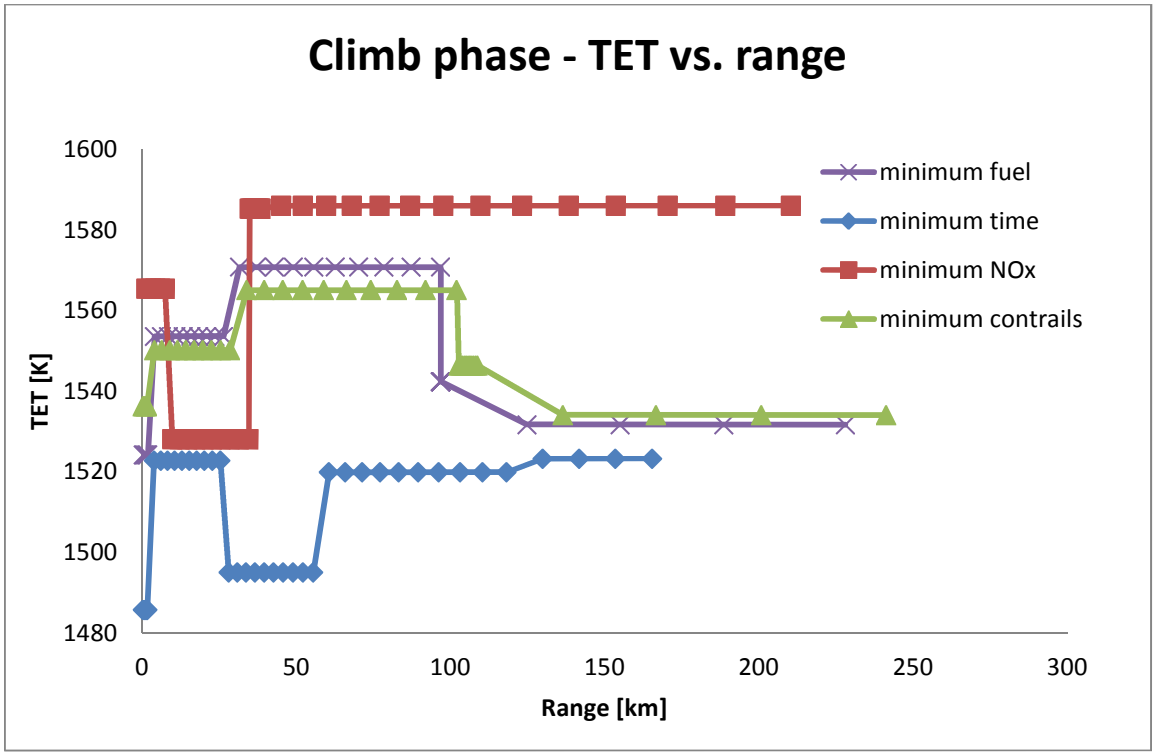

Figure 50 - TET vs. range for the minimum fuel, minimum time, minimum NO_x and minimum contrails for the climb phase

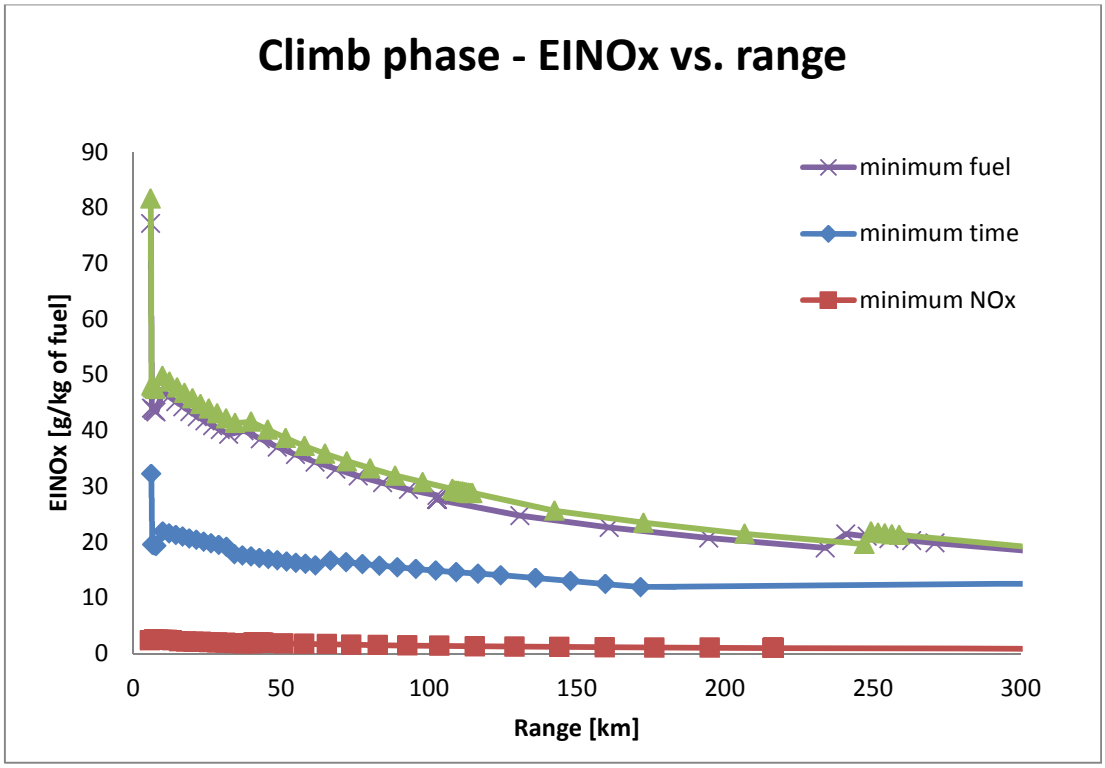

Figure 51 - EINO$_x$ vs. range for the minimum fuel, minimum time, minimum NO_x and minimum contrails for the full trajectory

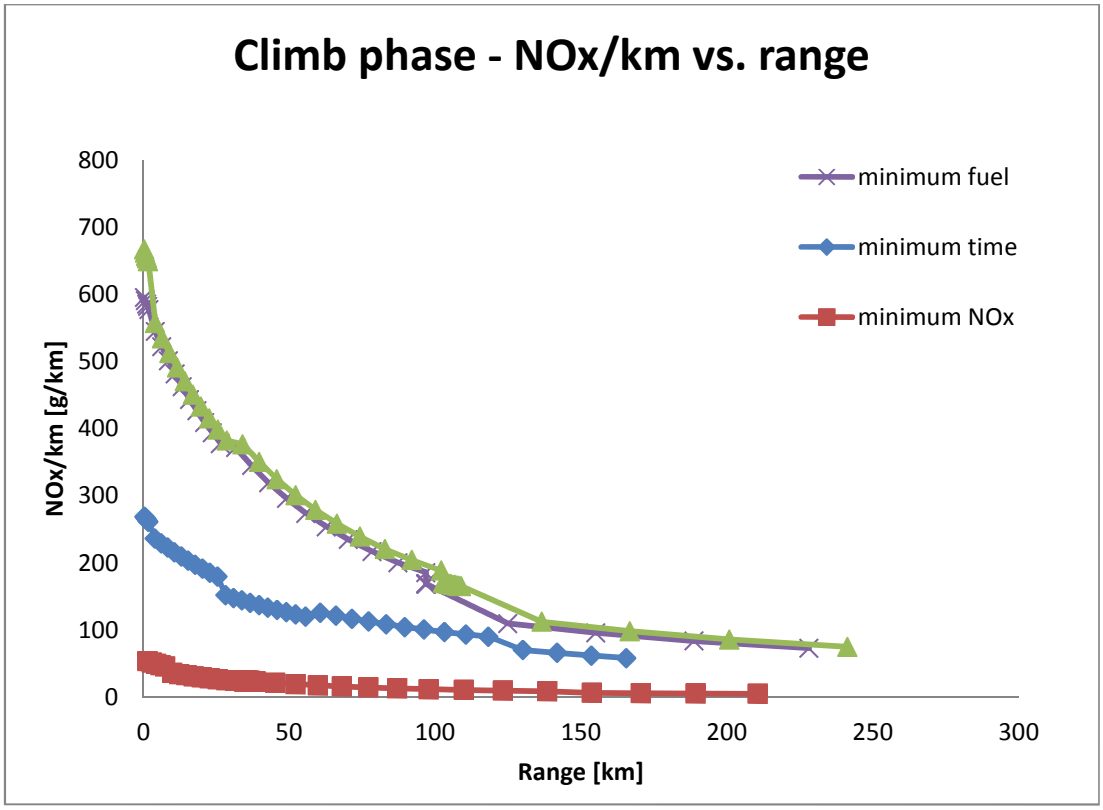

Figure 52 - NO_x/km vs. range for the minimum fuel, minimum time, minimum NO_x and minimum contrails for the climb phase

The reason behind is that the emissions model uses inputs such as pressure and temperature at combustor inlet, air and fuel mass flow rates, but TET is never directly specified. In fact TET is used by the engine model to derive the input required by the emissions model. In the case of the minimum NO_x solution, the engine has been designed in such a way that it minimises the overall pressure ratio and compressor delivery temperature (while still keeping the same thrust level) to ensure low level of NO_x emissions. As shown in Table 18, the overall pressure ratio selected by the optimiser is 19.3 (FPR of 1.61, low pressure compressor pressure ratio of 1.5 and high pressure compressor pressure ratio of 8), which is the minimum available. To compensate for this low OPR in term of engine thrust (design point thrust has to be 121440 N), the by-pass ratio at design point has been reduced to 4.52 and TET at design point has been increased to 1600K. To summarise, the optimiser has been able to find a solution that effectively minimises the flame temperature (by reducing combustor inlet pressure and temperature) while keeping the same thrust requirements. However, this NO_x efficient engine design have strong fuel efficiency drop. At take-off, the SFC of the original engine was 9.3 mg/Ns and it increases to 13.1 mg/Ns for the low NO_x engine design. From the results of the emissions model, it is possible to obtain the temperature calculated for the flame front and primary zone of the combustor along the whole trajectory. Figure 53 represents the equilibrium temperature calculated by the emissions model plotted against the range. Figure 53 clearly shows that the temperature

within the flame front and primary zone is significantly lower for the minimum NO_x solution which definitely proves that reducing combustor inlet pressure and temperature has the strongest impact on reducing the NO_x emissions.

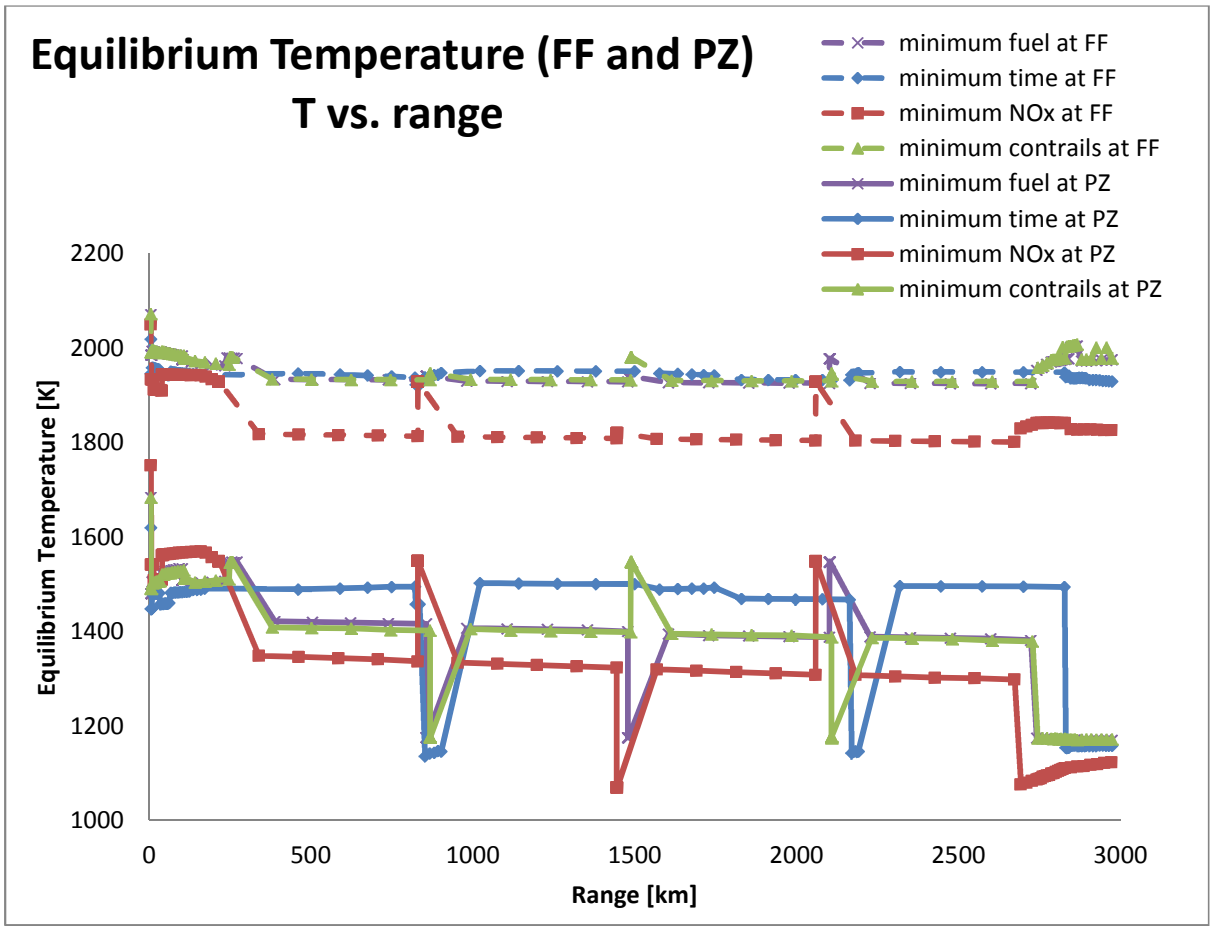

Figure 53 – Equilibrium temperature calculated at the flame front (FF) and primary zone (PZ) for the minimum fuel, time, NOx and contrails solution. The temperature is plotted against the range

5.3.3.2 Conclusion and further work

The main conclusion of this case study is that allowing the variables of the trajectory and the engine design parameter to vary in the same optimisation run led to improved overall objectives values. This is especially true for the minimum fuel and the minimum NO_x solutions which were reduced by 2.9% and 83% respectively compared to case study 1. For the minimum fuel solution the reduction of fuel consumed is relatively small. The reason is that the original engine is already well optimised for fuel consumption. The main differences with the newly fuel optimum engine is a higher OPR (42 instead of 32), higher BPR (5.5 instead of 5.2) and higher TET (1559 K instead of 1510 K). The outcome is that the engine efficiency in term of SFC at design point improves from 16.2 mg/Ns to 15.3 mg/Ns.

The design Mach speed was allowed to vary from 0.75 to 0.85, the design Mach speed of the original engine was 0.8. In all cases, the minimum solutions opted for design Mach speed of 0.75-0.77. Given that the cruise was flown at relatively low Mach speed (around M = 0.67, except for the minimum time solution), it is logical that a readjustment of the design Mach speed of the engine was needed in order to match that of the cruise phase speed.

Similarly to case 1, the same remark can be made regarding the relative weakness of the climb speeds, climb altitudes and climb de-rate thrust variables to the final objective value. Here again, only the minimum NO_x solution shows a strong tendency at reducing as much as possible the climb de-rate thrust.

In term of trade off, the addition of engine cycle parameters has generated a much broader Pareto front for the fuel/NOx optimisation.

Overall, this case study has shown that simultaneous optimisation of trajectory and engine cycle can be beneficial in generating and identifying optimal engine/trajectory parameter with respect to given objectives and constraints. This method can especially be useful during the early design phase to quickly identify promising solutions for a given aircraft range.

Based on the results obtained in this case study, it would be interesting to improve on the following points:

- Run an optimisation for more generations to see to which extent optimum solution variables are modified.
- Perform the same type of optimisation but on the climb, cruise and descent segment separately. This would allow the use of more variables per phase and thus would increase the ability of the optimiser to provide better minimisation of the objectives considered in this work.
- Addition of models such as engine weight model to allow for broader range of engine design as well as higher accuracy for the objectives calculation.
- Another aspect not considered in this thesis is the estimation of the noise generated over populated area resulting from each aircraft trajectory. This would require two additional models to be integrated in the framework. One model to estimate the noise generation and propagation from the engine/aircraft, the second model would be necessary to estimate the impact of noise for the population around the aircraft trajectory.

6 Conclusions and further work

6.1 CONCLUSIONS

The first part of the work has provided an overview of the different modelling approaches available to predict the level of NO_x emitted by aircraft gas turbine engines. It was also described how todays NO_x regulation is enforced by the ICAO. A section was dedicated to the genetic algorithm optimisation technique used in this work and provided some advantaged and disadvantages of such technique compared to other optimisation methods. The last part of the literature review focused on previous work related to aircraft trajectory optimisation, subsequently contribution to knowledge was identified.

The following chapter was dedicated at the testing and benchmarking of different genetic algorithm using mathematical test function to ensure that the performance in term of convergence, diversity, and algorithm capability were sufficient to cope with two-objectives aircraft trajectory optimisations. It was also checked that the optimiser was capable of dealing with constraints while still quickly reaching the theoretical Pareto front of the test functions. The optimisers tested showed an overall very good performance in reaching quickly the theoretical Pareto front of the various test functions used. In addition the spread (or diversity) of the solutions was found to be very good.

Chapter 4 was focused on the description of the work done with respect to the emissions modelling. Firstly, a reactor based emissions model was modified with the aim to improve the NO_x emissions prediction of conventional single annular combustors. The model obtained was validated against ICAO data for 4 different engines and showed very good agreement. All 4 engines were modelled using the Cranfield in-house Turbomatch engine simulation software. The emissions model was further improved by including a new type of fuel. The added fuel was natural gas. The NO_x emissions model was validated using information from an LM2500 stationary gas turbine modelled using Turbomatch. Using the same reactor based modelling approach, a NO_x emissions prediction model was developed for a novel conceptual lean pre-mixed pre-vaporised combustor. The last section of chapter 4 detailed the modelling methodology used to predict persistent contrails produced by aircraft flying at cruise altitude. The model developed is state of the art and follow the methodology of Appleman and Schumann. The model was also validated using data from public domain and showed a very good agreement.

Finally chapter 5 described how all the models were integrated and linked to the optimiser using the GATAC software. This chapter contains three case studies. The first two case studies focused only on the optimisation of aircraft trajectories. The optimisation used a

multi-objective approach in which two competing objectives were simultaneously minimised. Pairs of objectives to minimise were as follows: fuel/time, fuel/NO_x and fuel contrails. This led to the generation of Pareto fronts for which a whole population of optimum solutions was found. This Pareto was used to obtain the extremum solution and can also be used to perform trade off analysis. The difference between case 1 and case 2 was the usage of different combustor emissions models. In Case 1, the conventional single annular combustor model was used while in case 2 a hypothetical LPP combustor adapted for aircraft engines was used. Some of the main results from case study 1 were as follows: the difference in fuel consumed for the minimum fuel and minimum time solution is 25%. In addition the minimum time solution shows a significantly higher NO_x emitted (around 128% more NO_x emitted compared the minimum NO_x solution). The NO_x emitted by the minimum NO_x solution is 3.1% lower with only 0.7% fuel penalty when compared to the minimum fuel solution. Case study 2 showed a drastic reduction of NO_x emitted for the minimum NO_x solution, which comes from the use of a conceptual low emissions combustor technology. The optimisation has shown that the change of combustor technology does not lead to significant change in the optimum trajectory when compared to case 1. The third test case was a set of optimisation run in which both trajectory and engine design variables were modified. This last test case showed consistent improvement in terms of fuel and NO_x objectives due to the introduction of engine design point variables. A reduction of 2.9% in fuel consumption was found when compared to case 1. In addition, the NO_x emitted by the minimum NO_x solution was found to be dramatically reduced (83% less compared to case 1) mainly by using a lower overall pressure ratio.

In all cases, and based on the vertical atmospheric profile chosen, contrails were completely avoided with a relatively small fuel penalty (0.5% fuel penalty in case 1 and 2 and 0.3% for case 3).

The main purpose of the work was to develop a methodology and a number of models to assess the potential reduction of aircraft environmental impact in term of fuel burned, NO_x emitted and persistent contrails formation. The work carried out proved to fulfil the objectives set in the introduction section. The use of a genetic algorithm integrated with a framework of model was successfully applied to multi-objective aircraft optimisation problems. One case study using aircraft trajectory and engine design parameters simultaneously was optimised for fuel, time, NO_x and contrails in pairs. The development of a LPP combustor NO_x emissions model and its integration to the optimiser and model framework produced a unique way of assessing the level of NO_x by generating optimum Pareto fronts.

The main conclusions of the work with respect to the research questions stated in the introduction are as follow:

- The validation of the NO_x emissions model as well as the test cases described in this work have demonstrated that the developed NO_x emission model is capable

of providing reasonable and representative estimation of NO_x emitted by aero-engine for a wide range of aircraft trajectories.

- The development and use of the Lean Pre-mixed Pre-vaporised combustor emissions model show the versatility and adaptability of the reactor based model. With further validation the model can be used to assess NO_x emissions level from aero-engine gas turbine.
- The case studies developed for this work have demonstrated that all the models developed could be effectively used as part of a multi-disciplinary optimisation framework and also yielded usable output for inter-comparison of competing design solutions.
- For the first two case studies the optimiser has shown good ability to handle the problem complexity with relatively small dispersion in the optimum variable values. However the last case study which includes more variable and a more complex problem due to the engine cycle optimisation has displayed a wider variable dispersion. Even though the optimisation can be improved by increasing the number of generation and the population size, it shows that largely increasing the complexity by adding variables, objectives and constraints could quickly become a limiting factor for genetic algorithm based optimisation.
- In term of benefits of simultaneous optimisation of trajectory and engine, it has been shown that it is possible to obtain improved Pareto fronts for all objectives selected in this study. However the addition of engine cycle parameters to the problem setup did not fundamentally changed the optimum trajectories found in the first 2 case studies. This means that if optimum trajectories have been identified in a previous optimisation there is little benefits to setup a simultaneous trajectory and engine cycle optimisation. On the other hand, if the optimiser is capable of handling the problem complexity (this was the case in this work) then time can be saved since a single optimisation run will provide the optimum trajectory and engine cycle parameters.

Finally, the main result from this research work is the development and assessment of a methodology to compare in a systematic way potential optimum trajectories and/or engine cycles for minimum fuel, NO_x, contrails and time of flight. The model developed through this work have proved to be fast and flexible to be used as part of a multi-disciplinary optimisation framework and the results obtained by each model are representative of the physics involved. It is the author's belief that the models as well as the optimiser can easily be reused and/or adapted and thus expend the method to a wider range of optimisation problems which will contribute to the overall reduction of aircraft fuel consumption and emissions impact.

6.2 FURTHER WORK

From the work described in this thesis, a number of interesting research topics includes the following:

- 3D trajectory: All the trajectories in the present work were defined by their vertical profile. An interesting improvement is to extend the trajectory setup to include the horizontal profile. This would allow optimising trajectories using more realistic air traffic constraints. Selection of the optimum route would become an important part when considering air traffic management and weather forecast.
- Engine weight model: test case 3 was designed in such a way that engine weight variation would be small enough to be ignored in the optimisation process. However it would be of great interest to add an engine weight model so that final objective performance can be evaluated for a wider range of engine design. Additionally it would be important to add a module to the aircraft model to update the drag generated by engines with different fan diameter.
- Noise model: some phases of the flight such as the take-off, early climb, approach and landing can have impact on the population in term of noise perceived. In order to ensure that new optimum flight paths are not increasing noise level around populated area (especially around airports), it is necessary to include a noise model linked with a noise impact assessment model. Such models would prove even more useful when considering 3D trajectories.
- New combustor models: A first attempt at modelling an advanced combustor was successfully completed in the present work. Similarly, other potentially advantageous advanced combustor technology need to be assessed. Combustors technology such as dual annular (or staged combustors as they are called), Lean Direct Injection (LDI), Rich Quench Lean (RQL) combustors are all promising technologies that would allow reduction of NO_x while maintaining high level of reliability and combustion efficiency. As such formal emissions modelling is deemed to be useful.
- Sensitivity analysis: Based on all the assumptions made in the models used in this work a more in depth analysis on the sensitivity of each models is required. Especially the NO_x emissions model is very sensitive to model parameters such as air flow splits and combustion zone volumes thus comprehensive sensitivity analysis would prove useful to better assess the level of modelling uncertainty.
- Alternative fuels: thanks to the modular architecture of the emissions model presented in this work, it is relatively easy to add various type of fuel to assess their impact on the NO_x emissions. Alternative fuel such as hydrogen, biofuels and others can be implemented.
- Improving the optimiser: The optimiser used in this work has proved efficient and robust, however when considering optimisation problems in which the number of variable is greatly increased might reveal limitations of the genetic algorithm

technique. Due to the inherent randomness of the search of GA, increasing the number of variable leads to require more evaluations to reach convergence to an optimum Pareto front. Finally the number of variables that can be changed will depend on the computing resources available. Otherwise improving the optimisation technique can help in scaling up the complexity of optimisation problems. Technique such as hybridisation of GA with other classical search methods (in particular with direct search methods) is one possible way forward. This hybridisation technique would take advantage of the GA to initially look for the most promising set of solutions, while the direct search method would be used at a later stage to converge more quickly to the final solution. In the frame of the Clean Sky, a Tabu search method was implemented and used for aircraft trajectory optimisation with good results. Additionally, the test case results have proved the performance of the genetic based optimiser. It is expected that similar studies can be carried out in which the number of objectives is increased. Three or more simultaneous objectives optimisation can be done provided the population size and the number of generation are increased to ensure good overall Pareto convergence.

- Improved contrails model: the contrails model developed for the purpose of the work is considered state of the art. However such model is still fairly crude since the accuracy is only about 80%. Clearly no consideration is given towards how droplets can form. Especially it does not take into account of the presence of possible soot which can serve as nucleation sites for water droplets. Since different aircraft engine will produce different level of soot, it would be important to investigate whether the effect is significant.
- Improved atmospheric model: In this work the atmospheric model was simply provided by a vertical profile. In order to assess the level of contrails generated by aircraft in real flight route, it will be necessary to have a vertical and horizontal atmospheric model at least. Time dependency in the atmospheric model would also improve the ability to assess contrails formation.

7 References

[1] Scottish parliament website, “Report on sustainable Aviation CO2 Roadmap, http://www.scottish.parliament.uk/s3/committees/ticc/inquiries/documents/SARoadMapfinalDec08.pdf”, accessed 10/09/10

[2] “UK parliamentary Office of Science and Technology Report April 2003”, www.parliament.uk/documents/post/pn195.pdf, accessed 10/09/10

[3] Royal Commission on Environmental Pollution, ”The Environmental Effects of Civil Aircraft in Flight”, Special Report, http://www.rcep.org.uk/reports/index.htm, 2002, accessed 10/09/10

[4] European Commission, http://ec.europa.eu/environmentclimat/emission/index_en.htm, accessed 10/09/10

[5] European Commission, “Aeronautics and Air Transport Report by the Advisory Council for Aeronautics Research in Europe”, Directorate – General for Research, Communication Unit, Brussels, 2010

[6] Rizk, N. K., Mongia, H. C., “NOx Model for Lean Combustion Concept”, AIAA92-3341, AIAA conference, Nashville, 1992.

[7] Lefebvre, A. H., “Fuel Effects on Gas Turbine Combustion—Liner Temperature, Pattern Factor, and Pollutant Emissions,” Journal of Aircraft, Vol. 21, No. 11, pp. 887–98, 1984.

[8] Lefebvre, A., H., “Gas Turbine Combustion”, 2nd edition, ISBN: 1560326735, 1998.

[9] Odgers, J., and Kretschmer, D., “The Prediction of Thermal NO x in Gas Turbines,” ASME Paper 85-1GT 126, 1985.

[10] Rizk, N. K., and Mongia, H. C., “Emissions Predictions of Different Gas Turbine Combustors,” AIAA Paper 94-0118, 1994.

[11] Mellor, A. M., “Semi-Empirical Correlations for Gas Turbine Emissions, Ignition, and Flame Stabilization,” Progress in Energy and Combustion Science, Vol. 6, No. 4, pp. 347–58, 1981.

[12] Lewis, G. D., “A New Understanding of NO_x Formation,” Tenth International Symposium on Air-Breathing Engines, ISABE 91-7064, Nottingham, UK, AIAA, Washington, DC, pp. 625–9, 1991.

[13] Rokke, N. A., Hustad, J. E., and Berg, S., “Pollutant Emissions from Gas Fired Turbine Engines in Offshore Practice—Measurements and Scaling,” ASME Paper 93-GT-170, 1993.

[14] SAE, “Procedure for the Calculation of Aircraft Emissions”. SAE Committee A-21,

Report SAE AIR 5715, 2009.

[15] International Civil Aviation Organisation (ICAO), "Aircraft Emissions databank", http://easa.europa.eu/environment/edb/aircraft-engine-emissions.php, accessed 10/09/10.

[16] F. Jelinek, S. Carlier and J. Smith, "The Advanced Emission Model (AEM3) Version 1.5 _ Appendices A, B and C to the Validation Report", EUROCONTROL Experimental Center Report EEC/SEE/2004/004, 2004.

[17] B. Kim et al., "System for Assessing Aviation's Global Emissions (SAGE)". Federal Aviation Administration, Report FAA_EE_2005_01, 2005.

[18] Deidewig, F., Dopelheuer, A., Lecht, M., "Methods to Assess Aircraft Engine Emissions in Flight", Proceedings of the 20th Congress of the International Council of the Aeronautical Sciences (ICAS), pp 131-141, 1996.

[19] P. Madden and K. Park, "Methodology for Predicting NOx Emissions at Altitude Conditions from Ground Level Engine Emissions and Performance Test Information", Rolls Royce Technical Report DNS 90713 Issue 1, 2003.

[20] NEPAIR, "Development of the technical basis for a New Emissions Parameter Covering the Whole Aircraft Operation: NEPAIR", Final Technical Report, NEPAIR/WP4/WPR/01, 2003.

[21] Celis, C., "Evaluation and optimisation of environmentally friendly aircraft propulsion systems", Cranfield University, PhD Thesis, 2010.

[22] Aksit, I. M., "A Stochastic Model for Aircraft Gas Turbine Combustor Emissions", Ph.D. Thesis, School of Mechanical Engineering, Cranfield University, 1995.

[23] Pratt, D., T., "Mixing and Chemical Reaction in Continuous Combustion", Prog. Energy Combustion Sci., Vol. 1, pp73-86, 1976

[24] Fletcher, R. S., and Heywood, J. B., "A Model for Nitric Oxide Emissions from Aircraft Gas Turbine Engines", AIAA Paper 71-123, AIAA 9th Aerospace Sciences Meeting, New York, US, 1971

[25] Swithenbank, J., Poll, I., Vincent, M., W., Wright, D., D., "Combustion Design Fundamentals", 14th Symposium (International) on Combustion, pp627-638, 1973.

[26] Gordon, S., and McBride, B. J., "Computer Program for Calculation of Complex Chemical Equilibrium Compositions and Applications. I. Analysis", References 240 NASA Reference Publication 1311, National Aeronautics and Space Administration, Lewis Research Center, Ohio, US, 1994

[27] McBride, B. J., and Gordon, S., "Computer Program for Calculation of Complex Chemical Equilibrium Compositions and Applications. II. User's Manual and Program Description",

NASA Reference Publication 1311, National Aeronautics and Space Administration, Lewis Research Center, Ohio, US, 1996

[28] Hammond, D. C. JR., and Mellor, A.M., “Analytical Calculations for the Performance and Pollutant Emissions of Gas Turbine Combustors”, *Combustion Science and Technology,* Vol. 4, pp.101-112, 1971

[29] Hammond, D. C. JR., and Mellor, A. M., “Analytical Predictions of Emissions from and Within an Allison J-33 Combustor”, *Combustion Science and Technology,* Vol. 6, pp. 279-286, 1973

[30] Mellor, A. M., “Gas Turbine Engine Pollution”, *Progress in Energy and Combustion Science,* Vol. 1, pp. 111-133, 1976

[31] Sturgess, G. J., “An Account of Fuel/Air Unmixedness Effects on NOx Generation in Gas Turbine Combustors”, IECEC-98-353, 33rd Intersociety Engineering Conference on Energy Conversion, Colorado Springs, US, 1998

[32] Sturgess, G. J., Zelina, J., Shouse, D., and Roquemore, W., “Emissions reduction technologies for military gas turbine engines”, *Journal of Propulsion and Power,* Vol. 21, No. 2, pp. 193-217, 2005

[33] Allaire, D., L., Waitz, I., A., Willcox, K., E., “A Comparison of Two Methods for Predicting Emissions from Aircraft Gas Turbine Combustors”, ASME Turbo Expo 2007: Power for Land, Sea and Air, Montreal, Canada, GT2007-28346, 2007.

[34] Bowman, C. T., "Control of Combustion-Generated Nitrogen Oxide Emissions: Technology Driven by Regulation," Twenty-Fourth Symposium (International) on Combustion/The Combustion Institute, Sydney, Australia, 1992

[35] Miller, J. A., and Bowman, C. T., "Mechanism and Modelling of Nitrogen Chemistry in Combustion", *Progress in Energy and Combustion Science,* Vol. 15, pp. 287-338, 1989

[36] Heywood, J. B., Fay, J. A., and Linden, L. H, "Jet Aircraft Air Pollutant Production and Dispersion," *AIAA Journal,* Vol. 9, No. 5, pp. 841-850, 1971

[37] De Soete, G. G., “Overall Reaction Rates of NO and N_2 Formation from Fuel Nitrogen”, 15th Symposium (International) on Combustion/The Combustion Institute, Tokyo, Japan, 1975

[38] FLUENT, Flow Modelling Software, “FLUENT 6.2 User’s Guide”, Fluent Inc., Lebanon, NH, US.

[39] Marini, A., Bucchieri, L. and Peschiulli, A., “CFD aerodynamic and reactive study of an innovative lean combustion system in the frame of the NEWAC project”, Proceeding the 2010 ASME Gas Turbine Technical Congress and Exhibition, ASME Turbo Expo 2010, Glasgow, UK, June 14-18, 2010

[40] Frassoldati, A., Cuoci, A., Faravelli, T., Ranzi, E., Colantuoni, S., Martino, P. D., Cinque, G., Kern, M., Zarzalis, M. S. N., "Fluid dynamics and detailed kinetic modeling of pollutant emissions from lean combustion systems", MCS6 Sixth Mediterranean Combustion Symposium. Ajaccio Corsica France, 7-11 June 2009, p. 1-11, 2009

[41] Frassoldati, A., Cuoci, A., Faravelli, T., RANZI E.M., "Global kinetic mechanism of kerosene combustion for CFD applications", In: Proceedings of the European Combustion Meeting 2011. Cardiff (UK), 28/6/2011-1/7/2011, p. 1-6, 2011

[42] International Civil Aviation Organisation (ICAO) website, accessed 10/09/10, http://www.icao.int/env/

[43] ICAO Environmental Report, Environmental Branch, International Commercial Aviation Organisation, Montreal, Canada, 2010.

[44] Sethi, V., "Introduction to Gas Turbine Emisisons", Short Course Lecture, Cranfield University, 2013.

[45] Green, J. E, *"Civil Aviation and the Environmental Challenge",* Aeronautical Journal, 107(1072), 281-300, 2003.

[46] Lentini, D., *"Prediction of NO(x) emissions in gas turbine combustors inclusive of the N2O contribution",* Proceedings of the Institution of Mechanical Engineers, Vol 217 Part A: J. Power and Energy, 2003.

[47] Air France, Sustainable Development- Air France, http://developpementdurable. airfrance.com /FR/en/local/environnement/N4_gaz_qualitair_en.htm, (accessed on 15 Oct 2010), 2010.

[48] Rao, S. S., "*Engineering Optimization: Theory and Practice",* 3rd Edition, John Wiley, New York, US, 1996

[49] Kalyanmoy Deb, "Multi Objective Optimisation using Evolutionary Algorithms", John Wiley and Sons, New York, USA, 2002

[50] Holland, J. H., "Adaptation in Natural and Artificial Systems", 1st Edition, University of Michigan Press, Michigan USA, 1975

[51] Kalyanmoy Deb, Amrit Pratap, Sameer Agarwal, and T. Meyarivan, "A Fast and Elitist Multiobjective Genetic Algorithm: NSGA-II", IEEE Transactions on Evolutionary Computations, Volume. 6, Number 2., Pg 182-197, 2002

[52] Antoine, N. E., and Kroo, I. M., "Framework for Aircraft Conceptual Design and Environmental Performance Studies", *AIAA Journal,* Vol. 43, No.10, pp. 2100-2109, 2005

[53] Antoine, N. E., Kroo, I. M., Willcox, K., and Barter, G., “A Framework for Aircraft Conceptual Design and Environmental Performance Studies”, AIAA-2004 4314, 10th AIAA/ISSMO Multidisciplinary Analysis and Optimization Conference, Albany, NY, US, 2004

[54] Le Dilosquer, M., “Influence of Subsonic Aero Engine Design and Flight Routes on Atmospheric Pollution”, Ph.D. Thesis, School of Mechanical Engineering, Cranfield University, UK, 1998

[55] Bower, G. C., Kroo, I. M., “Multi-objective aircraft optimization for minimum cost and emissions over specific route network”, ICAS 2008, 26th International congress of the aeronautical sciences, 2008.

[56] Celis, C., Long, R., Sethi, V., Zammit-Mangion, D., “On trajectory Optimization for Reducing the Impact of Commercial Aircraft Operation on the Environment”, ISABE-2009-1118, AIAA, 2009.

[57] Pervier, H., Nalianda, D., Espi, R., Sethi, V.,Pilidis, P., Zammit-Mangion, D., “Application of Genetic Algorithm for Preliminary Trajectory Optimization”, SAE International J. of Aerospace, Vol. 4, Issue 2 (Nov. 2011), 2011-01-2594, doi:10.4271/2011-01-2594, 2011.

[58] Chircop, K., Xuereb, M., Zammit-Mangion, D., Cachia, E., “A Generic Framework for Multi-Parameter Optimization of Flight Trajectories”, ICAS 2010, 27th International Congress of the Aeronautical Sciences, 2010.

[59] E. Zitzler, et al., “SPEA2: Improving the Strength Pareto Evolutionary Algorithm”. Tech. Rep. 103, Gloriastrasse 35, CH-8092 Zurich, Switzerland, 2001

[60] Rogero, J.M., “A Genetic Algorithm based Optimisation tool for preliminary design of Gas Turbine Combustors”, PhD Thesis, Cranfield University, 2002.

[61] MATLAB, “The Language of Technical Computing”, Version 7.7 (R2008b), The MathWorks, Inc., <www.mathworks.com>.

[62] M. Tanaka, “GA-based decision support system for multicriteria optimization,” in Proc. IEEE Int. Conf. Systems, Man and Cybernetics-2, pp. 1556–1561, 1995.

[63] Samaras, C., “Emissions Estimation from Industrial Gas Turbine Combustors”, MSc Thesis, Cranfield University, 2010.

[64] Penner, J. E., Lister, D. H., Griggs, D. J., Dokken, D. J. and McFarland, M., “Aviation and the Global Atmosphere”, Ed. 1999, Cambridge University Press, 365 pp.

[65] Appleman H., “The formation of exhaust Contrails by jet aircraft”, Bull. Amer. Meteor. Soc., pp14-20, 1954.

[66] Schumann, U., “On conditions for Contrails formation from aircraft exhausts”, Meteorol. Zeitschrift, Vol. 5, February 1996, pp. 4–23.

[67] Noppel, F., Singh, R., “An overview on Contrails Cirrus Cloud Avoidance Technology”, AIAA, Journal of Aircraft 2007, 0021-8669, vol.44 no.5 (1721-1726), doi: 10.2514/1.28655, 2007.

[68] http://cires.colorado.edu/~voemel/vp.html from Smithsonian Tables, 1984, after Goff and Gratch, 1946, accessed 21-09-2011.

[69] Shull, J., D., “A Validation Study of the Air Force Weather Agency (AFWA) Jetrax Contrails Forecast Algorithm”, MSc Thesis, Air Force Institute of Technology, AFIT/GM/ENP/98M-10, 1998.

[70] Schrader, M., L., “Calculations of Aircraft Contrails Formation Critical Temperature”, Notes and Correspondence, Air Weather Service, Illinois, 1996.

[71] Sethi, V., “Presentation on the concept and application of Techno-Economic and Environment Risk Assessments”, Cranfield University, Cranfield, UK, 2011

[72] Pascovici, D.S, Colmenares, F, Ogaji, S.O.T, Pilidis, P., “An Economic and Risk Analysis Model for Aircrafts and Engines”, Proceedings of Gt2007 ASME Turbo Expo 2007: Power for Land, Sea and Air May 14-17 2007, Montreal, Canada. GT2007-27236, 2007.

[73] Goulos, I., Pachidis, V., Celis, C, D’Ippolito, R., Stevens, J., “Simulation Framework Development for Aircraft Mission Analysis”, GT2010-23379, Proceedings of GT2010, ASME Turbo Expo 2010, Power for Land, Sea and Air, Glasgow, UK, 2010.

[74] Nalianda, D., K., “Impact of Environmental Taxation Policies on Civil Aviation – A Techno-Economic Environmental risk assessment”, PhD thesis, Cranfield University, 2012.

[75] Eurocontrol, “User manual for the base of aircraft data”, EEC Technical/Scientific Report No. 2010-003, Eurocontrol, France, 2010.

[76] Pachidis, V., “Gas Turbine Performance Simulation”, Simulation and Diagnostics Course Notes: School of Engineering, Cranfield University, 2008.

[77] University of Wyoming, Atmospheric sounding data, http://weather.uwyo.edu/upperair/sounding.html, accessed 15/05/2011.

[78] Saravanamuttoo, H.,I.,H., “Gas Turbine Theory”, Longman Scientific & Technical, 3rd edition, ISBN 0-582-30539-X, 1987.

[79] Mair, A. W., Birdsall, D. L., “Aircraft Performance”, Cambridge University Press, Cambridge, United Kingdom, 1996

[80] Nuic, A., Poles, D. and Mouillet, V., “BADA: An advanced aircraft performance model for present and future ATM systems”, International journal of adaptive control and signal processing 2010, Volume 24, pg 850–866, 2010.

[81] Jenkinson, L. R., Simpkin, P., Rhodes, D., “Civil jet aircraft design”,1st edition, Butterworth Heinmann, MA, USA, 1999.

[82] CFM, “CFM Technical specification engine database”, available at: http://www.cfm56.com/products/cfm-technical-data, sourced on 26 April 2011, 2011.

[83] CFM56-7B emissions datasheet sourced from ICAO emissions databank, available at http://www.caa.co.uk/default.aspx?catid=702, sourced on 12 June 2011, 2011

[84] Gunston, B., “Janes Aero Engines”, Janes Information Group, London England, 1996.

[85] Mattingly, J.D, “Elements of gas turbine propulsion”, McGraw-Hill series in aeronautical and aerospace engineering, McGraw-Hill book co., Singapore, 1996.

[86] Aircraft performance data-737, Boeing, available at - http://www.boeing.com/commercial/airports/acaps/737sec3.pdf, sourced on 13 March 2011

[87] GE Marine Engines, “LM2500 Military Marine Gas Turbine Installation Design Manual”, MID-IDM-2500-18, January 1999.

[88] Clarke, J. P., 2003, “The Role of Advanced Air Traffic Management in Reducing the Impact of Aircraft Noise and Enabling Aviation Growth”, *Journal of Air Transport Management,* Vol. 9, No. 3, pp. 161-165.

[89] Riddlebaugh, and Stephen, M., (edit.), 2007, “Research & Technology 2006”, NASA/TM – 2007-214479, NASA Glenn Research Center, Cleveland, Ohio, US.

Annex A - Aircraft model description

This annex describes in detail the principle used to model the aircraft used in this work. This section comes from the work of Nalianda [74]. The model has been design as an improvement of another model developed within Cranfield University. This model was named Hermes.

The primary requirement of the generic aircraft model is to be modular in structure and be easily interchangeable to simulate of various fixed wing civil aircraft. The model has been therefore been structured to enable the following:

1. Facilitate easy interchanging of aircraft type and engine using input text files and GUI
2. Input files to change mission requirements such as payloads, load factors
3. Detailed output flies to enable the user to access various information such as gradient angles, ROC/D, speeds (airspeeds & Mach numbers) etc.
4. Easy interfacing of other models such noise , emission, DOC and contrails
5. Analysis of individual flight segments (take-off, climb, cruise, descent, approach and landing)
6. Analysis of a full mission
7. Facilitate engine cycle optimisation

Apart from the necessity to incorporate the above mentioned requirements, a secondary motivation was also to develop a code to understand better application and implementation of theories in aircraft performance modelling. The fundamental differences from the original version include the following:

- Unlike the previous version which utilises a database, this version interlinks the engine performance code (Turbomatch) directly with the aerodynamic model in order to process engine thermodynamic calculations.
- Modelling of some of the phases such as take-off is more detailed
- The drag polar is adapted from the euro control database for aircraft (BADA) and hence switching of aircraft models is more convenient [75]

Utilising the generic aircraft model described in this annex, specific models based on the characteristics of the conventionally used short/medium range single aisle aircraft (Boeing 737-800 equipped with two twin spool turbofan CFM56-7B27 engines) was modelled. This annex includes a description of the Boeing 737-800 aircraft model.

Total energy model

The model is based on the Total Energy Model [75] which equates the rate of work done by forces acting on the aircraft to the rate of increase in potential and kinetic energy

$$(T_{HR} - D)V_{TAS} = mg_0\frac{dh}{dt} + mV_{TAS}\frac{dV_{TAS}}{dt} \quad [A.1]$$

THR: Thrust acting parallel to the aircraft velocity vector (in Newton)

D: Aerodynamic drag

m: Aircraft mass (in kg)

h: altitude (in m)

g_0: Gravitational acceleration (9.80665 m/s^2)

V_{TAS}: True airspeed (m/s)

d/dt: time derivative (s^{-1})

Aerodynamic drag

The lift coefficient C_L is determined using equation A.2

$$C_L = \frac{2mg_0}{\rho V_{TAS}^2 A cos\emptyset} \quad [A.2]$$

cosϕ: Bank angle

A: Aircraft wing reference area

ρ: Air density (in kg/m^3)

Under nominal conditions the drag coefficient C_D is specified as a function of lift coefficient and C_{D0} and C_{D2} (being the parasitic drag coefficient and induced drag coefficient respectively) [75], as described in the BADA model specification. These coefficients are specific to aircraft and flap setting and hence are varied through the trajectory as per aerodynamic surface requirements for a particular phase of flight.

$$C_D = C_{D0} + C_{D2}.C_L^2 \quad [A.3]$$

$$D = \frac{1}{2}\rho V_{TAS}^2 A C_D \quad [A.4]$$

Take off

The primary objectives of the take-off phase during engine cycle and mission optimisation analysis are field length, noise and LTO emissions. The take-off segment therefore has been designed to calculate speeds distances and thrust variations through the phase. The calculations in the model during the take-off phase assumes the standard procedure wherein the aircraft starting at rest , accelerates along a runway at a low angle of attack altitude and passes the stall speed V_s . After increasing the speed to V_r (speed of rotation) and an increased angle of attack the aircraft continues to move along the runway until the speed increases to V_{LOF} . The aircraft then lifts off the ground and begins to gain height until it reaches screen height (35 ft/10.7m). At this point the aircraft reaches a speed V_2 , a critical parameter in the estimation of take-off performance. [79, 80].

On resolving forces during ground roll (Figure 54)

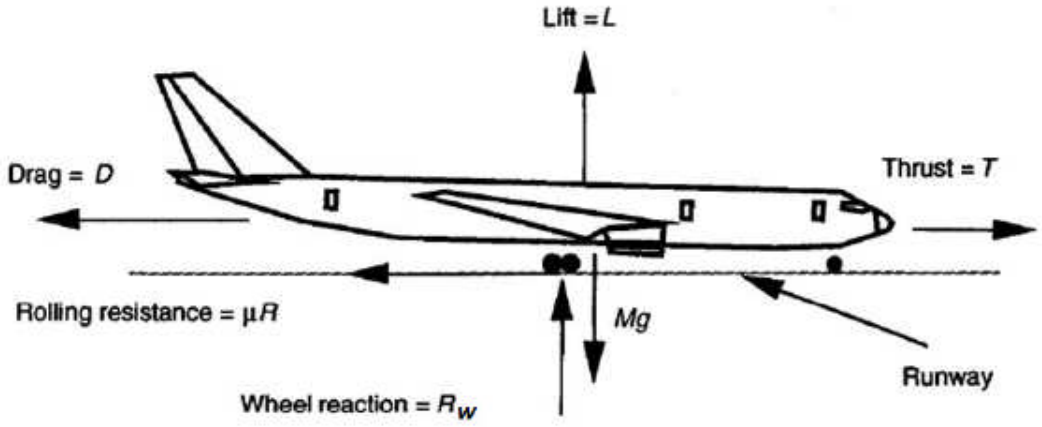

Figure 54 - aircraft at take-off [81]

Resolving forces horizontally

$$T_{HR} = D + m\left(\frac{dV_{TAS}}{dt}\right) + \mu R_w \quad [A.5]$$

μ: Runway coefficient of friction (paved runway μ = 0.02)

Resolving force vertically

$$R_w = mg_0 - L \quad [A.6]$$

Combining

$$m\left(\frac{dV_{TAS}}{dt}\right) = T_{HR} - D - \mu(mg_0 - L) \quad [A.7]$$

$$W = mg_0 \quad [A.8]$$

$$L = \frac{1}{2}\rho V_{TAS}^2 A C_L \quad [A.9]$$

$$\frac{dV}{dt} = \left[\left(\frac{T}{W} - \mu\right) + \rho\left(\frac{2W}{A}\right)(-C_D - \mu C_L)V^2\right] g_0 \quad [A.10]$$

The ground run s_g is then calculated using the integral

$$s_g = \int_0^{V_{LOF}} \frac{1}{2(dV/dt)} dV^2 \quad [A.11]$$

The speeds are calculated as follows

$$V_s = \sqrt{\frac{2mg_0}{\rho A C_{L_{max}}}} \quad [A.12]$$

$$V_{LOF} = 1.1V_{stall} \quad [A.13]$$

Two constants K_T and K_A are defined as follows [81]

$$K_T = \frac{T}{W} - \mu \quad [A.14]$$

$$K_A = \rho\left(\frac{2W}{A}\right)(-C_D - \mu C_L)g_0 \quad [A.15]$$

Substituting equations

$$\frac{dV}{dt} = (K_T + K_A V_{LOF}^2)g_0 \quad [A.16]$$

Therefore the ground roll distance is

$$s_g = \frac{1}{2gK_A} ln\left[\frac{K_T + K_A V_{LOF}^2}{K_T}\right] \quad [A.17]$$

Transition to climb

During Transition the aircraft accelerates from V_{LOF} to V_2 the model uses a simplified method as recommended by reference [81] (Figure 55). The following assumptions are made:

- The aircraft is flying at 0.9 C_{Lmax}
- The speeds V_{trans} and V_2 are fractions of V_{stall}
- The aircraft flies along an arc
- For small angle cosθ=1

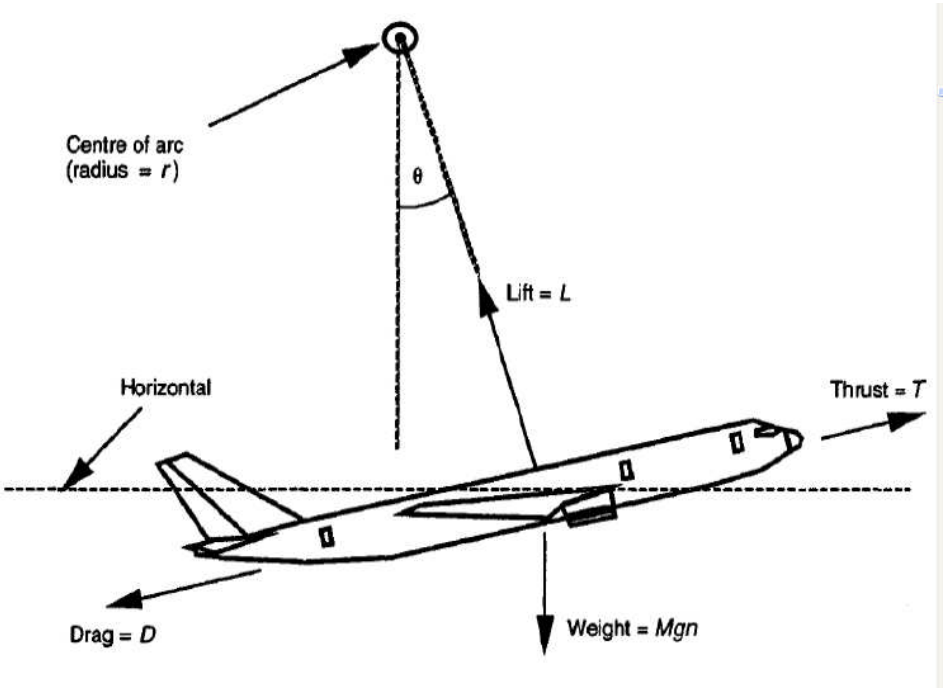

Figure 55 – Aircraft in transition to climb [81]

$$V_{trans} = 1.15V_{stall} \quad [A.18]$$

$$V_2 = 2V_{trans} - V_{LOF} \quad [A.19]$$

Resolving the forces normal to the flight path

$$L = mg_0 cos\theta + \frac{mV_{trans}^2}{r} \quad [A.20]$$

r: radius of arc

If $n = \frac{L}{mg_0}$ and $L = \frac{1}{2}\rho V_{trans}^2 A \times 0.9C_{L_{max}}$

Substituting

$$n = 1 + \frac{V_{trans}^2}{rg_0} \quad [A.21]$$

$$r = \frac{V_{trans}^2}{g_0(n-1)} \quad [A.22]$$

Knowing the radius of the arc and final gradient γ, the ground distance s_t covered and height at the end of transition may be approximated by

$$s_t = \gamma r \quad [A.23]$$

$$h_t = \frac{r\gamma^2}{2} \quad [A.24]$$

As per regulations the height at the end of transition must exceed 35 ft. The take-off segment is completed at 1500ft and aircraft is assumed to have reached a velocity of V_2+10.

Climb

The climb phase of the trajectory begins at 1500ft and continues up to the cruise altitude. This phase is further divided into 4 sub-segments:

- 1500 ft-3000 ft - The aircraft climbs at constant V_{CAS} and speed V_2+10.
- 3000 ft-10000 ft -the aircraft climbs at constant V_{CAS} 250 kt
- 10000 ft-Transition altitude - The aircraft climbs at constant V_{CAS} 310 kt till transition/ crossover altitude, which if airspeed and a Mach number are specified, is defined as the (geo-potential pressure) altitude at which the V_{CAS} and Mach number will represent the same TAS value.
- Transition altitude - cruise altitude: The aircraft climbs at constant Mach number

The two main independent control inputs available for affecting the aircraft trajectory in the vertical plane include the throttle and the elevator. These inputs in turn allow three main variables to be controlled during climb namely the thrust, speed and rate of climb. The

model essentially uses thrust and speed to control the rate of climb of the aircraft. The speed profile in the climb segment is defined as explained previously and the thrust is controlled by a variable power setting and maximum climb rating.

Climbing at constant equivalent/calibrated airspeed will result in a corresponding increase in true airspeed as altitude increases and climbing at constant Mach number below the tropopause implies a decrease in equivalent airspeed. Therefore the calculation of climb performance takes these effects into account.

Equation A.1 is then rearranged to give

$$(T_{HR} - D)V_{TAS} = mg_0 \frac{dh}{dt} + mV_{TAS} \frac{dV_{TAS}}{dh} \frac{dh}{dt} \quad [A.1]$$

$$\text{Climb gradient } = \frac{T_{HR}-D}{mg_0} \quad [A.25]$$

$$\frac{dh}{dt} = \frac{(T_{HR}-D)V_{TAS}}{mg_0}\left[1 + \left(\frac{V_{TAS}}{g_0}\right)\left(\frac{dV_{TAS}}{dh}\right)\right]^{-1} \quad [A.26]$$

dh/dt is the vertical speed or change of altitude with time.

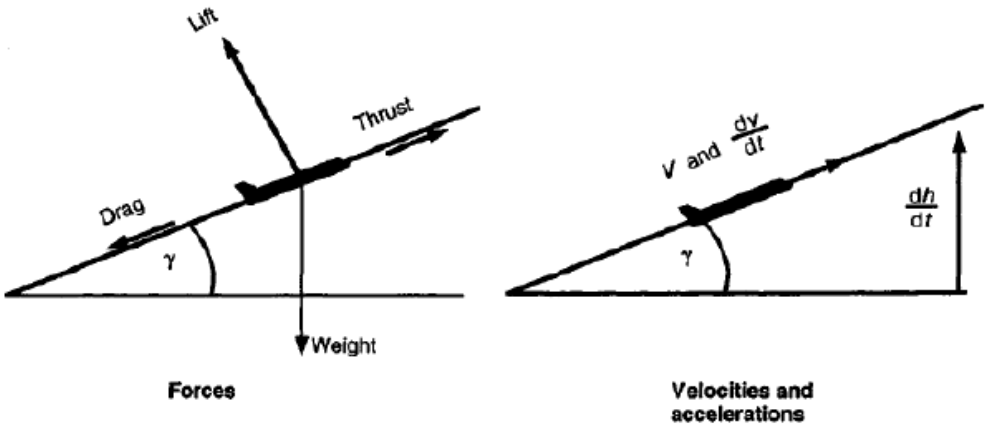

Figure 56 – Aircraft in climb [81]

Assuming standard constant gravity field and hence identical geodetic and geo-potential altitudes, the ROC/D or variation of geo-potential pressure altitude Hp with time is given as

$$ROC = \frac{(T_{HR}-D)V_{TAS}}{mg_0}\left[1 + \left(\frac{V_{TAS}}{g_0}\right)\left(\frac{Vd_{TAS}}{dh}\right)\right]^{-1} \quad [A.27]$$

If $f\{M\} = \left[1 + \left(\frac{V_{TAS}}{g_0}\right)\left(\frac{dV_{TAS}}{dh}\right)\right]^{-1}$

Then

$$\frac{ROC}{D} = \frac{(T_{HR}-D)V_{TAS}}{mg_0} f\{M\} \quad [A.28]$$

where $f\{M\}$ is defined as the acceleration factor or the energy share factor which essentially specifies the amount of power available to the aircraft to climb as opposed to acceleration while following a selected constant speed/Mach profile.
$f\{M\}$ for particular flight conditions are defined as follows:

a. Constant Mach number in stratosphere

$$f\{M\} = 1.0 \quad [A.29]$$

b. Constant Mach number below tropopause

$$f\{M\} = \left[1 + \frac{kR\beta_{T,<}\beta}{2g_0} M^2 \frac{T-\Delta T}{T}\right]^{-1} \quad [A.30]$$

R = 287.05 $J.kg^{-1}.K^{-1}$

g_0 = 9.81 m/s^2

$\beta_{T,<}$ = -0.0065 K/m (ISA temperature gradient below the tropopause)

M = Mach number

k = 1.4 (adiabatic index of air)

ΔT= Temperature deviation from ISA conditions

c. Constant calibrated airspeed below tropopause

$$f\{M\} = \left[1 + \frac{kR\beta_{T,<}\beta}{2g_0} M^2 \frac{T-\Delta T}{T} + \left(1 + \frac{k-1}{2} M^2\right)^{\frac{-1}{k-1}} \left\{\left(1 + \frac{k-1}{2} M^2\right)^{\frac{k}{k-1}} - 1\right\}\right]^{-1} \quad [A.31]$$

d. Constant calibrated airspeed above tropopause

$$f\{M\} = \left[1 + \left(1 + \frac{k-1}{2} M^2\right)^{\frac{-1}{k-1}} \left\{\left(1 + \frac{k-1}{2} M^2\right)^{\frac{k}{k-1}} - 1\right\}\right]^{-1} \quad [A.32]$$

Cruise

In cruise the aircraft is neither accelerating or climbing and will be assumed to fly at a constant Mach number and altitude

$$(T_{HR} - D)V_{TAS} = mg_0 \frac{dh}{dt} + mV_{TAS} \frac{dV_{TAS}}{dt} \quad [A.1]$$

Hence from equation A.1

$$\frac{dh}{dt} = 0 \quad [A.33]$$

$$\frac{dV_{TAS}}{dt} = 0 \quad [A.34]$$

Therefore for the cruise segment

$$T_{HR} = D \quad [A.35]$$

Descent

The descent phase is calculated similar to climb with the exception that in order to descend the thrust is less than the drag. However $f\{M\}$ (deceleration factor in descent) is calculated similar to the climb phase.

$$ROD = \frac{(D-T_{HR})V_{TAS}}{mg_0}\left[1 + \left(\frac{V_{TAS}}{g_0}\right)\left(\frac{Vd_{TAS}}{dh}\right)\right]^{-1} \quad [A.36]$$

The descent phase of the trajectory begins at end of the Cruise segment and continues up to an altitude of 3000ft. This phase is further divided into 3 sub-segments:

- Cruise altitude-Transition altitude: The aircraft descends at constant Mach number.
- Transition altitude – 10000 ft- The aircraft descends at constant V_{CAS} 330 kt till an altitude of 10000 ft.
- 10000 ft-3000 ft- The aircraft descends at a constant V_{CAS} 250 kt.

Similar to Climb phase, the control inputs for this segment will include thrust (set by the flight idle rating), speed (as set through a speed schedule) or a fixed rate of descent (ROD). A key assumption in this phase is that the decent is continuous and speed changes between sub segments are assumed to be instantaneous. As per standard procedure, the ROD of descent is controlled so as to ensure that rate of descent in cabin pressure does not exceed 300 ft/min.

Approach and landing

The approach phase for the aircraft is considered to begin at 3000 ft till 1500 ft and is currently calculated similar to the last sub-segment of descent (constant V_{CAS} 200 kt). From 1500 ft the gradient angle is fixed at 3° to the horizontal with a speed of 1.3 V_{stall} . The current version of the model does not calculate the ground run during landing.

Key assumptions

The BADA database [75], from where the calculations for this aircraft performance model originates, has drag coefficients available for over 60 different aircraft and hence converting the aircraft performance model to simulate different aircraft is convenient. References [79] and [81] have also been extensively used to formulate this model. The speed profiles, power settings, segment altitudes and aircraft weight in terms of load factors may all be used as

variables for trajectory optimisation. Some of the main assumptions in calculation of aircraft performance were:

- Change of speeds between sub-segments are instantaneous as the implication on overall fuel consumption due to change in calibrated speeds and Mach numbers in the speed profile is negligible.
- Bank angles and wind effects have been neglected in all phases of flight
- Cos γ=1
- All segments (climb, cruise and descent) are considered to be continuous and have no step segments
- Currently all calculations are done for the mission and do not account for block calculations. However the program calculates the ground idle and taxi thrusts and hence block calculations may be calculated if required
- As the aerodynamic data for a modelled aircraft is adapted from the BADA database which is verified and validated [80], the model assumes the basic characteristics, dimensions and aircraft/propulsion system limitation parameters remain unchanged and follow those as specified by the data sheets for an individual aircraft. These include the aircraft mass and balance (comprising maximum take-off weight (MTOW), maximum landing weight (MLW), maximum zero fuel weight (MZFW), operating empty weight (OEW), fuel capacity, max payload), number of passengers, mean centre of gravity position, maximum operational altitude, environmental envelope and aircraft dimensions (wing span, overall length, tail height, wing span, reference wing surface area).

Annex B – Engine model

Annex B details the modelling of the engine used in the current work. The model used is the same as in the work of Nalianda [74]; for sake of completeness an extract of the design point parameter selection for the engine is provided. Off-design trends are also extracted from Nalianda work [74].

The engine performance model to be used in conjunction with the aircraft performance model is built using Cranfield University's in-house gas turbine simulation and diagnostics software TURBOMATCH. The engine model currently used with the aircraft performance model simulates the performance of a typical twin spool high bypass engine similar in design characteristics to a CFM56-7B27 engine which is currently used by the industry to power a Boeing 737-800 aircraft.
The design point of the engine model was chosen at top of climb (i.e. Alt 10668 m, Mach speed 0.8, and the pressure recovery of 0.99) under International Standard Atmosphere (ISA) conditions. Several iterations were performed using the model at design and off-design point conditions to match the performance of the model with data obtained from the public domain for the engine on which the design was based. A summary of this data is presented in Table 22 [82-84].
The mass flow rate at the engine intake was estimated based on the measured intake area and assuming an average inlet Mach number of 0.55 – 0.65. The design point (top of climb) bypass ratio (BPR) and the turbine entry temperature (TET) were determined based on the overall pressure ratio and the net thrust at top of climb. The optimum fan pressure ratio corresponding to the calculated TET, overall pressure ratio (OPR) and bypass ratio (BPR) was also determined.
Additionally, values of component pressure ratios, component efficiencies, and compressor bleed for turbine cooling, and other parameters, were guessed and iterated to match the required engine performance at off design (maximum take-off and cruise) conditions. It was observed that the discrepancies between the required and achieved values are minor and hence the engine performance model was deemed acceptable.

Table 22 – Comparison of design and performance data of simulated engine with public domain data [74]

	Public domain data	Model value
Design point altitude	10668	10668
Design flight Mach number	0.8	0.8
Top of climb thrust	26511	26600
Top of climb SFC	-	16.21
Top of climb TET	-	1510
Top of climb mass flow	-	140
Take-off thrust	121400	121400
Take-off fuel flow	1.235	1.12
Take-off TET	-	1670
Take-off BPR	5.1	5.1
Take-off mass flow	358	350
Fan pressure ratio	-	1.77

Booster pressure ratio	-	1.881
HPC pressure ratio	-	9.829
Overall pressure ratio	32.8	32.7
Isentropic compressor efficiencies	-	0.86
Isentropic turbine efficiencies	-	0.91
Combustor efficiency	-	0.99

Off-design performance

Several off-design performance simulation calculations utilising the simulated engine model were performed. These simulations yielded off-design performance charts highlighting the effects of altitude, flight Mach number, ambient temperature and turbine entry temperature on net thrust and specific fuel consumption.

Figure 57 highlights the variation of net thrust (FN) as a function of altitude (Alt) and flight Mach number (M) for a fixed value of turbine entry temperature (TET). The value of TET chosen was the design point i.e. top of climb (TET = 1340K).

Figure 58 highlights the variation of specific fuel consumption (SFC) as a function of altitude and flight Mach number for the same fixed value of TET. Figure 59 highlights, in turn, the variation of net thrust (FN) as a function of ambient temperature (T_{amb}) and turbine entry temperature (TET) at Sea Level Static Conditions (Alt = 0 m, M = 0). Finally, Figure 60 highlights the variation of specific fuel consumption (SFC) as a function of ambient temperature (T_{amb}) and turbine entry temperature (TET) at Sea Level Static Conditions. It may be noted that for these analyses, the maximum TET considered was the TET corresponding to take-off conditions. The three figures broadly follow the expected trend lines. Reference [85] provides detailed qualitative descriptions of the effects of altitude, flight Mach number, ambient conditions and turbine entry temperature on gas turbine performance.

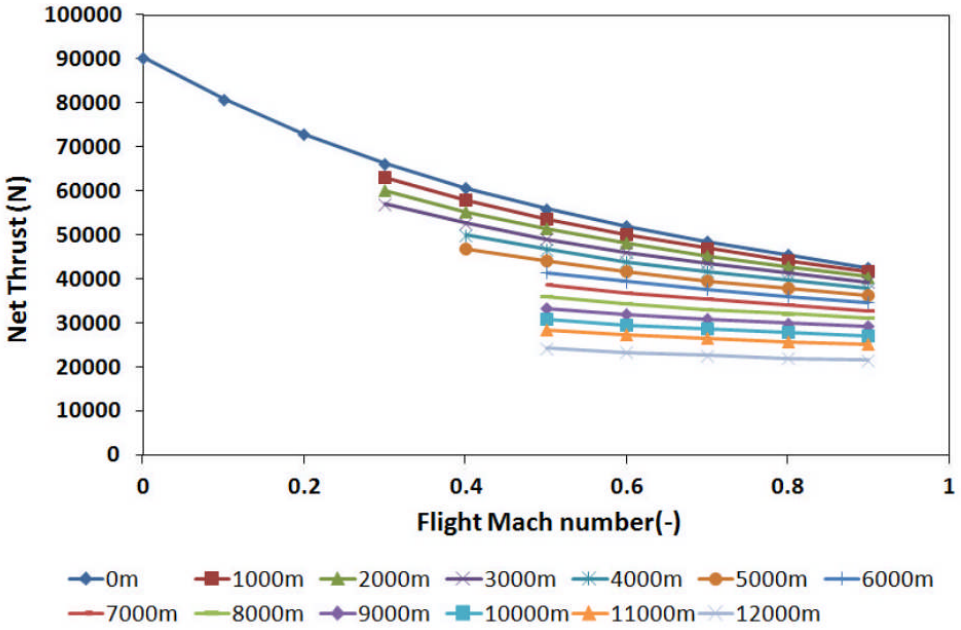

Figure 57 – Variation of net thrust as a function of altitude and flight Mach number for the same fixed value of TET (DP TET = 1510K) [74]

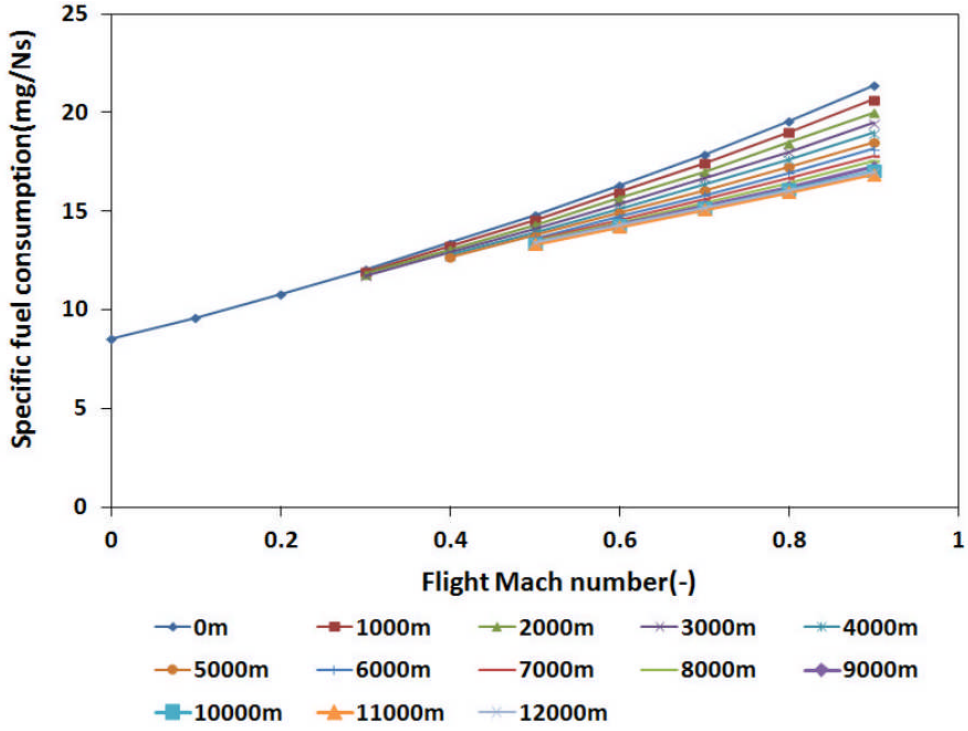

Figure 58 – Variation of specific fuel consumption (SFC) as a function of altitude and flight Mach number for the same fixed value of TET (DP TET = 1510K) [74]

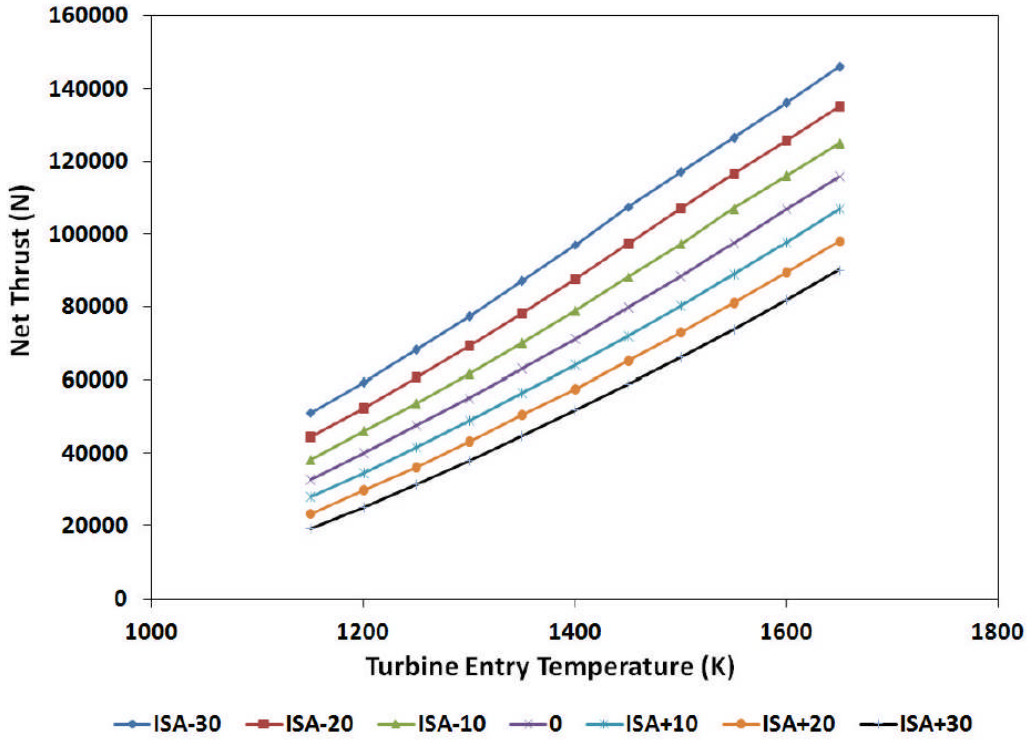

Figure 59 – Variation of net thrust as a function of ambient temperature (T_{amb}) and turbine entry temperature (TET) at sea level static conditions [74]

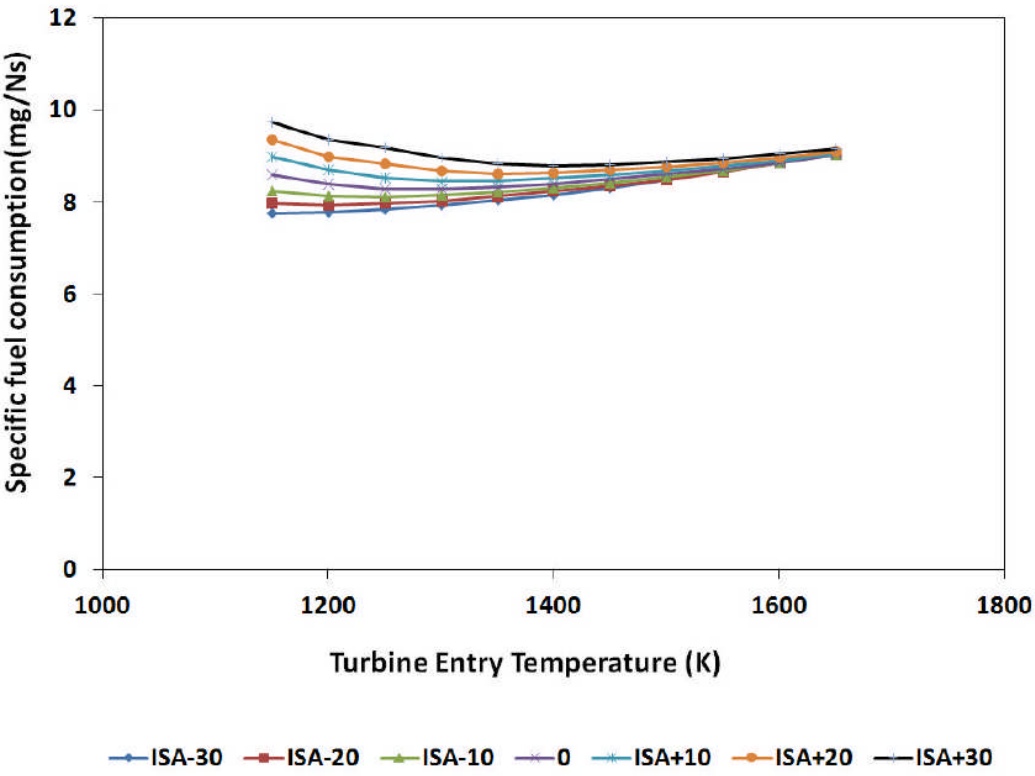

Figure 60 – Specific fuel consumption (SFC) as a function of ambient temperature and TET at sea level static conditions [74]

Annex C – Validation of aircraft/engine model

The aircraft and engine model were integrated and a series of validation tests were performed to validate/ verify the performance of the models. This section comes from the work of Nalianda [74].

Performance assessment on the payload range chart: The payload range (PR) chart is an important assessment tool for decision making, during an aircraft or fleet selection process. It depicts the maximum allowable revenue generating payload that may be carried by a particular aircraft. It also defines the combined mass of payload and fuel that may be allowed to achieve any particular range, within the aircrafts' performance ability. The payload range chart is usually accompanied by a specified flight profile wherein the performance calculation of each point is based on a set of International Flight Rules (standard assumptions on fuel reserves, diversion fuel and contingency fuel).

The PR chart has effectively four critical points (as shown in the Figure 61). The point A shows the maximum volumetric payload carried by a particular aircraft, while keeping within its structural limitations. Line AB is essentially the line wherein the aircraft's range is increased by increasing the quantity of fuel on board. Point B is the maximum range flyable by the aircraft with maximum payload on board as it reaches its Maximum Take-off Weight (MTOW) limit. Line BC then depicts the range at which the aircraft will fly at MTOW, and therefore will result in reduction of payload with an increase in fuel on board. Point C is the range at which the fuel on board is maximum and hence the payload is reduced to level at which the aircraft is still at its MTO weight. A further reduction in payload, with maximum fuel on-board, allows an increase in range along line CD, but only because the reduction of total weight increases the specific range R_{ac} .

$$R_{ac} = -\frac{dR_a}{dm} = \frac{V}{SFC\beta W} \qquad [C.1]$$

Where

β: drag to lift ratio

W: weight of aircraft

SFC: specific fuel consumption

One of the ways of assessing the performance of the simulated aircraft is to compare its performance on a payload range chart against that of the original aircraft on which it is modelled. Figure 61 indicates the payload range capability of the simulated model compared with that of the aircraft it is based on (Boeing 737-800 with a CFM56-7B27 engine) [86]. This is done for the three critical points (B, C and D) and as mentioned previously, for a specific flight profile assumed for all missions as discussed earlier.

Therefore in establishing the payload range performance, similar to a standard flight profile found in BADA [80] the following flight profile was assumed:

1. Take off - sea level, ISA conditions, max take-off thrust, take off configuration, accelerate to 155 kt (V_2+10)
2. Initial climb - Constant CAS (155 kt), clean configuration, maximum climb thrust to altitude 1500 ft.
3. Initial climb - CAS (193 kt), clean configuration, maximum climb thrust until altitude 3000 ft.
4. Enroute climb - Constant CAS (250 kt), clean configuration, maximum climb thrust until altitude 10000 ft.
5. Enroute climb - Constant CAS (300 kt), clean configuration, maximum climb thrust until crossover altitude 25756 ft.
6. Enroute climb - Constant Mach (0.75), clean configuration, maximum climb thrust until cruising altitude 35000 ft.
7. Cruise - Constant altitude and speed cruise (35000 ft and Mach 0.78), clean configuration. The cruise speed and altitude were based on long range cruise data for this aircraft and engine.
8. Descent - Constant Mach (0.75), clean configuration, descent idle thrust until crossover altitude (25756 ft)
9. Descent - Constant CAS (300 kt), clean configuration, descent idle thrust until altitude 10000 ft.
10. Descent - Constant CAS (250 kt), clean configuration, descent idle thrust until altitude 3000 ft.
11. Approach and landing – Constant path angle (3°), approach configuration, approach thrust until altitude 0 ft.

All missions were simulated with standard assumptions for hold, diversion and on board reserves fuel. Therefore at the end of the mission that the fuel onboard included the following:

- Fuel for 20 minute hold (760 Kg)
- Fuel for 200 nm diversion route which includes a climb to 20000 ft, cruise at constant altitude and speed of 20000 ft and Mach 0.60 and descent (1633 kg).
- Fuel for onboard reserves - 5% of trip fuel consumed.

Table 23 indicates the mission specific data for the three simulated points and Figure 61 illustrates the PR performance of both aircraft. Given the various assumptions made in modelling, flight profile of the trajectories and numerical discretisation errors, discrepancies between the required and achieved ranges are observed. However, as this is an attempt to simulate the generic performance of a short to medium range aircraft, the errors are considered small and hence deemed acceptable.

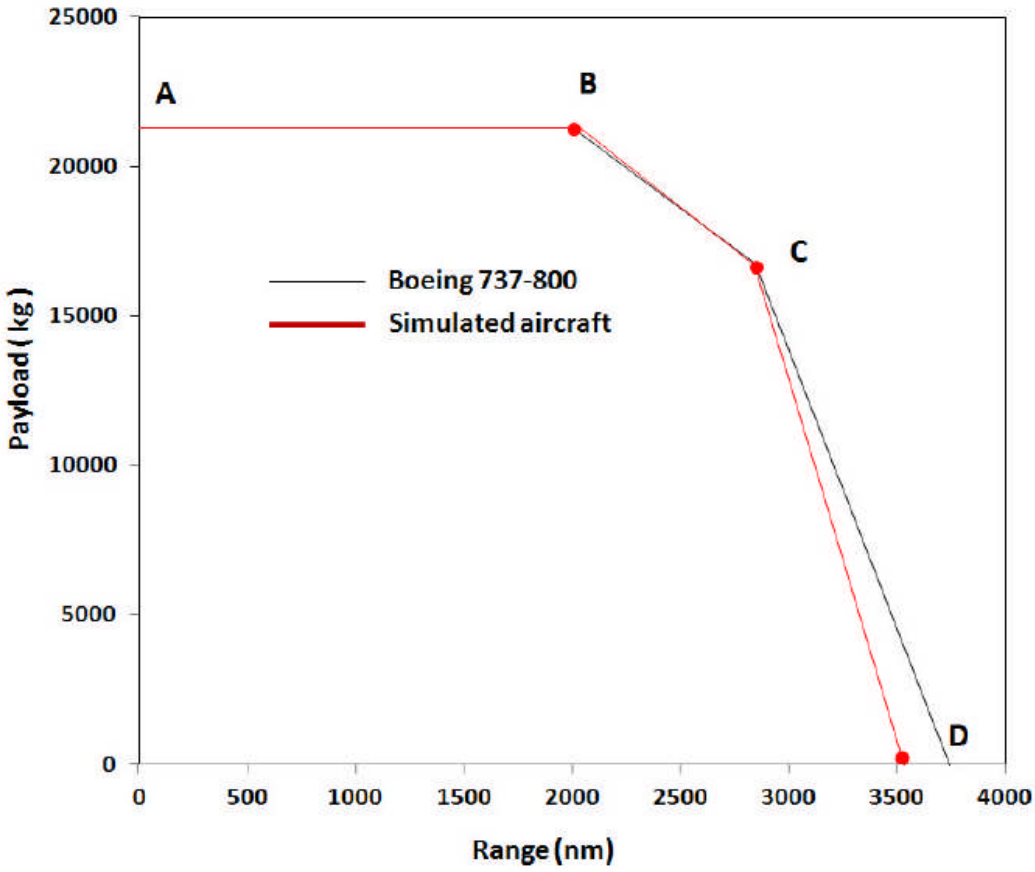

Figure 61 – Payload-range validation of aircraft/engine model [74]

Table 23 – Payload range validation of aircraft/engine model [74]

	Max payload range (B)	Max fuel range (C)	Max ferry range (D)
Cruise flight Mach number (-)	0.78	0.78	0.78
Altitude at cruise (ft)	35000	35000	35000
Maximum take-off weight (kg)	79016	79016	62307
Maximum payload (kg)	21319	16709	0
Operating empty weight (kg)	41413	41413	41413
Maximum fuel onboard (kg)	16284	20894	20894
Hold (20min) + diversion (200nm) fuel (kg)	2394	2394	2394
5% contingency fuel (kg)	661	870	862
Fuel consumption – Model (kg)	13219	17630	17638
Range Boeing 737-800 (nm) (nm)	2000	2850	3750
Range simulated aircraft (nm)	2033	2847	3531
Range error % (in ref to B737 data)	**1.6**	**0.1**	**5.8**